A STUDY OF ELECTROLUMINESCENCE IN ZINC SELENIDE SCHOTTKY DIODES WITH PARTICULAR EMPHASIS ON REVERSE-BIASSED DIODES FREE OF INTENTIONALLY ADDED LUMINESCENCE CENTRES.

A thesis presented by

K. Turvey, B.Sc.,M.Sc.

to the

University of St. Andrews

in application for the degree

of Doctor of Philosophy.

I hereby certify that this thesis has been composed by me, and is a record of work done by me, and has not previously been presented for a Higher Degree.

This research was carried out in the Physical Science Laboratory of St. Salvator's College, in the University of St. Andrews, under the supervision of Mr. J.W. Allen.

I certify that K. Turvey has spent at least nine terms of research work in the Physical Science Laboratory of St. Salvator's College, in the University of St. Andrews, under my direction, that he has fulfilled the conditions of Ordinance No. 16 (St. Andrews) and that he is qualified to submit the accompanying thesis in application for the degree of Doctor of Philosophy.

Research Supervisor.

ACKNOWLEDGEMENTS

The author is indebted to his supervisor, Mr. J. W. Allen, for the guidance he rendered throughout the conduct of the work reported in this thesis.

Dr. J.F. Cornwell provided valuable assistance in the interpretation of certain published selection rules governing electronic transitions between symmetry points of the Brillouin zone. These rules are referred to in chapter 3.

Financial support for the programme of research which led to the submission of this thesis was obtained from the Science Research Council and from the Wolfson Foundation.

ABSTRACT

The passage of a reverse current through Schottky diodes of ZnSe not containing intentionally added luminescence centres excites a broad band of electroluminescent emission which extends from 2.65eV to 0.4eV. It has been shown that the electronic transitions giving rise to this emission band are between certain valleys of the ZnSe conduction band. Structure in the spectrum has been explained in terms of transitions between several pairs of conduction band valleys. It is suggested that similar studies of the light emission from reverse biassed Schottky diodes could be used as a method of gaining experimental information on the band structure for a wide range of semiconductors.

Electroluminescence has also been studied in ZnSe Schottky diodes in which Mn or Cu centres were present. For the Mn- doped diodes the reverse bias emission is yellow in colour and the photometric power efficiency compares favourably with commercially available yellow light electroluminescent sources. The mechanism of excitation in reverse biassed ZnSe diodes containing luminescence centres is by impact of these centres with energetic electrons.

A weak electroluminescent emission has been observed in forward biassed ZnSe Schottky diodes. The field for this polarity of bias is insufficient to impact excite or impact ionize luminescence centres and a model of excitation by hole injection is discussed for this case.

CONTENTS

1. INTRODUCTION

During the past few years the electronics industry has devoted considerable effort in attempts to produce light-emitting diodes of high photometric power efficiency. Lamps are commercially available using p - n junctions of GaP and Ga $As_x P_{1-x}$, amongst other materials. With the trend of a steadily reducing price per unit these are finding increasing application, especially in alpha-numeric displays and as indicator lamps on instruments. For the manufacture of efficient diode sources of visible light a semiconductor of band gap greater than about 2eV is required. Many of the II-VI zinc-blende semiconductors satisfy this condition and have therefore frequently been considered as potential lamp materials.

Zinc selenide, which is a member of the above class of compounds and has a band gap of 2.7eV, has not been neglected by other workers as a possible lamp material but one reason for its non-adoption is the difficulty of making it usefully p-type thus precluding the manufacture of suitable p - n junctions. This difficulty is encountered in several other II-VI compounds, some of which are efficient phosphors, and hence otherwise likely to be suitable as a visible light source material. In the present work Schottky diodes have been prepared on n-type ZnSe and the excitation of the luminescence centres achieved in an impact process by energetic carriers in reverse biassed diodes. The usual method of excitation employed in p - n junctions is by minority carrier injection in forward bias. The preparation of Schottky diodes is a much cheaper procedure than the preparation of p - n junctions so that, in this respect, the former type has a cost advantage as a practical device.

A part of the work of this thesis has been a study of the electro-luminescence in ZnSe doped with Mn or with Cu as luminescence centres. Possible practical applications arising from the work have been given some consideration.

The main area of study has been the light emission which occurs

in reverse bias of Schottky diodes on ZnSe free from deliberately added luminescence centres. The emission spectrum under these conditions is a broad band extending over a range of about 2.1eV from the visible into the infra-red regions of the electromagnetic spectrum. A study of this spectrum was of interest because it was expected to reveal information regarding the interaction of energetic carriers with the ZnSe lattice. Since structure was observed in the broad emission band this was anticipated to be associated with the nature of the ZnSe band structure which could therefore be studied from diode spectra. It has been noted in the introductory remarks of chapter 3 that other authors have reported observations of similar broad-band spectra in other materials, but they used reverse-biassed p - n junctions rather than the simpler Schottky diode structure used in the present work. These other studies, however, have been less intensive than has the work of this thesis.

The research fields outlined above, in which D.C. reverse bias electroluminescence in ZnSe was investigated both with and without the deliberate inclusion of luminescence centres, are two related projects on the behaviour of free carriers in high fields ($\sim$ 100 kV/cm); in the former case energetic carriers lose energy in interactions with luminescence centres and in the latter case, since the density of such centres is small, higher average free carrier energies are achieved. The behaviour of carriers at high fields is a topical branch of semiconductor physics largely on account of the device application of the Gunn effect.

A minor part of this thesis is the investigation of light emission in forward bias of ZnSe diodes. This is of interest for purposes of comparing the spectra with the corresponding reverse bias emission and because a completely different excitation mechanism is involved.

2. EXPERIMENTAL METHODS

2.1. Preparation of ZnSe for diode manufacture

The preparation of the ZnSe used in the manufacture of the Schottky diodes for the experimental work of this thesis was not performed by the author and therefore only a very brief outline of the preparation procedure is appropriate here. The ZnSe was made by direct synthesis of the elements and grown into crystals by a vapour phase transport method. The Zn (99.999% purity) and the Se (99.9998% purity) used in the synthesis were both obtained from Koch-Light Laboratories. Al was added as a donor to obtain n-type conductivity. In some preparations luminescence centres were deliberately introduced by the incorporation of either Mn or Cu into the ZnSe. The product contained crystallites of about 1mm size.

2.2 Diode fabrication

The ZnSe prepared as described above was cut into chips of typical dimensions 2mm x 2mm x 1mm. Ohmic contact was provided by alloying on In dots in an evacuated chamber. Suitable heating conditions to obtain ohmic contact had been determined in preliminary experiments and two In dots were alloyed onto each chip to enable checks to be made that the contacts were indeed ohmic. On one of the larger faces of each chip a Schottky barrier contact was prepared by evaporation of the contact metal through a mask and the diameter range for these rectifying contacts was 0.4mm to 1.0mm. The evaporation was from an electrically heated tungsten filament and was performed at a vacuum of 10^{-5} torr. On account of its chemical inertness Au was chosen as the barrier contact metal for the manufacture of most diodes. A few diodes were prepared with Al rectifying contacts, with this metal chosen because of the readily available and not very highly reactive metals, it differs most in work function from Au.

Surface preparation of the ZnSe prior to the application of both ohmic

and rectifying contacts consisted of rubbing down the chip on fine (600 mesh) moistened carborundum, followed by etching with a solution of bromine in methanol (5% by volume) and finally treating the chip with CS_2. The purpose of the CS_2 treatment was to remove the layer of Se which formed on the surface of the ZnSe during etching. The surface was prepared in the above way immediately before the application of the In contacts and again just before placing the ZnSe chips in the evacuable chamber for the evaporation of the barrier metal. Precautions were taken to minimize the exposure of surface-treated chips to the atmosphere by keeping these wet with methanol until placement in the appropriate chamber which was then immediately evacuated. The In contacts were protected during the second etch by coating them with a suitable wax which was later removed with a solvent.

2.3 Diode capacitance measurements

Measurements of the differential capacitance (C) of the ZnSe Schottky diodes were made to determine the donor concentration (N_D). A plot of C^{-2} against applied bias, V, is linear for an ideal Schottky barrier and for all of the diodes tested in this work, with the exception of the first few diode fabrications. The slope of a C^{-2} vs. V plot for an ideal Schottky barrier on an n-type semiconductor is given by

$$\frac{dC^{-2}}{dV} = \frac{2}{\varepsilon e N_D A^2} \qquad \ldots\ (2.1)$$

where ε is the permittivity of the semiconductor at the measuring frequency (essentially ε is equal to the static value), e is the electronic charge and A is the area of the rectifying contact. Equation 2.1 is given for the rationalized M.K.S. system of units. Goodman[1] has shown that for diodes of the metal-insulator-semiconductor form, if C^{-2} is experimentally found to vary linearly with V, then N_D is related to dC^{-2}/dV as for an ideal Schottky diode. For an intimate metal to n-type semiconductor contact the intercept on the voltage axis in a C^{-2} vs. V plot is the electron barrier height but a larger intercept is obtained for a metal-insulator-semiconductor

diode. From the experimentally determined value of this intercept many diodes showed evidence of an insulating layer between the metal contact and the ZnSe. In evaluating N_D from equation 2.1 the value $9.1\varepsilon_o$ [2] was taken for ε, where ε_o is the permittivity of free space.

Apart from the determination of N_D, capacitance measurements were also of value in obtaining the bias-dependent diode depletion width and, from this, the mean electric field in the depletion layer.

The capacitance measurements were made using a Marconi TF 2700 bridge. This instrument operates as a Schering bridge when switched to capacitance ranges. Measurements were made at frequencies in the range 200 Hz to 100 kHz. Although Marconi recommended that the bridge only be used at frequencies below 20 kHz it was found, by preparing a parallel capacitance-resistance network to simulate the capacitance and loss of typical diodes, that the capacitance as measured at 100 kHz differed by less than 2% from the value obtained at 1 kHz. This latter frequency is the frequency for optimum accuracy of the bridge. The A.C. signal at the diode during capacitance measurements was arranged to be less than 20 mV pp. Balancing of the bridge was performed using two plastic handles, each about one foot in length, to eliminate the effects of hand capacitance. Batteries were used to bias the diode and as the power-source for the oscillator. In plotting C^{-2} against V the value of C was taken as the effective parallel capacitance of the diode chip, although, since measurements were restricted to a bias range in which losses were small, this was not normally significantly different to the equivalent series capacitance.

2.4 Spectrum measurements

Luminescence spectra were measured using a Zeiss SPM2 monochromator. The dispersive element used in the SPM2 was a glass prism except for measurements which encompassed a spectral range with photon energies less than 1.0 eV, in which case a LiF prism was used. The spectrum measuring equipment is shown in Fig. 2.1. Light from the D.C. excited diode, S, was

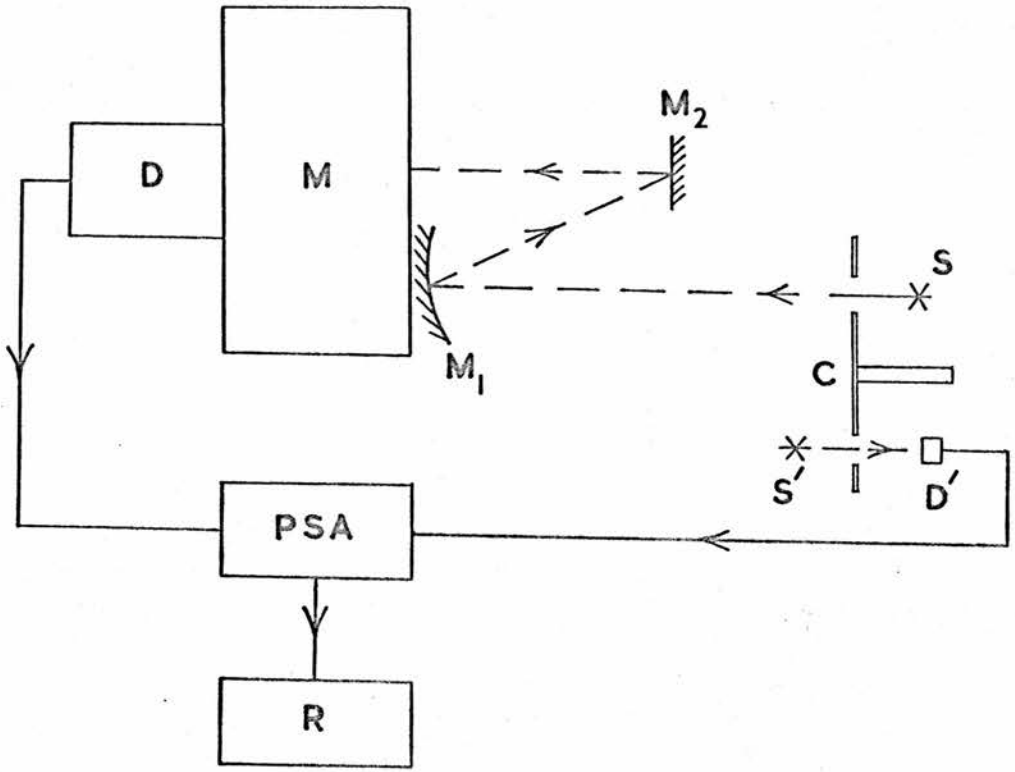

Fig. 2.1 Block diagram of apparatus used for spectrum measurements. C-Chopping disc, D-Detector, M-Monochromator, M_1 and M_2 -Mirrors, PSA-Phase-sensitive amplifier, R-Recorder, S-Diode source, D′-Photodiode, S′-Subsidiary source for obtaining reference signal.

mechanically chopped at 800 Hz by the chopping disc C, then after reflection from each of the mirrors M_1 and M_2 entered the monochromator M. At the exit slit of M radiation was detected by the detector, D, with this connected to the input terminal of the phase-sensitive amplifier PSA. A reference signal, in fixed phase relationship to the signal from D, was obtained by interrupting with C the light received at a photodiode (D') from a small source S'. For continuous drive of the prism in M the emission spectrum of S was displayed by the recorder, R, which was connected to the output terminals of PSA.

For some measurements C, S' and D' were removed and S then driven in the bias polarity of interest from a square wave generator which was also the source of the reference signal.

Photoluminescence spectra were measured using PSA, without the use of C, by utilizing the 100 Hz modulation of the 365 nm exciting light from a mains-operated mercury lamp. The reference signal was derived from the mains through a simple frequency doubler.

Depending on the spectral range to be covered in any particular measurement the detector, D, was an E.M.I.9558 photomultiplier (S20 response), a Mullard 150CVP photomultiplier (S1 response), or for measurements further into the infra-red, a Mullard 62SV PbS cell. The latter two detectors were always cooled when in use. The upper wavelength limit that could be reached in spectrum measurements was about 3.0μ with this limit set by room temperature radiation from the opaque parts of C causing spurious results at longer wavelengths. Painting of C with aluminium paint, in an attempt to reduce its emissivity did not appreciably improve the situation. The use of the measuring system in the form without C was not successful when the spectral range necessitated use of the PbS cell. This was because the electrical pick-up signal in the cell circuit, due to power radiated from the diode circuit, was greater than the signal attributable to the optical modulation, even for a screened system. When attempting to measure spectra for diodes at room temperature in the wavelength range greater than 2.5μ it was found essential

to provide effective diode cooling, for example by an air blast directed at the diode, otherwise, for the usually necessary few hundred milliwatts dissipation in the diode, temperature radiation obscured the luminescence emission. This effect occurred if the diode temperature exceeded 40°C.

Wavelength calibration of the monochromator was achieved by measuring several emission lines from Na, Cd, Hg and Ne lamps. In the infra-red range, wavelength calibration was based on standard absorption lines of benzene and chloroform.

To obtain the true shape of the spectrum it is necessary to apply corrections for the response of the measuring system, particularly if the detector response changes appreciably over the width of the spectrum. Distortion from the true spectrum shape is also caused by a photon energy dependent dispersion of the monochromator prism and, usually less importantly, by a photon energy dependent absorption in the prism. Many authors of papers in which luminescence spectra are published do not appear to have considered these effects or to state precisely the definition of the ordinate in their spectra. This leads to ambiguities when comparing results obtained by different workers. In this thesis corrections for the measuring system response, which include the above effects together with any effects due to the optics external to the monochromator, have always been applied and the ordinate, which is denoted by N(E), is the relative number of photons emitted per unit photon energy interval at a photon energy E. The spectra are plotted with E as the abcissa.

To express spectra in the terms just described requires calibration of the measuring system using a source of a known and continuous spectrum. The most obvious such source is a black-body radiator but this is difficult to construct for radiation emission of a single temperature if this temperature is more than a few hundred degrees centrigrade. As a standard source for the calibration work a tungsten filament lamp was used and reference made to tungsten emissivity data given by De Vos[3] to

determine the spectrum shape. The filament temperature, which was required for this purpose, was estimated from filament resistance measurements and the known[4] temperature dependence of the resistivity of tungsten. Accurate resistance measurements were made by placing the lamp in one arm of a D.C. Wheatstone bridge. To obtain good thermal isolation of the filament from its supports, and hence a good approximation to temperature uniformity, a lamp with a long thin filament (240 volt, 15 watt) was chosen. The optical system for coupling light from the tungsten lamp into the monochromator was the same as that used in measuring the ZnSe spectra. As a check on the reliability of De Vos's data for the spectral emissivity of tungsten it was noted that similar measurements[5] on the light emission properties of hot tungsten were in good agreement.

From the detector output signal obtained with the tungsten lamp as a source and from the calculated emission spectrum for this lamp, a quantity S(E) was determined for a series of photon energies, where S(E) is the detector relative output (standardized to a constant E.H.T. voltage in the case of photomultipliers) for unit number of photons emitted by the source per unit energy interval per unit time. The values of S(E) were determined for a series of filament temperatures ranging from a red to a white filament colour and without alteration of the monochromator slit widths or of the position of the lamp. Stated more precisely, the filament temperature range was from 1400K to 2300K. (These temperatures were deduced after the application of a certain correction procedure which is discussed in the next paragraph.)

It was discovered that at any photon energy there was a small regular shift of the determined S(E) values with filament temperature, and this was attributed to a small systematic error in the temperature determination. Since, according to De Vos[3], the spectral emissivity of tungsten is only very weakly dependent on temperature, a semilogarithmic plot of detector output against the reciprocal of filament temperature, at a fixed photon energy,E,

($E \gg kT$) should be linear and have absolute slope E/k. When the filament temperature was measured as indicated above these plots were linear but with absolute slope $0.95E/k$ independently of E. This suggested that the temperature estimates were 5% too low, and in accord with this, it was found that the temperature-coefficient of resistance for the filament, as directly measured in the range $0^{\circ}C$ - $120^{\circ}C$, was 5% higher than that deduced from the resistance tables previously used in the temperature estimation.

Redetermination of S(E) values, taking all filament temperatures as 5% higher than the values used earlier, yielded results which exhibited only small and random variations for changes in the filament temperature. This was shown by plotting, on a common graph, points of S(E) against E obtained in experiments with several different filament temperatures. The variation of S(E) with E obtained by drawing a smooth curve through the points was subsequently used to correct ZnSe spectra. The same calibration procedure was repeated for each combination of detector and prism used in the measurement of ZnSe spectra. In cases where spectra were measured separately with an S20 response photomultiplier and an S1 response photomultiplier, each forming the detector of a calibrated spectrum measuring system, excellent agreement was obtained between the corrected spectra even if the shape was appreciably changed by application of the corrections.

For certain spectra, which are discussed in chapter 3, a correction was applied for the distortion of the spectral shape caused by wavelength dependent absorption in the diode chip.

2.5 External quantum efficiency

An S20 response photomultiplier was calibrated for absolute light emission measurements and then, by using the photomultiplier to measure the light output from diodes operated at known currents which were usually in the range 0.5mA to 10mA, the external quantum efficiencies were determined.

The calibration procedure involved measuring the photomultiplier output, V_o, for a known photon current of L_o photons per unit time incident upon the photocathode. This photon current was obtained by a large and known attenuation of a laser beam of known pre-attenuation power. The source was a Spectra-Physics model 132 He - Ne laser ($\lambda = 632.8$ nm) with nominal laser light output of 1.5 mW. For reasons to be given later a concave lens was introduced in the laser beam and the beam power, with no other attenuation apart from that due to the lens, was measured using a Spectra-Physics 401 laser power meter. This instrument is claimed by its manufacturers to be accurate to within 5% for He - Ne laser powers in the 1.5mW region. The large and known attenuation was produced by a series of two or three filters. Each individual filter caused an attenuation which had been determined from transmission measurements of He - Ne laser light. Several combinations of the calibrated filters were used, with an overall attenuation in the range 2×10^2 to 5×10^4. For the upper decade of this attenuation range the attenuated beam power was of similar magnitude to the radiant power from a typical ZnSe diode operated at a reverse current of 1mA. Over the entire attentuation range the ratio V_o/L_o was constant to within the limits of experimental error. The laser beam, as delivered by the source, was narrow ($\sim$ 1mm wide at a distance of 1m from the source) and of small divergence. The purpose of the concave lens was to increase the beam divergence so that a larger part of the photocathode was illuminated by the beam than would otherwise have been practicable. This had the benefit of reducing the possibility of overloading a small part of the photocathode and also meant that the results obtained were more representative of the properties of the whole of the photocathode surface. With the lens in position the illuminated zone of the photocathode was about 1cm in diameter.

To measure the external quantum efficiency of a diode this was placed at a known distance in front and along the axis of the photocathode of the calibrated photomultiplier. From this distance and the known radius

of the photocathode the solid angle, Ω, subtended by the diode at the photocathode, was calculated. It was arranged that Ω was a large fraction of the maximum possible value of 2π. If the photomultiplier output, after standardization to the same E.H.T. voltage as in the calibration, was V then assuming spatial uniformity of emission, the total rate, L, of emission of photons from the diode was obtained from the equation,

$$L = L_o \cdot \frac{V}{V_o} \cdot \frac{Q_o}{\bar{Q}} \cdot \frac{4\pi}{\Omega} \qquad \ldots.(2.2)$$

where Q_o is the quantum efficiency of the photocathode for light of wavelength 632.8nm and $\bar{Q}$ is its mean value for the diode spectrum. Q_o and $\bar{Q}$ were obtained by reference to the photocathode sensitivity data provided by the manufacturer of the photomultiplier. For sufficiently broad spectra the determination of $\bar{Q}$ required a numerical integration over the entire emission spectrum. Since Ω was large any error in the assumption of spatial uniformity of emission is not, for the purpose of obtaining approximate results, critical. The diode current was always noted when measuring L and therefore the external quantum efficiency could be found.

By obvious modifications to the definitions of L and $\bar{Q}$ the external quantum efficiency for photons within a specified energy band, rather than for the whole of the spectrum, was found for certain broad spectra.

For some of the diodes studied in this thesis the external power effiency, expressed in photometric terms, has been quoted as this is a more useful quantity than the external quantum efficiency for gauging the technological value of the diodes. The determination of the external photometric power efficiency from the external quantum efficiency was trivial.

2.6 Relative light output as a function of diode current and voltage

The output of an S20 response photomultiplier, placed with respect to a diode under test as in the external quantum efficiency determination, was measured for a series of known diode currents and corresponding voltages to

study the relative light output as a function of diode current and voltage. The light emission intensity in each diode was typically measured over a range of more than six decades and sometimes over as much as eight decades. To make measurements over such large ranges it was necessary to vary the E.H.T. voltage applied to the photomultiplier and then to reduce the photomultiplier outputs all to the basis of a certain standard E.H.T. voltage.

Some measurements were made with diodes excited by D.C. and in other measurements diodes were operated from a square wave generator at a frequency of 80Hz. In the former case the photomultiplier output was measured directly as the signal voltage across the anode load resistor and in the latter case a phase-sensitive amplifier was used. The limit of sensitivity for light emission measurements with the square wave method of diode excitation was better by about an order of magnitude compared with that for the D.C. method. For some diodes the experiment was performed both for D.C. and square-wave excitation and good agreement was obtained when the results were reduced to a common basis by use of the previously measured gain of the phase-sensitive amplifier for square wave input.

For measurements over a range of currents for which heating effects would be caused for D.C. or square wave excitation diodes were pulsed to avoid these effects.

2.7. Measurements of light rise and fall times.

The rise and fall times for the light emission from ZnSe diodes were obtained by pulsing the diodes from a pulse generator source. The light was collected, without a spectrometer or filter in its path, by a photomultiplier, the output of which was fed to either an oscilloscope or a boxcar detector. The rise and fall times were obtained from the oscilloscope trace or from the output of the boxcar detector.

In measurements for diodes with no deliberately added luminescence centres there was particular interest in obtaining high time resolution. The rectifying contacts on the ZnSe were made as small as conveniently possible

(0.4 mm. diameter) to minimize diode capacitance. The photomultiplier employed in these measurements was an R.C.A. model IP28, which was chosen because it has small physical size and hence probably a small spread in the electron transit time. The pulse generator was an Advance PG55A unit which, according to its specifications, has output voltage rise time and fall time each less than 15ns. The current rise and fall times, with a diode driven in reverse bias as the load, are less than the corresponding output voltage response times of the pulse generator on account of the form of the current-voltage characteristics of the diode. The measured diode reverse current rise and fall times were about 3ns, and this time is not much greater than the estimated charging time of the junction capacitance ($C \sim 20$ pF, total circuit series resistance $\sim 100\,\Omega$). The IP28 photomultiplier output was monitored on a Tektronix 561A sampling oscilloscope, which has input impedance of $50\,\Omega$. The light rise and fall times as measured for the diodes without deliberately added luminescence centres were each about 5.5ns (for 10%-90% rise and 90%-10% fall). This time is close to the time resolution of the instrument.

Other measurements of diode response time, particularly in cases where preliminary investigations had shown the response times to be longer than a few tens of nano-seconds or where there was less interest in obtaining high time resolution, were made using an E.M.I. 9558 photo-multiplier in conjunction with a Brookdeal 400 series boxcar detection system. The latter was used in place of the sampling oscilloscope and was usually operated with a gate time of 10ns.

The boxcar detection system was also used in the measurement of time-resolved spectra for certain purposes which are discussed in Chapter 4.

3. REVERSE BIAS ELECTROLUMINESCENCE IN SCHOTTKY DIODES OF ZnSe WITH NO DELIBERATELY ADDED LUMINESCENCE CENTRES

3.1 INTRODUCTION

At an early stage of the work presented in this thesis it was noted that there is a broad band electroluminescent emission (2.6eV - 0.5eV) which accompanies the passage of a reverse current through Schottky barriers on n-ZnSe free from intentionally added luminescence centres. In the past few years similar spectra have been observed for reverse currents in p - n junctions of Si[6-8], Ge[9], GaP[10,11], GaAs[12], $GaAs_xP_{1-x}$[13] and SiC[14], all of which exhibit a spectrum at least leV wide. The motivation for studying these spectra was to gain knowledge of the behaviour of energetic electrons in semiconductors. In the above papers the most generally favoured explanation for the light emission mechanism has been that free carriers are heated in the strong field of reverse-biassed junctions and the light results from the bremsstrahlung of these hot carriers within single valleys of the band structure. Necessarily, there is a change in free carrier wavevector in the emission process so that measurements of the quantum efficiency should enable conclusions to be reached regarding the scattering mechanisms for hot carriers. Figielski and Torun[15] first postulated the model of bremsstrahlen emission from hot free carriers within a single valley and were able to give a correct quantitative calculation of the efficiency obtained in one of the papers for Si p - n junctions[6], although certain quantities required in the calculation were estimated by rather indirect means. When the same theory was applied by Pilkuhn[10] in an attempt to explain his measurements on GaP it was found that the observed quantum efficiency exceeded the predicted value by a factor of 10^3.

The spectra observed for ZnSe show some structure which gives an indication that part of the emission may be due to inter-valley transitions. An important reason for pursuing the research was that from this spectral

structure it was hoped to gain information on the band structure of ZnSe and also on the occupancy of higher valleys under the influence of strong electric fields. With the exception of Ge[9], structure was not detected in the other materials referred to, but this lack of observed structure may be due to a restricted range of spectral measurements.

The present work was carried out using diodes of the metal to n - ZnSe form for two reasons. Firstly, p - n junction diodes cannot be readily made since ZnSe is difficult to prepare with p - type conductivity and, secondly, the basic simplicity of Schottky diodes facilitates the analysis of results. The range of experiments covered in this work is greater than in any of the papers 6-14 as is also the depth of treatment of the results. Both single-valley bremsstrahlung of hot free carriers and inter-valley transitions have been considered, each combined with several different types of interaction between carriers and lattice imperfections.

3.2 EXPERIMENTAL RESULTS

Schottky barrier diodes on n-type ZnSe were prepared as described in chapter 2. Nearly all diodes were prepared with Au as the metal of the rectifying contact. However, a few diodes were prepared with Al forming the rectifying contact so that tests could be made of any possible dependence of the optical behaviour on the nature of the barrier metal. The following measurements were made: reverse current and associated relative light emission as a function of bias voltage, the spectrum shape, the absolute efficiency of emission and the response time of the light emission for step changes in the applied voltage. Measurements were also made of the differential diode capacitance as a function of bias voltage for reasons discussed in section 2.3.

3.2.1. Capacitance-voltage characteristics.

The differential capacitance, C, of the diodes was measured as a function of applied bias, V, by the method described in the preceding

chapter. The bias range was determined by the requirement of a sufficiently small loss to enable satisfactory capacitance measurements to be obtained. The bias range was typically from about 0.7 volts forward bias (ie Au or Al positive with respect to the ZnSe) to 10 volts reverse bias. As expected for Schottky barriers, plots of C^{-2} against V were found to be linear.

For many of the diodes tested the slope of such a plot was independent of signal frequency over the range 300Hz to 100 kHz which was the frequency range in which measurements were normally made. Some diodes, however, exhibited a slope dC^{-2}/dV which was higher at 300Hz than at 100kHz by a factor as large as three. These diodes showed a constant slope at low frequencies and a larger constant slope at high frequencies, with the greatest rate of change of slope occurring at about 10kHz. A check on one such diode ensured that dC^{-2}/dV does not change further between 100kHz and 1.6MHz.

In the plots of C^{-2} against V the intercept on the voltage axis was, for 85% of the diodes in a sample of 30 Au - contact diodes, in the range of 2.0 volts to 3.0 volts. A typical C^{-2} against V plot for a diode exhibiting frequency-independent slope is shown in fig. 3.1.

The range of donor concentrations as determined from the slopes of capacitance plots was $2 \times 10^{21} m^{-3}$ to $6 \times 10^{25} m^{-3}$ but most diodes were within an order of magnitude of the donor concentration $2 \times 10^{22} m^{-3}$.

Cooling of a diode to $77^{\circ}K$ reduced the donor concentration (as deduced from 100kHz C-V data) by about 30% below its room temperature value. This effect is attributed to carrier freeze-out.

3.2.2. Current-voltage characteristics

The reverse bias current-voltage characteristics were always 'soft'. It was found that the logarithm of the current varied linearly with applied reverse voltage for a typical current range (at room temperature) of 10^{-6} to 10^{-2} amp. Departures from linearity outside this range are considered to be due to leakage at small currents and to the bulk series resistance of the ZnSe chip at high currents. In a family of ln i against V curves drawn for different

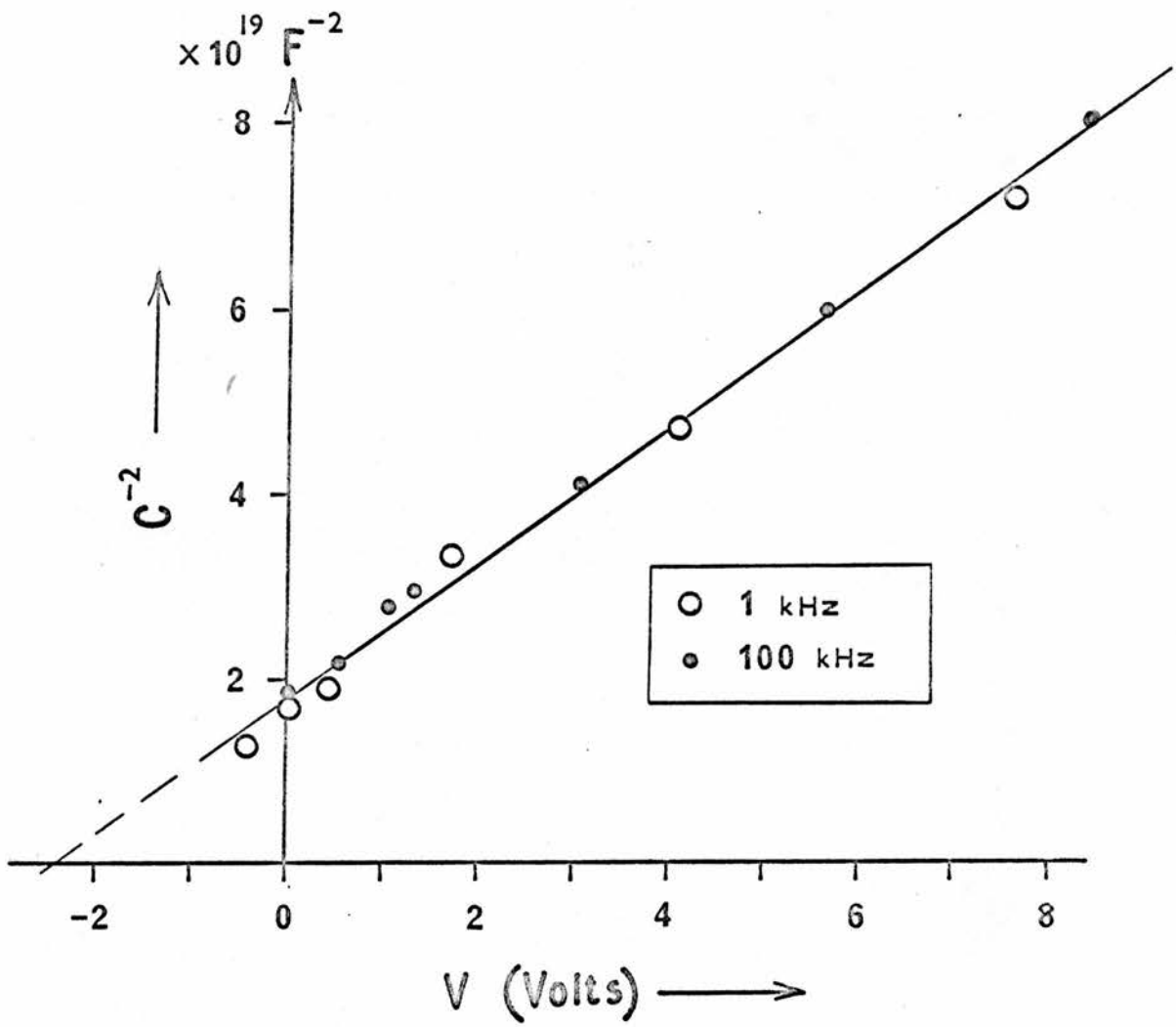

Fig. 3.1 C^{-2} vs. V plot for a Au-contact diode exhititing frequency independent capacitance. The measurements were made with the diode at room temperature.

temperatures of a given diode each curve exhibits a straight portion corresponding to several orders of magnitude of variation of the current and these straight portions are parallel to one another. This is shown for two temperatures in fig. 3.2. In another diode, which also exhibited good linearity in a semi-logarithmic plot of current against voltage for fixed temperature, measurements were made of the variation of the voltage at constant current when the temperature was changed. The results are given in fig. 3.3 in which it can be seen that between 100K and 340K the voltage at the fixed current increases linearly with temperature and, from the slope, $\partial V/\partial T\big|_i$ is determined as 1.8×10^{-2} volts K^{-1}. From the two lines of Fig. 3.2 the corresponding mean value of this derivative is 2.0×10^{-2} volts K^{-1}. In fact $\partial V/\partial T\big|_i$ was close to 2×10^{-2} volts K^{-1} for all diodes in which the temperature dependence of the voltage for fixed current was measured.

Usually, cooling a diode increases the range of exponential variation of current with voltage down to smaller currents, thus showing that the extent of shunt leakage is reduced by cooling. This is consistent with an observation that at fixed reverse bias the lossiness of the diodes, as determined in the capacitance measurements, is much reduced by cooling from room temperature to $77^{\circ}K$, even though the true junction current is known to increase on cooling with a fixed applied voltage.

Fig 3.4 shows the dependence of voltage on donor density for a fixed reverse-bias current density ($2mA/mm^2$) in many Au-contact diodes. The contact area was not the same for all diodes, hence the reason for reducing the results to a fixed current density rather than a fixed current. Although the scatter is large there is a trend for the voltage at constant current density to fall as the donor density increases from $10^{21} m^{-3}$ to $10^{24} m^{-3}$. For higher donor densities the voltage appears to rise with increasing donor density but this latter impression is of doubtful authenticity in view of its reliance on a single point of the graph.

In many papers in which observations of reverse bias light emission

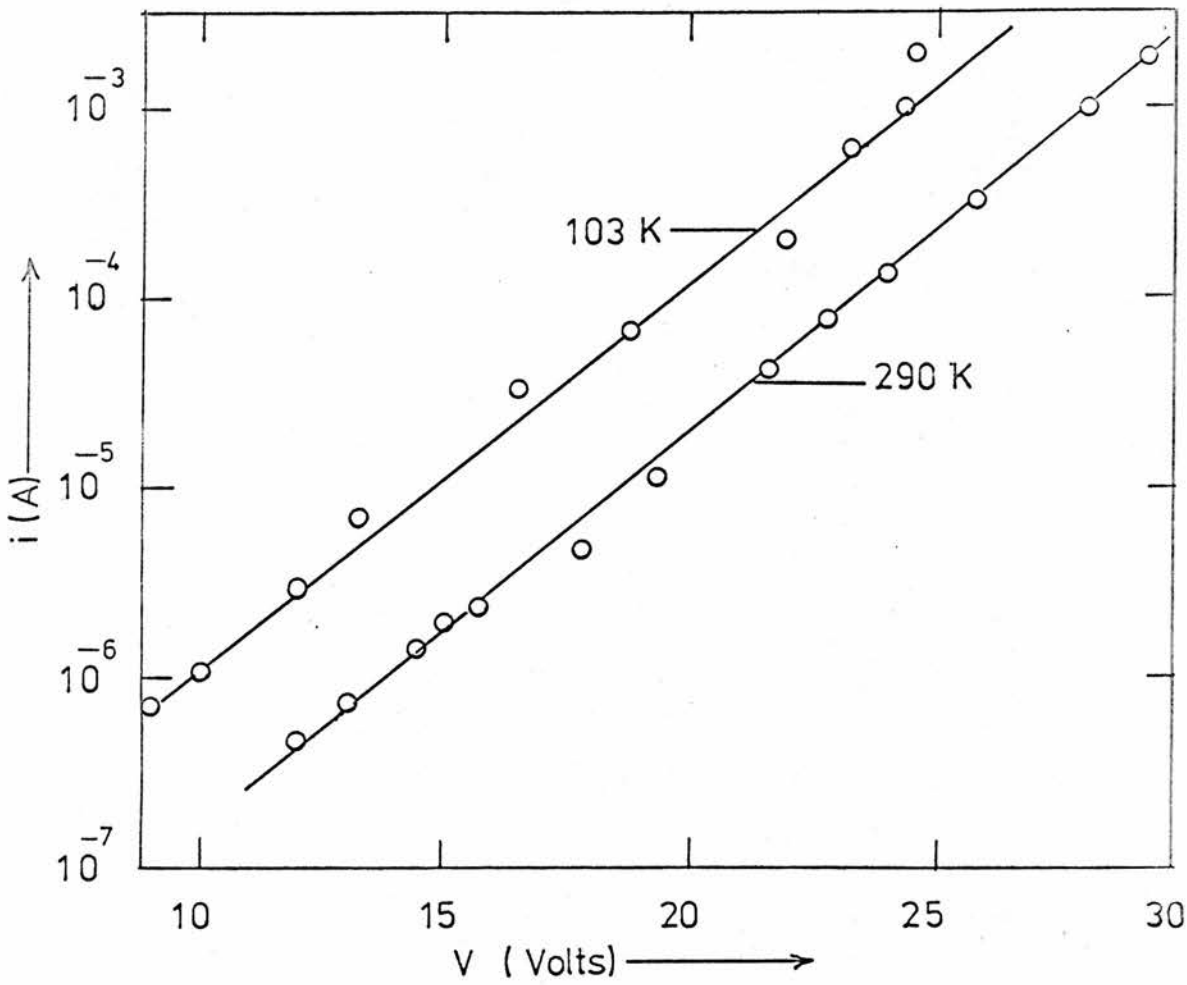

Fig. 3.2 Current-voltage characteristics for a diode at two temperatures.

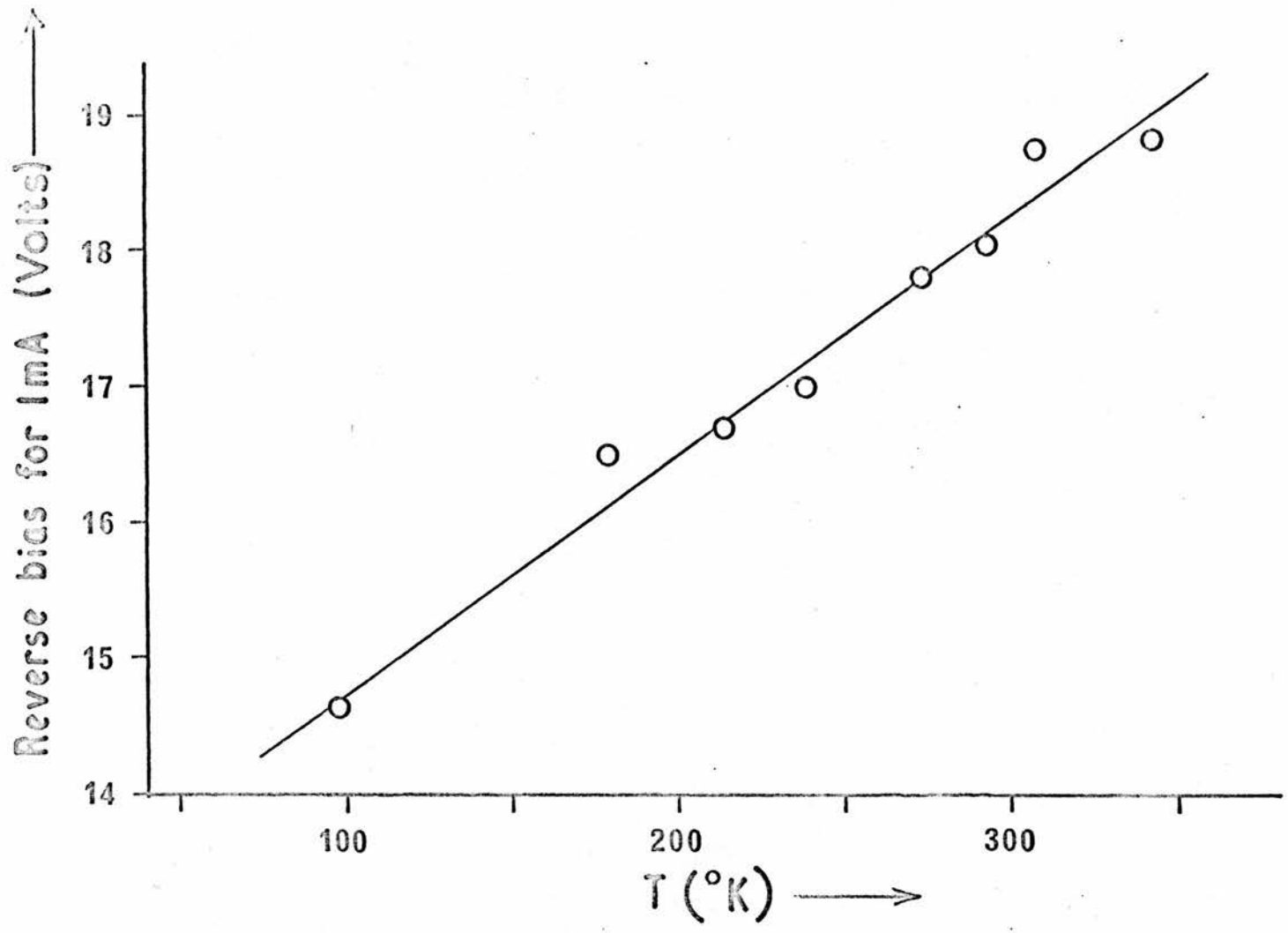

Fig. 3.3 Temperature dependence of the applied bias for a current of 1 mA in a typical diode.

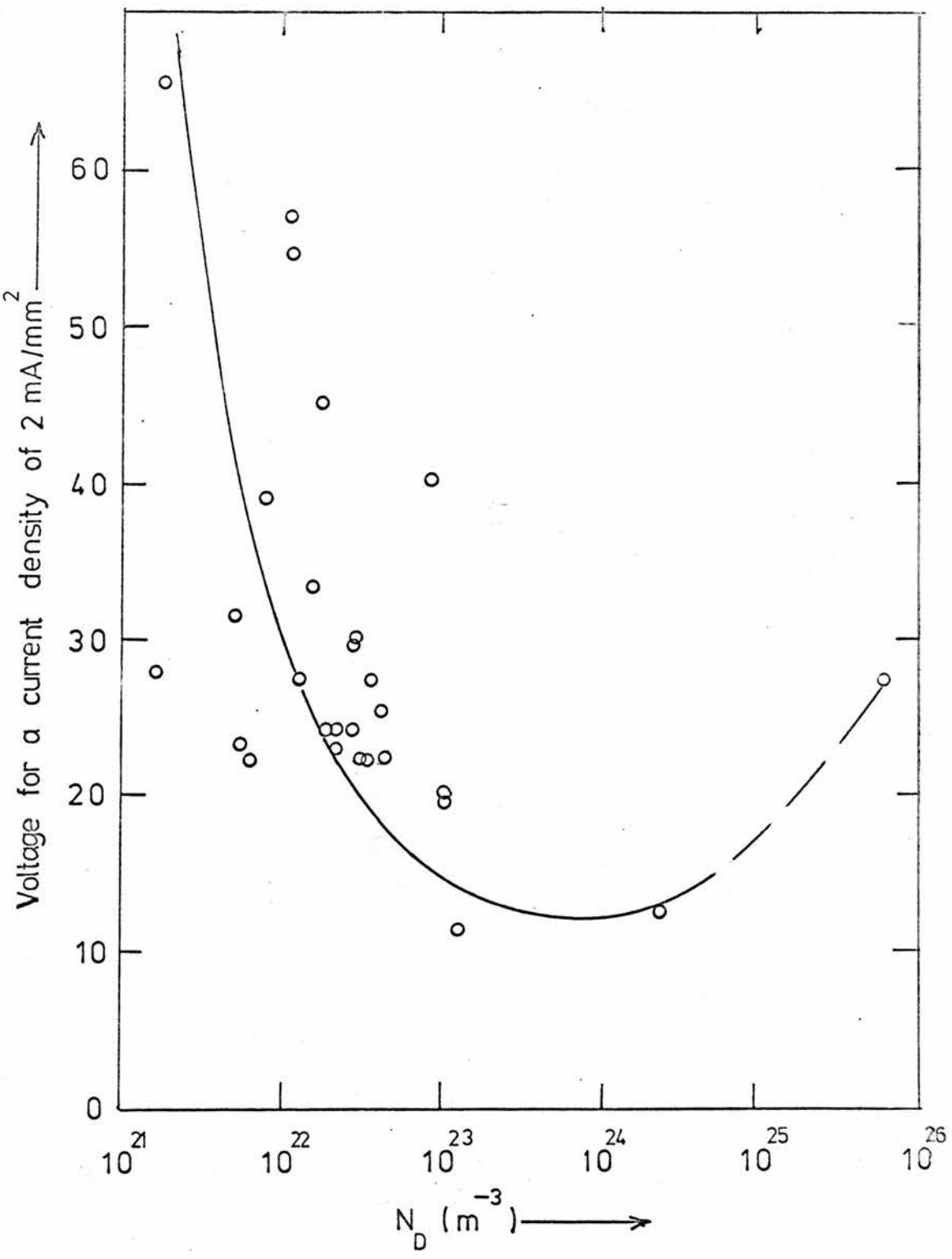

Fig. 3.4 Voltage for a fixed current density of $2mA/mm^2$ as a function of donor concentration (N_D) in diodes at room temperature.

have been reported the occurrence of microplasmas, shown by a spotty pattern of bright points across the diode junction plane, have been noted. There is no clear evidence for a similar behaviour in the ZnSe diodes discussed in this chapter but some bright spots have been seen around the periphery of the rectifying barrier.

In a later chapter results for the electrical and optical properties of ZnSe Schottky diodes in forward bias are presented and discussed but it is of interest to mention briefly a result here concerning the forward bias current-voltage characteristics, for purposes of comparison with reverse bias. In forward bias a parallel family of straight lines is obtained, for a given diode, when the logarithm of the current is plotted against the applied voltage, with temperature as a parameter. However, unlike reverse bias, the current increases as the temperature is raised. The slope, $\partial \ln i / \partial V \big|_T$, is widely different for the two polarities eg. in a typical diode this derivative for forward bias was greater than for reverse bias by a factor of 4.5.

3.2.3. Dependence of relative photon emission on reverse voltage and current

The relative light emission (L), taken as proportional to the output of an S20 response photomultiplier, was measured for diodes in reverse bias, as a function of diode current (i) and voltage (V). The experimental procedure was discussed in section 2.6. Semilogarithmic plots of L against V were linear over the entire range of measurements and these extended over several decades of L. Fig. 3.5(a) shows the variation of L with V for a diode at room temperature. For reference the corresponding variation of i with V in the same diode is also included in the figure. Fig. 3.5(b) shows similar results for a different diode. From the former figure it is seen that the exponential dependence of L on V holds over a range as large as eight orders of magnitude of L. The lowest light level displayed in the data of the figures is close to the limit of sensitivity of the apparatus used, so that as far as can be ascertained there is no threshold voltage for light emission. It is a consistent result that in plots similar to those of figs 3.5(a) and (b) the

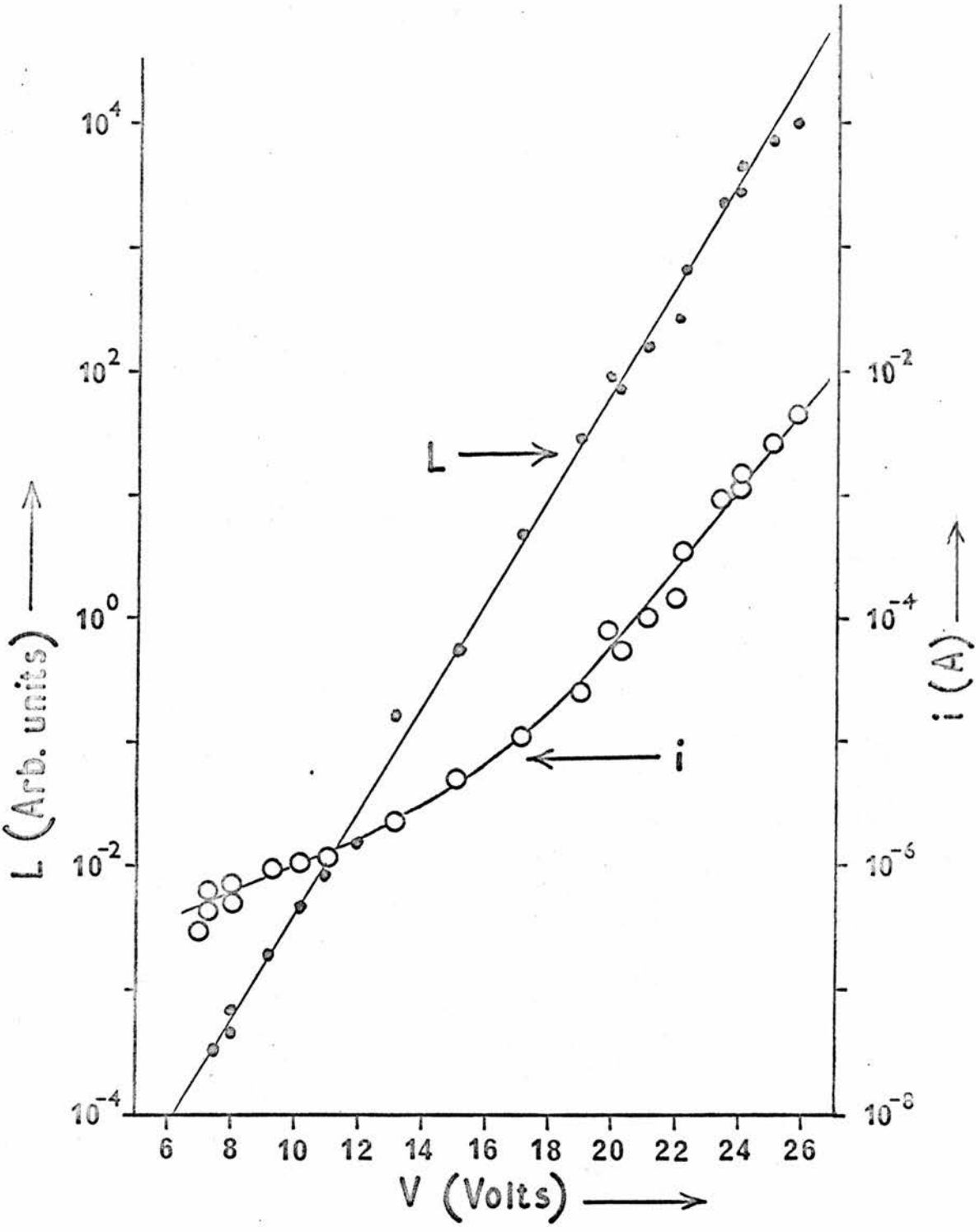

Fig. 3.5(a) Current and relative light emission as functions of applied reverse bias for a diode at room temperature.

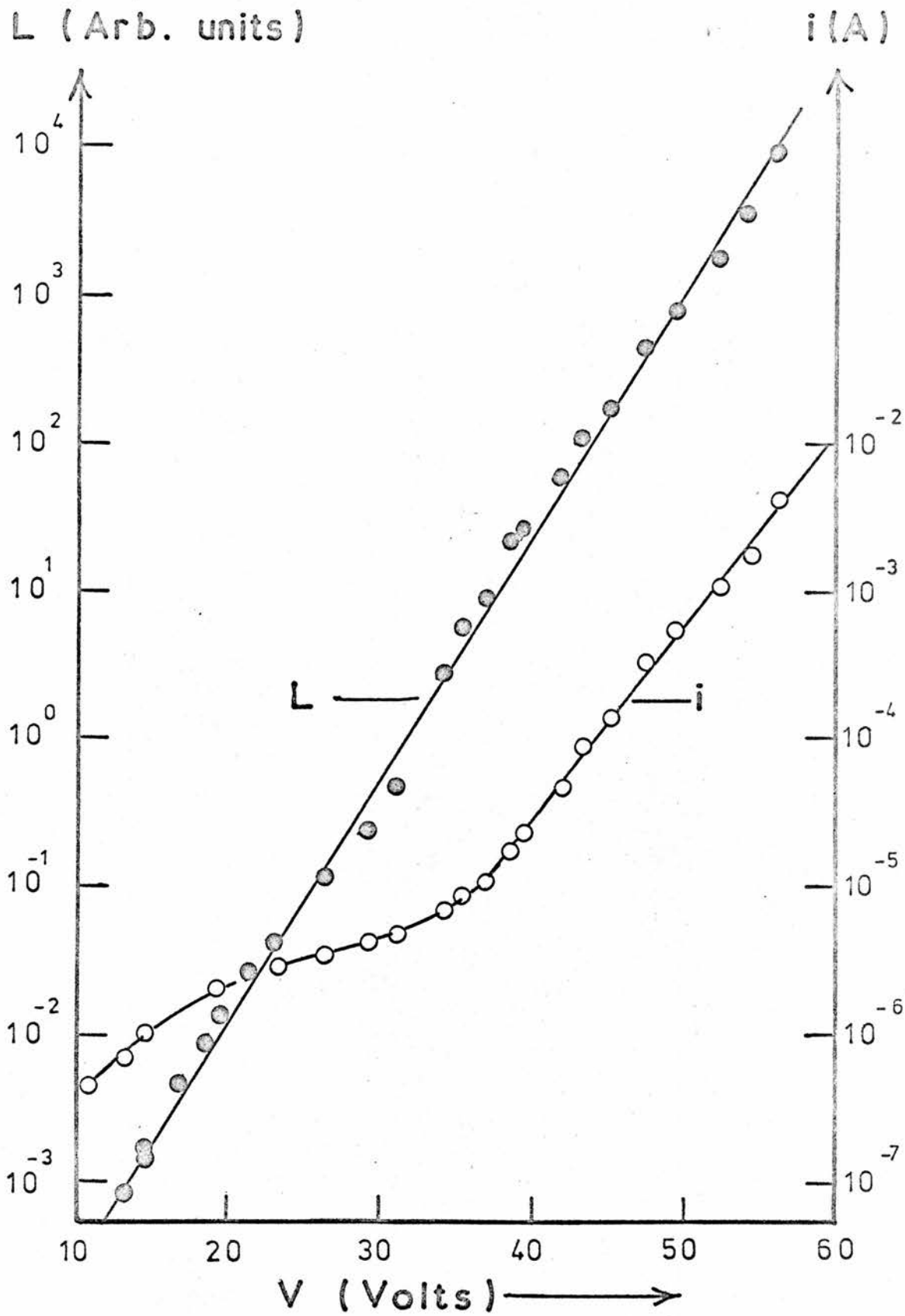

Fig. 3.5(b) Similar plots to those of fig. 3.5(a) obtained for a different diode also at room temperature.

line representing the light variation is steeper than that for the current variation in the same diode. Usually there is only a few percent difference between the two slopes for diodes of high working voltage ($V > 35V$ for 1mA) and a larger difference for low voltage diodes, although this difference does not exceed 35%. It follows that the relationship between light and current can be written in the form $L \propto i^n$ with n constant for a particular diode and $1.0 < n < 1.35$. In fig. 3.5(a) n is 1.29 but the power law dependence of light on current is valid up to much higher currents than those shown in the figure. This is demonstrated in fig 3.6 in which the light, measured as a function of current for pulse currents in the range 1mA to 110mA, is shown to be well described by the law $L \propto i^{1.2}$. The diode of fig. 3.6 is the same as that of fig. 3.5(a) hence n is nearly constant for four decades of variation of the current. Fig. 3.7 shows that plots of ln.L against V for a given diode at different temperatures are accurately parallel to each other. There is an increased emission at a given voltage on cooling below room temperature and, as may be inferred from section 3.2.2, also an increase in current. The light emission, however, increases by a larger factor than the current so that cooling from room temperature increases the quantum efficiency.

Examination of diodes showed that the light is generated at the rectifying contact.

3.2.4. Shape of emission spectra

Fig. 3.8 shows spectra of two diodes, measured at room temperature, using a Zeiss SPM 2 monochromator fitted with an S1 response photomultiplier as the detector and a glass G60 prism as the dispersive element. The spectra have been corrected for measuring system response and for absorption in the diode chip. The two spectra have been normalized to the same height at 1.99eV, and both spectra were measured at a diode current of about 1.5mA. The ratio of donor concentration for the two diodes from which the data of fig. 3.8 were obtained is 650:1 so it may be concluded that the spectrum is independent of donor concentration. Results have also been obtained which show that the

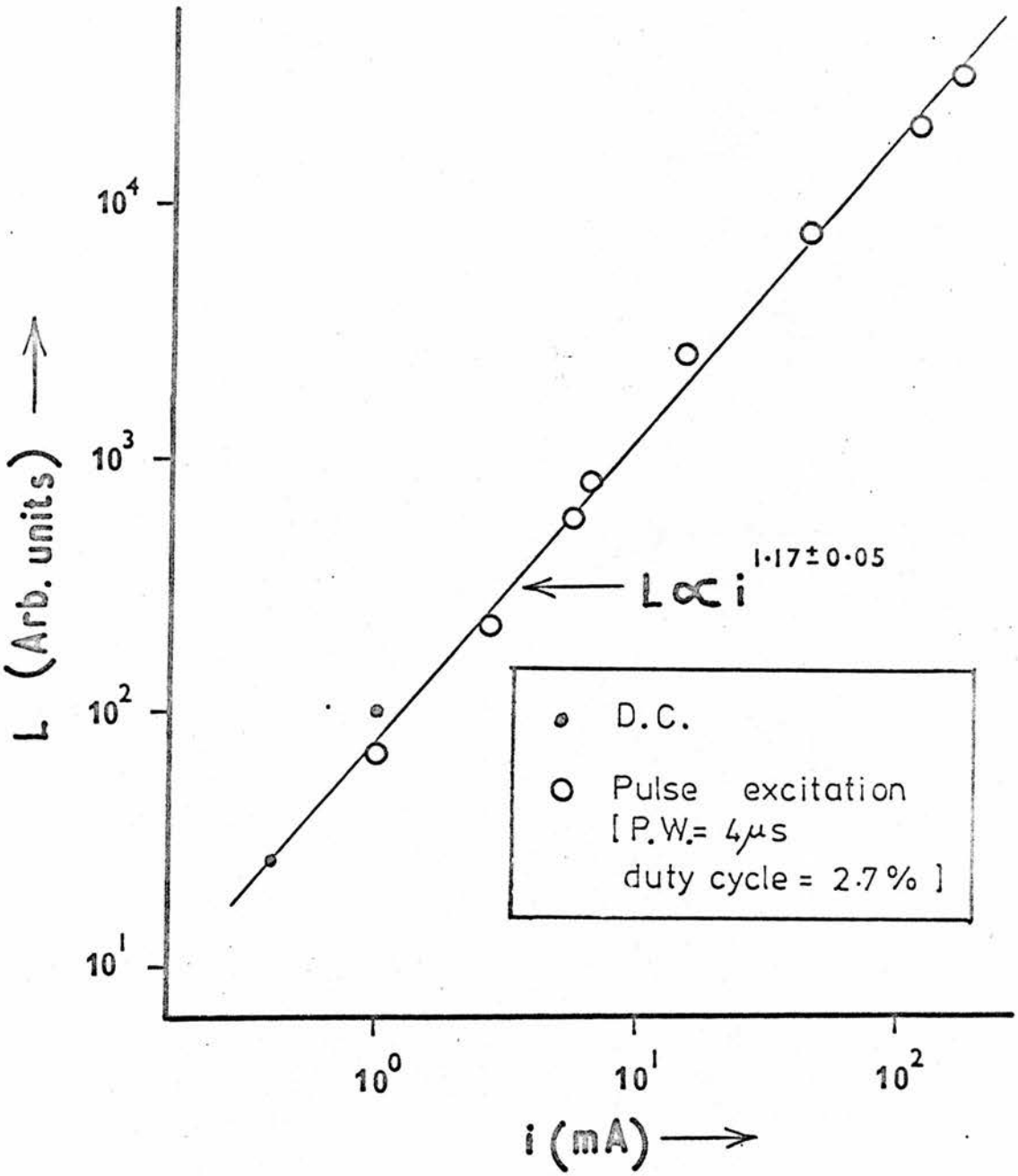

Fig. 3.6 Relative light emission, as detected by an S20 response photomultiplier, for a diode at room temperature.

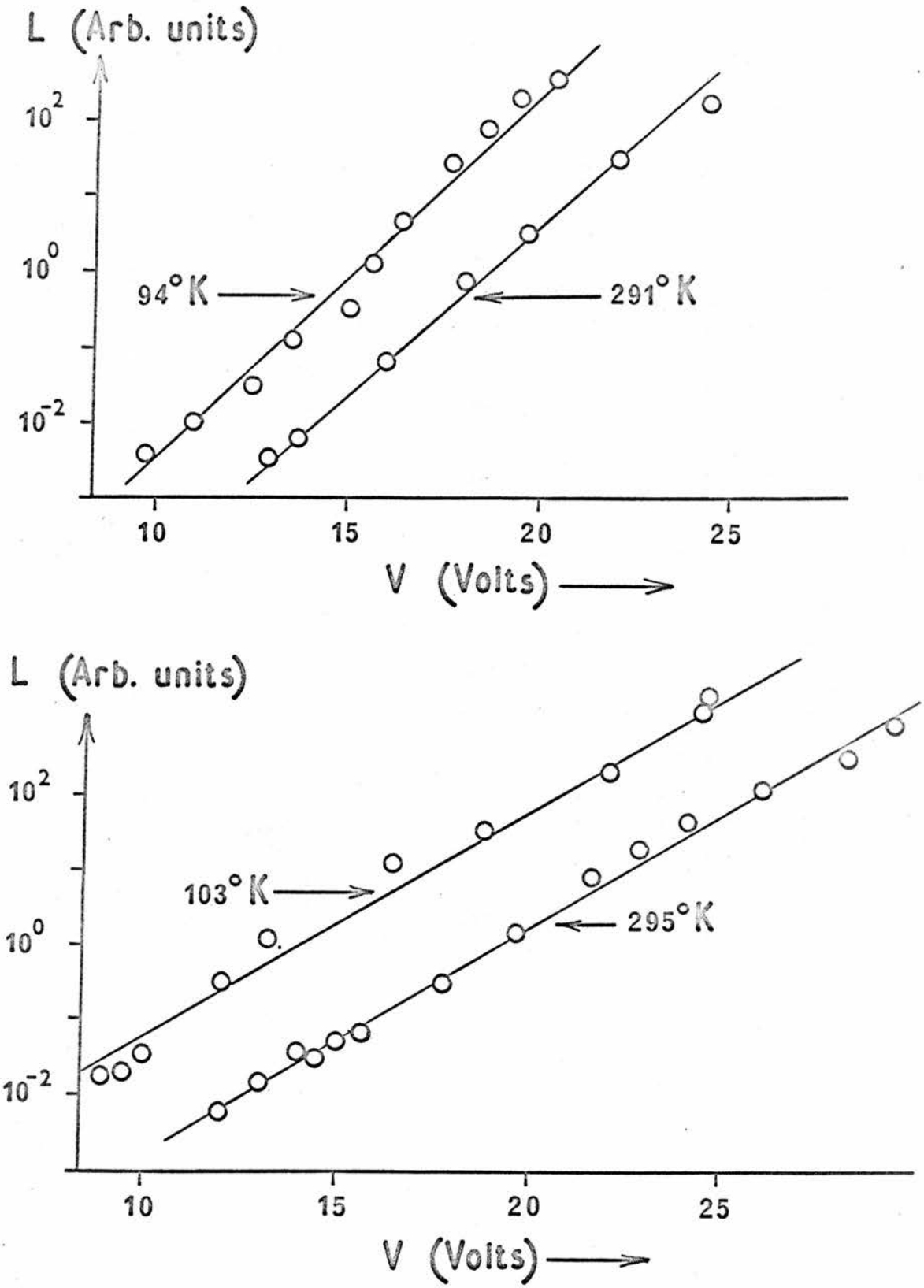

Fig. 3.7 Light vs. voltage characteristics, with temperature as a parameter, for two typical diodes.

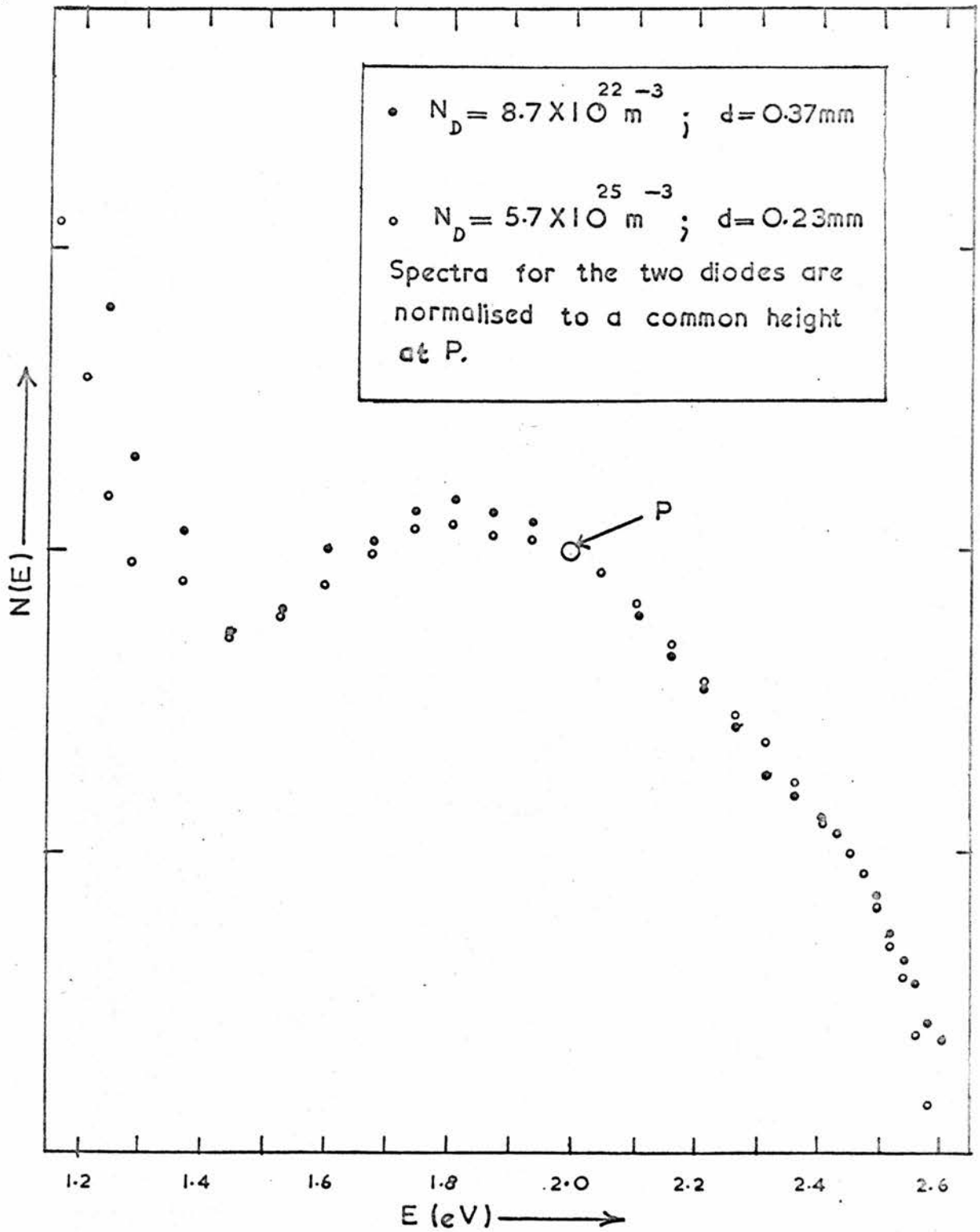

Fig. 3.8 Spectra for two diodes at room temperature. The detector was a cooled S1 respose photo-multiplier. Absorption corrections have been applied; d = light path length through ZnSe.

spectrum, at least for the photon energy range of fig 3.8 is also independent of diode current if the temperature is constant. In this connection spectra were measured for diode currents as high as 150mA by operating diodes under pulse conditions with a pulse width of about 3μs and a 0.5% duty cycle. From the results obtained in this way, together with D.C. measurements at small currents, it has been shown that the most energetic photons in the spectrum have an energy constant to within 0.02eV for the diode current range 100μA to 150mA.

Spectra of diodes made from different ingots of ZnSe have the same shape and this shape is identical whether Au or Al forms the rectifying contact. These results respectively suggest that the observed spectra are not determined by chance impurities or by the choice of contact metal.

A spectrum, measured with emphasis on the lower energy range, for diodes at room temperature, is shown in fig.3.9. This spectrum was obtained using a Zeiss SPM.2 monochromotor fitted with a LiF prism, and with a cooled Mullard 62SV PbS cell as the detector. The spectrum was obtained from the mean of a total of eight spectral scans on three different diodes (these diodes were all in the donor density range of $5 \times 10^{21} m^{-3}$ - $3 \times 10^{22} m^{-3}$). The current was steady at about 25mA for each measurement and diode heating was avoided by means of an air blast directed at the diode. The spectrum shown in fig. 3.9 has been corrected for the measuring system response and for absorption within the diode chips, although the latter correction was small compared with the uncertainties in the intensity measurements. The significance of the fact that absorption has been considered is that the steep fall at the low energy end of the spectrum is real and is not an artifact produced by free carrier absorption of light.

A spectrum, obtained using an S20 response photomultiplier, is shown in fig. 3.10 for a diode at 125K. In drawing this figure corrections have been applied for the measuring system response but not for the absorption of light in the ZnSe chip. The light path length through ZnSe for the spectrum of the figure was 0.34mm but, for a different diode in which the thickness of ZnSe traversed by the emergent light was nearly twice as great, the same

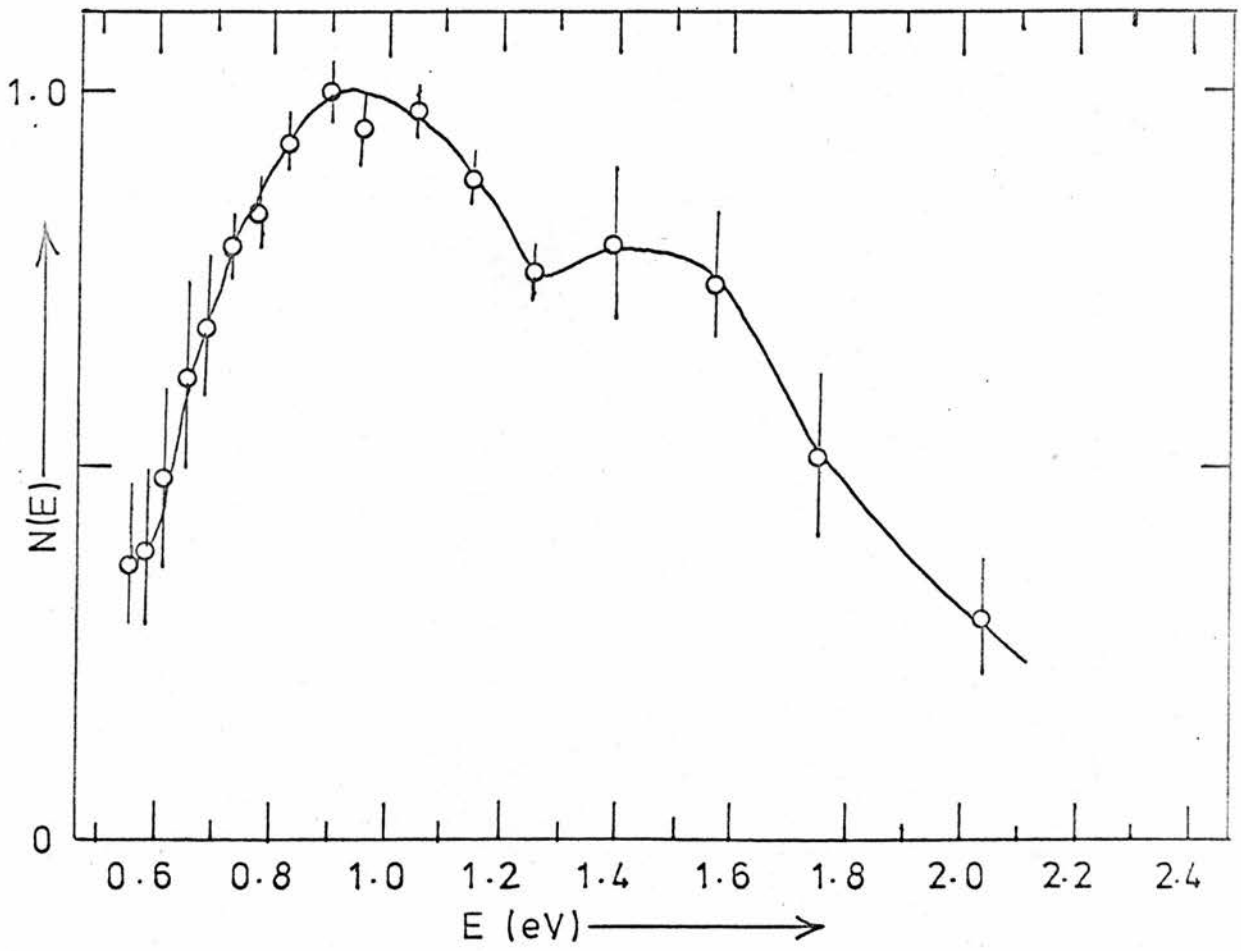

Fig. 3.9 Spectrum for diodes at room temperature. The detector used was a cooled PbS cell. The points are plotted from the mean of a total of 8 spectral scans on 3 diodes. Error bars indicate the degree of reproducibility. Absorption corrections have been applied.

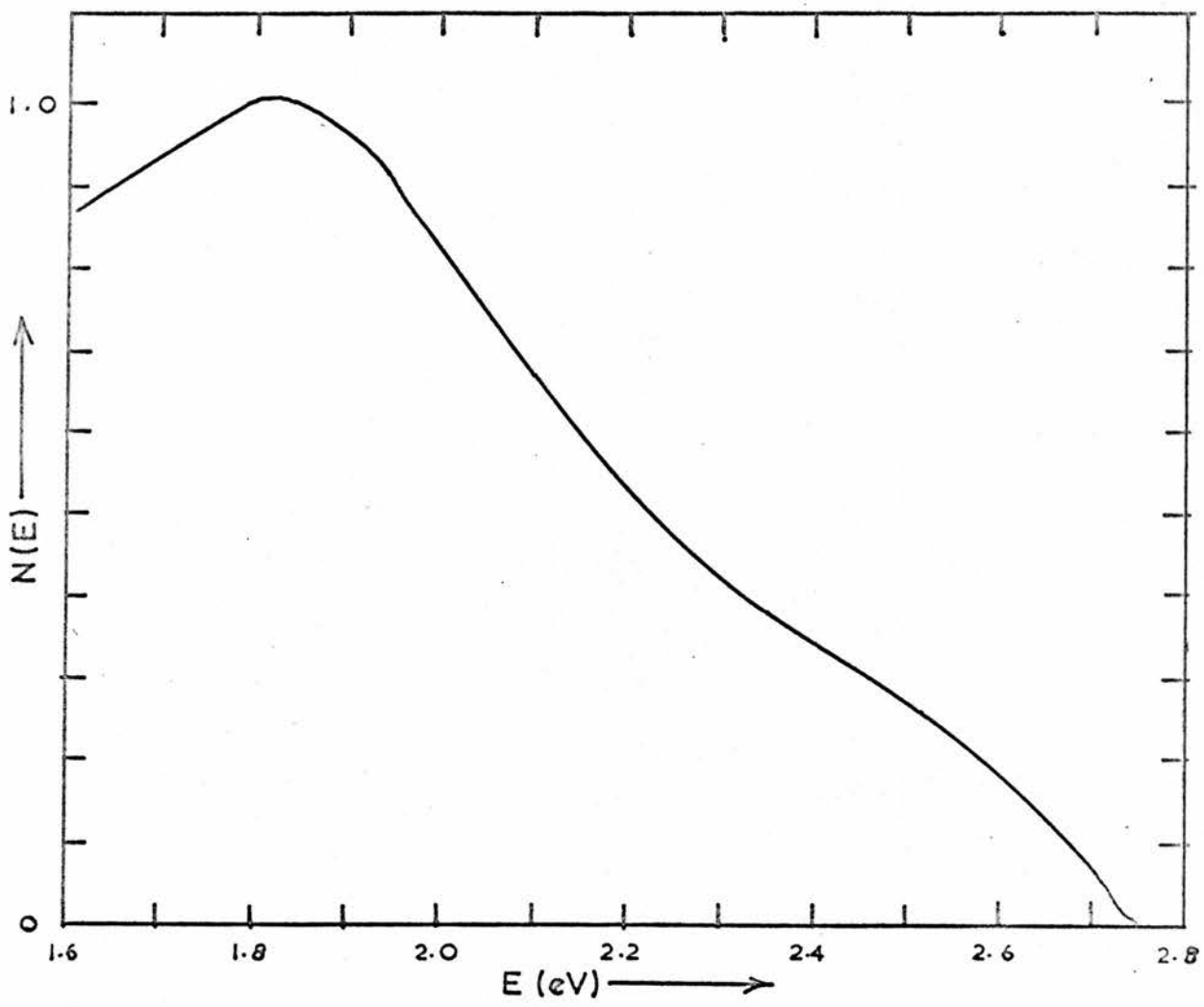

Fig. 3.10 Spectrum of a diode at 125 K. An S20 response photomultiplier was used as the detector. No correction has been applied for light absorption within the diode chip. The path length of the light through ZnSe was 0.34 mm.

high energy photon limit was found in the externally observed spectrum. This limit, which is evidently not changed by applying an absorption correction, is 2.74eV. For diodes at room temperature the most energetic photons in the spectrum have an energy of 2.65eV and this value was determined for spectra which were corrected for absorption.

Results for spectrum measurements, made with the same apparatus as used in obtaining the data for fig. 3.9, are shown in fig. 3.11 for three diodes at approximately 120K. Each curve in fig. 3.11 refers to a different diode and is drawn from the mean spectrum obtained in at least three spectral scans. It is observed, by reference to fig. 3.11 that, although the general reproducibility of the spectra is poor, there is consistency for the photon energies corresponding to each spectral maximum and minimum.

3.2.5 Light output at constant current as a function of temperature.

The temperature dependence of the reverse bias emission for a diode at a constant current of 1mA is shown in fig. 3.12. The light output was measured by collecting emission from the diode directly on to the photocathode of an S20 response photomultiplier. The output of this photomultiplier was taken as a direct measure of the diode emission and the results shown in fig. 3.12 were accurately reproduced in several experiments for the same diode. Referring to the figure it is seen that as the temperature is varied this diode exhibits a minimum quantum efficiency in the vicinity of 280K. All other diodes for which the necessary measurements were made exhibited a variation similar to that shown in fig. 3.12 and the temperature corresponding to the minimum quantum efficiency was apparently independent of donor concentration. Curves similar to fig.3.12 have been obtained both for

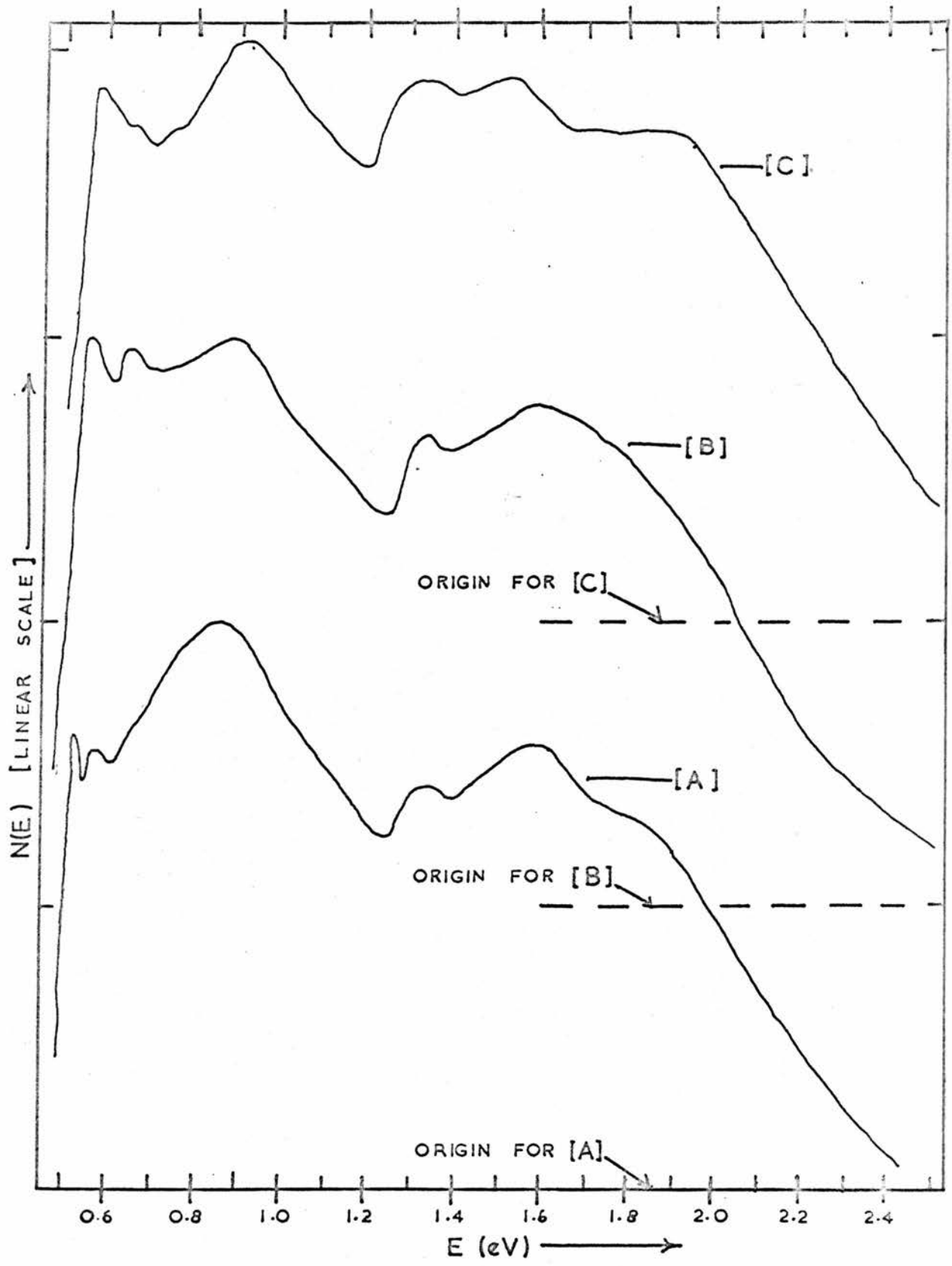

Fig. 3.11 Spectra for diodes at 123 K. The detector was a cooled PbS cell. Each curve refers to a different diode and was drawn from the results of at least 3 spectral scans. No absorption correction has been applied.

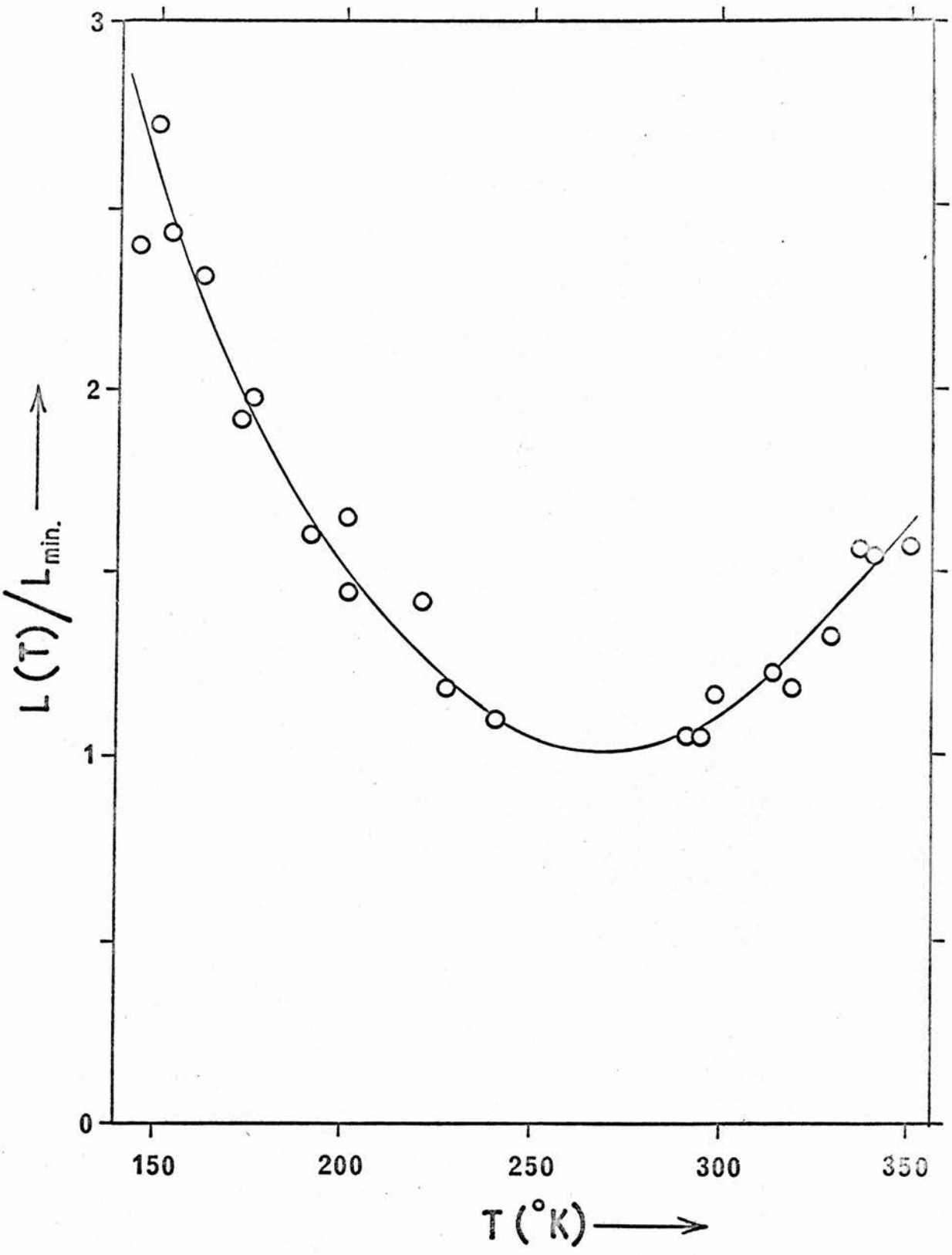

Fig. 3.12 Temperature dependence of light emission at constant current (1mA) for a typical diode.

diodes exhibiting frequency dependence and frequency independence in C^{-2}vs.V plots.

It was seen in section 3.2.2 that cooling of a diode causes the voltage at fixed current to fall. Hence, for temperatures below 270K, the rise in light output at constant current on cooling is associated with a reduction of the bias voltage.

In the last section it was shown that the high energy limit of the spectrum shifts to a slightly higher energy on cooling of the diode. This, of itself, would produce an increased signal from the photomultiplier but very much less than the change shown in fig. 3.12. In fact a variation indistinguishable from that in the figure has been obtained with a spectrometer between the source and detector to select a photon energy well below the high-energy cut-off.

3.2.6. Light emission rise and fall times

Diodes, made with Au contacts of small diameter (0.4mm) to minimize junction capacitance, have been tested for the rise and fall times of their light emission under pulsed current operation. The light was received by an R.C.A. IP28 photomultiplier and the signal from this device fed to a Tektronix 561A sampling oscilloscope. The light rise - time (10% - 90%) in the diodes testedwas determined, from the oscilloscope traces, to be 5.4ns with a corresponding light fall-time (90% - 10%) of 5.7ns. The current rise and fall times were respectively 3.3ns and 4.0ns , and these are not much greater than the RC time-constant of the diode circuit. The diode pulse current was about 10mA. In subsequent tests, pulses of various widths up to 2 msecs were applied in order to check whether the initial fast rise of the light is followed by a much slower component. No such slow component was observed, nor was any slow component present in the light decay.

The as - measured light rise and fall times quoted above are to be regarded as upper bounds of the true light response times because of the experimental time-resolution limits.

3.2.7. External quantum efficiency as a function of diode donor density.

The donor concentration (N_D) deduced from capacitance measurements and the absolute external quantum efficiency(η) for a diode current of 1mA, measured at room temperature as described in chapter 2 were obtained for thirty ZnSe diodes, each having a Au rectifying contact. It is expected that the quantum efficiency be proportional to the depletion width (W), and, since W is a function of N_D, the results are presented as a graph of(η/W) against N_D to exhibit any other dependence on N_D. This graph is shown in fig. 3.13. The width, W, used in evaluating η/W, is the width corresponding to the conditions under which η was measured and was obtained from the capacitance measurements by an extrapolation of the C^{-2} against V plots. There is a wide scatter in the results of fig. 3.13 as might be expected in view of a likely variation of about a factor of two in the reproducibility of both η and W, but over the range $10^{22} m^{-3} < N_D < 4 \times 10^{25} m^{-3}$ the relationship $(\eta/W) \propto N_D^{0.6}$ fits the results. For $N_D < 10^{22} m^{-3}$ it appears that (η/W) is independent of N_D but unfortunately the number of diodes in this range is too small, and their donor density insufficiently below $10^{22} m^{-3}$, to state this result more definitely. For an ideal Schottky barrier $W \propto \left[(V + \phi)/N_D\right]^{\frac{1}{2}}$ where $e\phi$ is the electron barrier height. Since V is only very weakly dependent on N_D the relationship $(\eta/W) \propto N_D^{0.6}$ effectively means that η is almost independent of N_D.

The range of observed quantum efficiency for diodes at room temperature and for a current of 1mA was from 1.8×10^{-5} to 1.4×10^{-4}. The quantum efficiency discussed in this section refers to the integrated emission for the entire spectrum.

3.3 DISCUSSION OF ELECTRICAL PROPERTIES

3.3.1 Diode capacitance and related quantities

The apparent barrier height, ϕ, expressed as a voltage and obtained from the intercept of plots of C^{-2} against applied bias V, is, for most Au contact diodes, in the range 2.0 volts to 3.0 volts. The lowest apparent barrier voltage

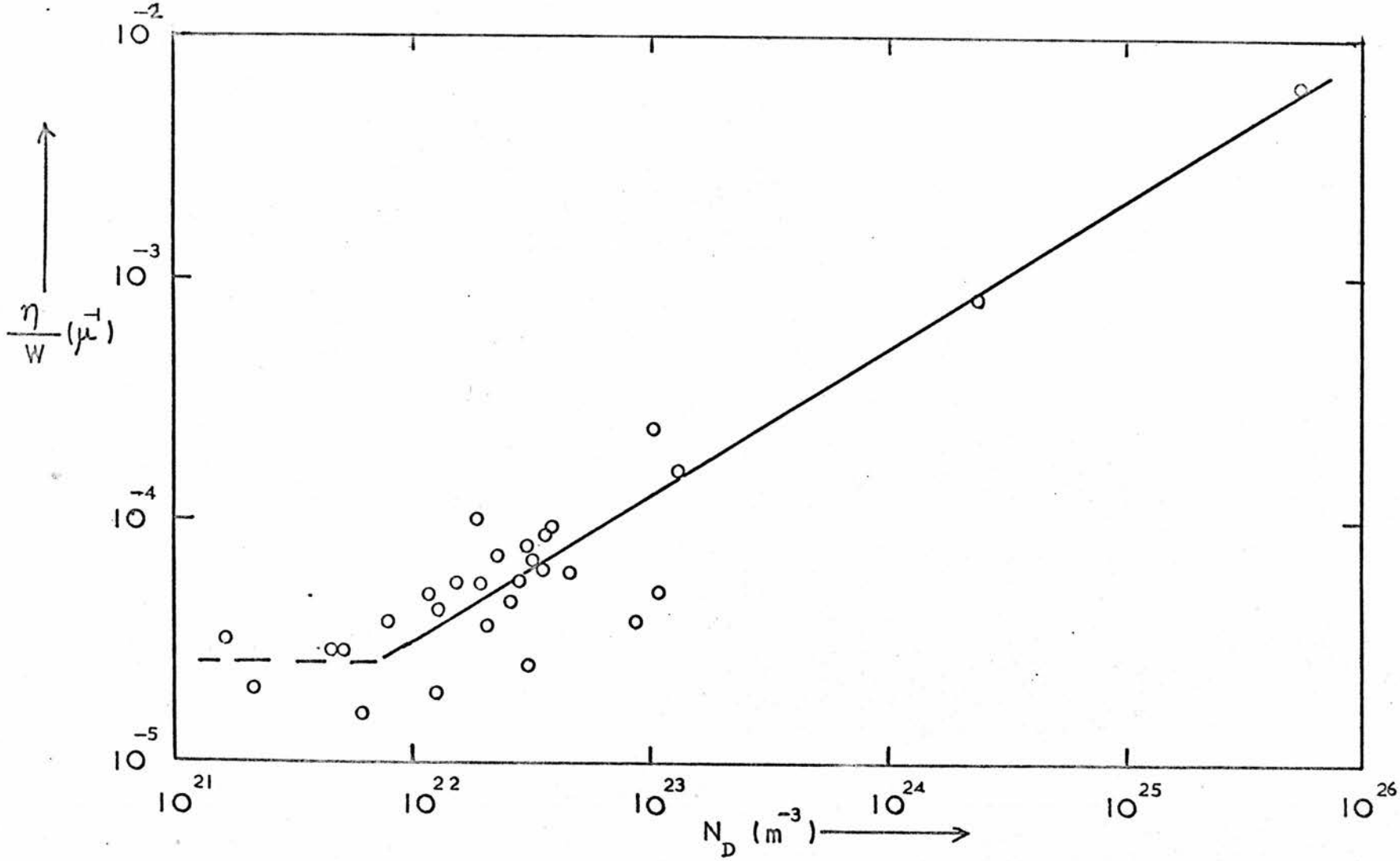

Fig. 3.13 Quantum efficiency per unit depletion width, $\frac{\eta}{W}$, plotted as a function of donor concentration, N_D. The photon

determined in this way is 1.85 volts and the highest is 4.5 volts. This is a wide spread and even the lowest result is considerably higher than the barrier voltage of a Au to ZnSe contact obtained by other workers. Mead[16] found the barrier height of Au - vacuum cleaved ZnSe surfaces to be 1.40eV from measurements of the photoresponse of the junction. The barrier height of a Au - etched 110 ZnSe surface has been determined as 1.53eV by Swank, Aven and Devine[17], who obtained this result as the mean barrier height from the current-voltage characteristics, the intercept on a C^{-2} against V plot and from the photoresponse as a function of photon energy. Employing the same methods these authors obtained a barrier height of 1.48eV for a Au - vacuum cleaved 110 ZnSe surface. Simple considerations show that in an ideal Schottky diode the barrier height cannot exceed the fundamental forbidden gap of the semiconductor since this simultaneously involves a high hole density with a high electric field and such a situation is not possible without current flow. The fundamental forbidden gap of ZnSe is 2.7eV hence some of the diodes which were made in the present work do not approximate ideality. As already noted in section 2.3 it has been shown by Goodman[1] that an anomalously high apparent barrier height is obtained from the intercept on the voltage axis in a C^{-2} against V plot if there is an insulating layer between the semiconductor surface and the metal contact. Since a major purpose of measuring the diode capacitance was to determine the donor concentration, N_D, it is reiterated that Goodman[1] also showed that if C^{-2} varies linearly with V for a metal-insulator - semiconductor diode then the slope, dC^{-2}/dV, which involves N_D, is given by the same equation (equation 2.1) as for an ideal metal-semiconductor contact.

In some diodes dC^{-2}/dV exhibited a systematic variation with the frequency, f, of the measuring signal, leading to an apparently higher donor density at low frequency compared with that at high frequency. A possible explanation for the observed behaviour of these diodes is that certain deeper lying donors do not become fully ionised in a time of the order f^{-1} at sufficiently high f. A second possibility is that there is additional capacitance contributed by the surface states and which becomes evident when f is less than the frequency

τ_{ss}^{-1}, where τ_{ss} is the time constant associated with surface states. This latter possibility is preferred because some ZnSe diodes exhibit a frequency dispersion of dC^{-2}/dV whilst other diodes, made from the same preparation of ZnSe, show constancy of this derivative over a wide frequency range. The density of surface states is liable to vary between diodes but the energy distribution of bulk donor centres amongst diodes made from a common batch of material is unlikely to vary much. There was a trend for the diodes made towards the end of the experimental period to exhibit no change of dC^{-2}/dV with f which would comply with the idea of surface state effects since techniques were presumably improving. As the surface states charge through a resistive equivalent circuit a large increase in loss would be expected for $f \sim \tau_{ss}^{-1}$. Experimentally, it was found that the reciprocal of the diode quality factor (Q) exhibited a maximum at the frequency corresponding to the maximum rate of change of dC^{-2}/dV with f.

In view of these remarks the donor density and the depletion width were calculated from the results of the highest frequency capacitance measurements.

3.3.2 The current-voltage characteristics

The reverse current in metal to n-type semiconductor diodes is almost entirely due to transport of electrons from the metal to the semiconductor. If the electrons are thermally excited over the contact barrier between the metal and semiconductor, then, neglecting image force corrections, the current density, j, is given by the modified Richardson equation

$$j = A^{*} T^{2} \exp\left(\frac{-e\phi}{kT}\right)\left[\exp\left(\frac{eV}{kT}\right) - 1\right] \quad \ldots.(3.1)$$

where $e\phi$ is the barrier height and A^{*} is a constant of the order of 100 amp cm^{-2} K^{-2}. In this equation j and V are reckoned positive for forward bias. For a contact area of $1mm^{2}$, which is typical of the diodes discussed in this chapter, and for a barrier height of 1.4eV, which is believed correct[16] for Au to ZnSe contacts, the saturation current at 300K, deduced from equation 3.1, is about 3×10^{-19} amps. The reverse currents observed in this work are many orders of magnitude greater than the above theoretical estimate.

According to 3.1, the saturation current density flows for any applied reverse voltage which is large compared with kT/e and, again assuming a barrier height of 1.4eV, there is a predicted decrease in the saturation current by the huge factor of 10^{46} for cooling from 300K to 100K. In total contrast to this, the experimental results, which were always obtained with applied reverse biases much greater than kT/e, show a strong dependence of current on the applied voltage and a weak dependence on the temperature. As may be seen by reference to fig. 3.2, for cooling from 300K to 100K, the current at fixed reverse bias changes by less than one order of magnitude and this small change is actually an increase.

A weak dependence of junction current on temperature and an associated strong dependence on voltage is typical of a tunnel injected current. Since the ZnSe diodes evidently behaved qualitatively in accord with a tunnel-injection model, it was of interest to compare their quantitative behaviour with the predictions of this model.

All tunnel-injection theories for Schottky barriers lead to a relationship between the current, i, and the mean junction field, $\bar{\mathcal{E}}$, of the form

$$i = C\,\bar{\mathcal{E}}^{n} \exp\left(-\frac{B}{\bar{\mathcal{E}}}\right) \qquad \ldots.(3.2)$$

where B and C are constants. In this equation the term $C\,\bar{\mathcal{E}}^{n}$ is the current that would be transported in the limit of a perfectly transparent barrier and the exponential factor is the transmission coefficient of the barrier. The quantity $C\,\bar{\mathcal{E}}^{n}$ depends on the assumptions implicit in any particular tunnelling theory regarding the origin of the tunnel current, e.g. two different sets of assumptions [18,19] lead to respective values of one and two for n. There is, however, consistency amongst different tunnelling theories for the dependence on $\bar{\mathcal{E}}$ of the barrier transmission coefficient term, apart from small numerical differences in the coefficient B.

These small differences are attributable to different mathematical approximations involved in complete formulation of the theories rather than to different physical assumptions. The theories in the previously mentioned references 18 and 19, together with other sources, give for the coefficient $\mathcal{B}$, the equation

$$\mathcal{B} = \frac{2\sqrt{2}}{3} \cdot \frac{m^{*\frac{1}{2}} (e\phi)^{3/2}}{e\hbar} \qquad \ldots\ldots(3.3)$$

The mean field, $\bar{\mathcal{E}}$, across the depletion layer of a biassed diode is proportional to $\left[(V+\phi)^{\frac{1}{2}} \times N_D\right]$, with the constant of proportionality known, hence a plot of $\ln (i/V)$ against $(V+\phi)^{-\frac{1}{2}}$ is expected to be linear and comparison of the slope with the calculated value provides a quantitative test of whether tunnelling occurs. This is a test based only on the barrier transmission term and it is this term which dominates the variation of the current for changes of $\bar{\mathcal{E}}$. The reverse bias current-voltage data for four Au-contact diodes on ZnSe were plotted in the suggested form and for each diode approximately linear plots were obtained. In table 3A the slopes of the plots are compared with those based on equation 3.3. It will be seen from the table that the ratio of calculated to experimental slopes is about 6 if the barrier height is taken as 1.4eV and the ratio is even larger if the barrier height is taken as the intercept obtained in C^{-2}vs. V plots. Whilst an extension of the theory to allow for image force barrier lowering would reduce the absolute value of the calculated slope, reference to a tabulated function[20] giving the correction to be applied for this effect, showed it to be negligible at the electric fields encountered in the experiments. The large quantitative difference between the measured behaviour of the diodes and the predictions of the tunnel injection theory is probably caused by the presence of an insulating film between the Au contact and ZnSe in each diode.

TABLE 3A

(a) Diode No.	(b) ϕ (experiment) volts +	(c) N_D m^{-3}	(d) $\frac{d \ln\left(\frac{i}{V} R\right)}{d(V+\phi)^{-\frac{1}{2}}}$ $volts^{\frac{1}{2}}$ (experiment)	(e) $\frac{d \ln\left(\frac{i}{V} R\right)}{d (V+\phi)^{-\frac{1}{2}}}$ $volts^{\frac{1}{2}}$ (calculated) +	(f) ++	Ratio of theoretical result (column f) to experimental result (column d)
18.9.70A	1.85	5.1×10^{21}	-212	-1710	-1120	7.0
28.12.71E	2.0	1.1×10^{23}	-106	-1260	-739	5.3
24.12.71A	2.4	3.7×10^{22}	-96	-930	-410	4.3
6.4.71C	2.5	1.9×10^{21}	-296	-4040	-1690	5.7

\+ ϕ taken as intercept on voltage axis in C^{-2} vs. V plot.

++ ϕ taken as 1.4V.

R is a constant resistance introduced only so that the arguments of the logarithmic functions in columns (d), (e) and (f) are dimensionless.

It was anticipated that such a film would grossly affect the current-voltage characteristics and, therefore, in the test of the tunnel model, data were used only for diodes in which the voltage intercepts in C^{-2} vs. V plots were least.

It has been assumed in comparing the electrical properties of Schottky diodes with predictions based on the model of electron tunnelling, that impact ionization was negligible. The validity of this assumption was verified by reference to ionization coefficient data[21] for ZnSe.

For a reverse bias V in a Schottky diode formed on an n-type semiconductor the length (W_T) traversed by electrons in tunnelling at constant energy between the metal quasi Fermi level and the semiconductor conduction band is easily shown to be given by

$$W_T^2 = \frac{\varepsilon \phi^2}{2eN_D V} \qquad (V \gg \phi) \qquad \ldots.(3.4)$$

In this equation ε and ϕ are respectively the permittivity of the semiconductor and diode barrier height. Since tunnel current densities are strongly voltage dependent it is easily seen from equation 3.4 that, for constant current density, W_T decreases for an increase of N_D. It then follows that with increasing N_D the voltage for constant current density falls. In fig. 3.4 the voltage for a current density of $2mA/mm^2$ is plotted as a function of N_D from measurements obtained for many ZnSe diodes. It is seen that for $N_D < 3 \times 10^{24} m^{-3}$ the predicted qualitative variation of voltage with N_D is valid. For $N_D > 3 \times 10^{24} m^{-3}$ the curve shown in the figure is not in accord with expectation but, since only a single experimental point was obtained for this range of N_D, the apparent deviation from the expected behaviour may not be genuine.

As a summary to this section it is concluded that the injection of reverse current is certainly not a thermally activated process. The variation of current with voltage and temperature is qualitatively in agreement with the predictions of a tunnelling injection current model. The quantitative deviation from the model is possibly caused by an insulating layer between the metal contact and the semiconductor. Over the reliable part of the range of measurements, the variation of voltage (for fixed current density) as a function of donor concentration is in qualitative accord with tunnelling injection.

Finally, it may be added that in forward bias the diode current is also not injected by a thermal activation process. This follows from the observation that, for forward bias, linear semi-logarithmic plots of current against voltage are found, but with slopes independent of temperature rather than inversely proportional to temperature as would be the case for thermal activation.

3.4. DISCUSSION OF OPTICAL PROPERTIES.

3.4.1. General considerations of the origin of the light emission

In section 3.2.3. it was shown that there is good linearity between the logarithm of the relative light emission and the applied reverse voltage. This is displayed in figs. 3.5(a) and 3.5(b) in which the graphs extend down to the limit of sensitivity for light measurements for the sensitive apparatus used. From the ionization coefficient data for ZnSe given by Livingstone and Allen[21] and referred to in the last section, the current multiplication factor, M, due to impact ionization events, may be computed for various applied biases if the bias-dependent depletion width is first found from C-V measurements or from an extrapolation of these measurements.

In this way, using ionization data for the appropriate donor density, it is discovered that for the diode of fig. 3.5(a), if M is written as $1+\delta$, then $\delta < 10^{-4}$ for 9V bias, $\delta < 10^{-2}$ for 15 V bias and $\delta < 10^{-1}$ at 25V bias. For some diodes, in which there is also good linearity between ln L and V, the value of δ is of the order of unity at the high voltage end of the set of measurements of the L-V characteristics, but in all diodes for which such characteristics were obtained, δ was very much less than unity over the lower part of the voltage range. Thus the results show that there is appreciable light emission at voltages for which $\delta \ll 1$ and that L is a discontinuity-free, smooth and simple function of V across the entire range of δ from values very much less than unity to values greater than or about unity.

From these results it may be deduced that the light is generated when electrons rather than holes undergo transitions. This follows because there is light emission at voltages insufficient to produce appreciable impact ionization and, in this voltage range, the current is conveyed across the depletion layer essentially only by electrons. To explain the emission at low voltages in terms of hole transitions would require the assumption of an improbably high quantum efficiency, expressed as the number of photons radiated per hole transit through the junction. For applied voltages close to the level at which valence band-conduction band impact ionization becomes significant the free hole density is a strongly increasing function of voltage, thus if the light is assumed to be due to hole transitions the emission intensity would be deduced to also exhibit a strong voltage dependence. However, as previously mentioned, the experimental results show that the light intensity for any given diode is a smooth function of the reverse voltage over the entire range of the measurements and there is no evidence of an emission

threshold voltage.

Recombination of free electrons and free holes can be dismissed as a possible mechanism of the light generation for two reasons. Firstly, it involves free holes and is therefore ruled out for the above reasons and, secondly, most of the emitted photons have energy substantially less than the fundamental gap of ZnSe with even the most energetic photons having energy just less than this gap.

A spectrum as broad as that observed in the reverse bias electroluminescence is totally unlike that for electron transitions from the conduction band to centres in the forbidden gap or between centres in the forbidden gap and also if either type of transition does occur then a similar luminescence emission should be observed for ultra-violet excitation. However, the material of which the diodes are made exhibits, for excitation with a focussed beam of light of wavelength 365nm from a powerful (125 watt consumption) mercury lamp, a photoluminescence emission which is barely detectable by a dark-adapted eye. The weak photoluminescence that is excited is believed to be in the well known self-activated band for ZnSe and this band is different in many respects to the reverse bias spectrum since it is much sharper, of a different shape and has a different peak energy.

Since the light generated in reverse bias is not due to hole transitions of any description or electron transitions from the conduction band to centres in the forbidden gap or transitions between bound states the conclusion is reached that it is generated in intra-valley or inter-valley conduction band transitions. Both of these types of conduction band transitions would require for their excitation in electroluminescence an intense electric field. This is consistent with the observation that although some light is generated

in forward bias, (but with very much lower quantum efficiency than for reverse bias), the spectrum is entirely different from the reverse bias spectrum (the self-activated band is excited in forward bias). If electrons are assumed to make intra-valley transitions then it is reasonable to further assume that these occur in the lowest conduction band valley which, for ZnSe, is the Γ valley. If inter-valley transitions are considered to be the method of light generation then it is likewise reasonable to suppose that the majority of such transitions are to the Γ valley from the next higher valley or, possibly, from the next higher but one above Γ if the two valleys immediately above Γ are not widely separated. Of course, it is necessary to check for any proposed model that the emission spectrum observed is consistent with the band structure in so far as this is known.

The occupancy of the upper states involved in the radiative transitions, whether these transitions are of the inter-valley or intra-valley type, is evidently not strongly voltage dependent in the range of diode working voltages since the spectrum exhibits no clearly detectable change over a wide range of currents. From this voltage independence of the occupancy of the upper states it is expected, as a first approximation, that the light intensity would be proportional to the diode current for, at the high operating fields, the electron limiting drift velocity would be reached and thus the free electron density would be proportional to current. A refinement to this approximation for the current dependence of the light emission can be made by taking account of the change in the depletion layer volume with current, since it is this volume which is the source of the light. The width of the depletion layer is weakly dependent on the current since this width, for an ideal Schottky barrier, is proportional to the square root of the total (applied plus inbuilt)

barrier voltage. Hence, the light emission is predicted to vary slightly faster than the current when the voltage is raised, independently of whether the radiative transitions are in a single valley or between two valleys. This prediction is in qualitative agreement with experiment as may be seen by reference to figs. 3.5(a) and 3.5(b) in which, for a given diode, the slope d ln L/dV is slightly greater than the slope d ln i/dV.

In the following sections intra-valley and inter-valley electronic transitions are considered in greater detail in attempts to explain the mechanism of the light generation in the diodes at present under consideration.

3.4.2. The model of Bremsstrahlung of hot electrons in a single valley - theory and comparison with experiment.

The model of light emission envisaged here is that free electrons in the Γ valley are heated as they cross the high field region in a reverse biased Schottky barrier and transitions of the hot electrons down to lower parts of the valley give rise to a broad band of radiation emission. The light-emitting transitions involve a change of electron wavevector hence a scattering mechanism must be invoked. We will consider separately electron scattering due to ionized impurities, acoustic phonons and optical phonons. Two objectives of the theory are to predict the spectrum shape and the quantum efficiency, since these are amenable to experimental test. It will be assumed that the Γ valley is approximately parabolic and that the hot electron distribution can be adequately described by a drifted Maxwellian distribution corresponding to a certain electron temperature T_e. It might reasonably be supposed that the emission spectrum for such a model, over at least part of the energy range of the emitted photons, will have similarities to the radiation from a black-

body at temperature T_e, and indeed this is the case.

One of the first papers in which a model of the above type was considered, and in which the result of the theoretical analysis was in a convenient form for comparison with experimental quantum efficiency measurements, was published by Figielski and Torun[15]. These authors considered only scattering by ionized impurities and applied their formulation to explain the observations of Chynoweth and McKay[8] concerning a broad emission band in reverse-biassed Si p - n junctions. The agreement between theory and experiment for the spectrum shape and the quantum efficiency was quite good, although certain quantities required in the theoretical calculation were not given by the experimenters and these quantities were estimated by somewhat tenuous means. Pilkuhn[10] applied the theory of Figielski and Torun, retaining the assumption of ionized impurity scattering, to compute an efficiency which he compared with his measurements on GaP p - n junctions. The theoretical result for the quantum efficiency was less than the experimental result by three orders of magnitude.

In at least two papers[22,23] the validity of the assumption of a drifted Maxwellian distribution for the hot free carriers in reverse-biassed diodes has been questioned. The doubt concerning the applicability of the function for these conditions arises because the free carrier concentration is low and, as a consequence of this, there may not be sufficient interaction between carriers to maintain a Maxwellian distribution. For example, in a diode with an effective junction area of $1mm^2$ and passing a current of 1mA, the free carrier concentration, for any semiconductor, is only about $10^{11} cm^{-3}$. Theoretical forms for the spectrum shape were derived without the assumption of a Maxwellian

distribution, in the above two papers[22,23]. These forms provided a better fit to published spectra than that obtained from the theory of Figielski and Torun but, for one of them,[23] it is difficult to avoid the impression that this was not simply due to leaving a sufficient number of parameters adjustable to obtain the fit. In both papers only ionized impurity scattering was considered and no attempt was made to calculate a theoretical quantum efficiency which could be compared with experiments. This is in fact very difficult in view of the complexity of the formulations but, nevertheless, is a crucial test for a theory.

The present author has chosen to assume a Maxwellian function because of its simplicity and explore whether, by allowing for several separate scattering mechanisms, the results for ZnSe can be explained.

The bremsstrahlung model for intra-valley transitions is not able to account for the structure seen in the spectrum from ZnSe diodes but the model may be reasonably considered in an attempt to explain the shape and quantum efficiency for a part of the spectrum. The high energy tail of the spectrum has been selected for this purpose.

The high energy emission limit for ZnSe diodes operating at room temperature is 2.65eV. Referring to the ZnSe band structure diagram (fig. 3.14) and to table 3B, in which the latter contains a compilation of the positions of band structure critical points calculated by various methods and authors[24-28], it is seen that since the top of the Γ valley is higher than X_1 and about the same height as X_3, transitions as energetic as 2.65eV could conceivably occur within the Γ valley.

To evaluate the theoretical quantum efficiency for different scattering mechanisms an expression for $N(E)$, which

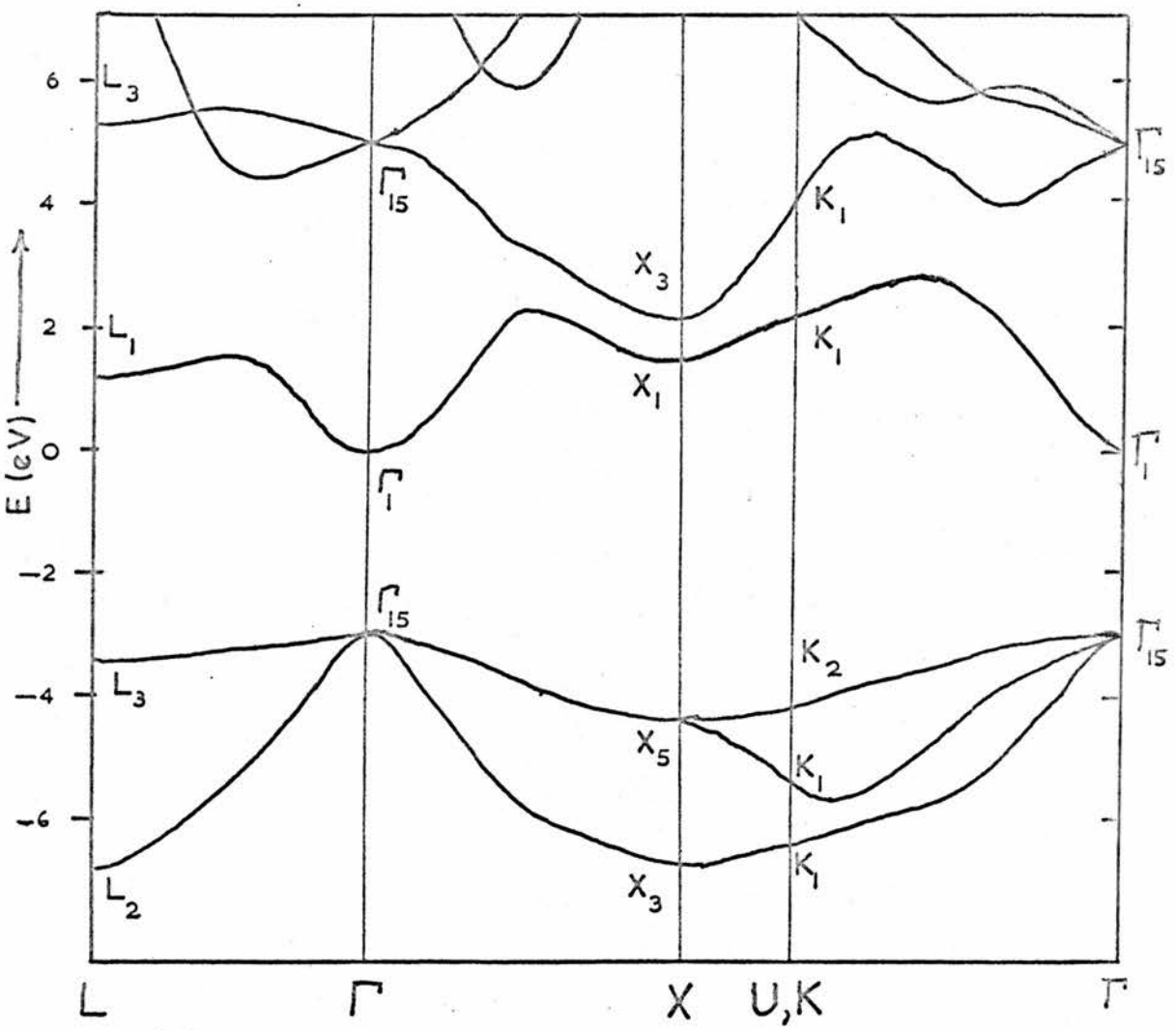

Fig. 3.14 ZnSe band structure (after Petroff et al[27]).

TABLE 3B

SUMMARY OF CRITICAL POINT ENERGIES IN THE

ZnSe BAND STRUCTURE AS CALCULATED BY VARIOUS METHODS

The critical point energies are given in eV with the origin taken at the lowest point of the conduction band.

Critical point	(a)	(b)	(c)	(d)	(e)	(f)	(g)	(h)
L_{3C}	4.5	4.9	5.3	5.6	5.0	5.7		5.6
Γ_{15C}	3.7	4.4	4.9	5.1	5.0	5.2	4.9	5.1
X_{3C}	1.6	1.9	2.6	2.2	2.5	2.1		3.0
X_{1C}	1.3	1.8	1.4	2.0	1.6	1.9		2.0
L_{1C}	0.9	1.1	1.7	1.4	1.6	1.4		1.9
Γ_{1C}	0.0	0.0	0.0	0.0	0.0	0.0	0.0	0.0
Γ_{15V}	-2.9	-3.2	-2.8	-2.9	-2.9	-3.3	-2.9	-2.8
L_{3V}	-3.5	-3.7	-3.2	-3.6	-3.4	-3.8		-3.0
X_{5V}	-4.6	-4.5	-4.2	-4.5	-4.4	-4.6		-3.9

		Ref.
(a)	First-principles, self-consistent; orthogonalised plane wave	24
(b)	" " non self-consistent; orthogonalised plane wave	24
(c)	Empirically refined; orthogonalised plane wave	24
(d)	Empirically refined; Korringa, Kohn, Rostoker method	24
(e)	Empirically refined; pseudo-potential method	25
(f)	First principles; Korringa, Kohn, Rostoker method	26
(g)	Empirically refined; pseudo-potential method	27
(h)	Empirically refined; orthogonalised plane wave	28

is defined as the number of photons emitted per unit energy interval centred at E, per unit time, per unit volume of emitting material, is first quoted or obtained. The quantity $N(E)$ is then multiplied by the volume of material in which there are hot electrons and integrated over the photon energy range E_1 to E_2 for which the quantum efficiency is required; this then gives the emission per unit time in the required range. Thus we have:-

$$\text{Rate of photon emission } (E_1 \leq E \leq E_2) = AW \int_{E_1}^{E_2} N(E)\, dE \quad \ldots\ldots(3.5)$$

where W is the depletion width corresponding to the diode current for which the calculation of the quantum efficiency is required and A is the effective cross section of the depletion layer perpendicular to the electron drift direction. The electron flux through the depletion layer is $n V_d A$, where V_d is the electron drift velocity and n is the concentration of free electrons. The required quantum efficiency, $\eta_{E_1}^{E_2}$, is the ratio of the photon emission rate given in 3.5 to the electron flux. Hence

$$\eta_{E_1}^{E_2} = \frac{W}{V_d} \cdot \int_{E_1}^{E_2} \frac{N(E)}{n}\, dE \quad . \qquad \ldots\ldots(3.6)$$

It should be noted that the term A has cancelled out so that, whether or not microplasms occur, the expression for the quantum efficiency is the same. Since $N(E)$ is proportional to n the value of this latter quantity is not required. The value taken for V_d is 4×10^7 cm sec^{-1}, which is the maximum possible electron velocity in the Γ valley and found by the steepest tangent that can be drawn to this part of the band structure diagram.

(i) Ionized impurity scattering.

An expression for N(E) has been given by Visvanathan[29] for ionized impurity scattering. This is

$$N(E) = \frac{32}{3}\left(\frac{\pi}{6}\right)^{1/2} \frac{n e^6 \varepsilon_\infty^{1/2} Z^2 N_D}{m^{*3/2} c^3 \varepsilon_s^2 (kT_e)^{1/2} h E} \cdot \exp\left(\frac{-E}{kT_e}\right) \quad \ldots.(3.7)$$

where $\varepsilon_\infty^{1/2}$ is the refractive index for photon energy E

ε_s is the static dielectric constant

m^* is the effective mass of electrons in the Γ valley

N_D is the concentration of ionized centres, which is here identified with the donor density.

Ze is the charge on each ionized centre

and other symbols which have not been previously defined have their usual significance.

The formula is most conveniently used in the e.s.u. system in which case the dielectric constants are dimensionless.

From 3.6 and 3.7 the quantum efficiency, for the photon energy range E_1 to E_2 is

$$\eta_{E_1}^{E_2} = \frac{7.72\, W e^6 \varepsilon_\infty^{1/2} Z^2 N_D}{v_d m^{*3/2} c^3 \varepsilon_s^2 (kT_e)^{1/2} h} \cdot \int_{u_1}^{u_2} u^{-1} e^{-u}\, du \quad \ldots.(3.8)$$

where $u_2 \equiv E_2/kT_e$

and $u_1 \equiv E_1/kT_e$.

Apart from the already mentioned assumptions the further

assumptions involved in obtaining 3.7 are satisfied for the high energy tail of the ZnSe emission spectrum. Figielski and Torun[15] found an expression equivalent to 3.8 except for a numerical factor of two. These authors expressed doubt regarding the appropriate dielectric constant to use in the denominator of 3.8, this term arising from the potential of an electron in the vicinity of an ionized centre. For ZnSe the radius of the first Bohr orbit is several lattice parameters so the form given in 3.8 should be valid.

The procedure adopted to analyse the results for ZnSe diodes was to draw, from spectrum measurements, graphs of $\ln[E\,N(E)]$ against E using accurate results for the high energy end of the room-temperature spectrum. From the slope of these plots T_e was determined and substituted into 3.8 to calculate the quantum efficiency. In practice the plots were not linear but were roughly fitted to a straight line for the photon energy range 1.8eV to 2.6eV, and from the line, $T_e \sim 7000K$. Insertion of this value of T_e into equation 3.8, together with $Z = 1$, $\varepsilon_s = 9.1$, $\varepsilon_\infty = 5.9$ and $m^* = 0.2X$ (free electron mass) gave, for the above photon energy range, a quantum efficiency per unit depletion width less by about a factor of 10^5 than the corresponding experimental result for all measured diodes with $N_D < 10^{23}\ m^{-3}$. This very large ratio of the experimental to the theoretical quantum efficiency per unit width is clear evidence that the light emission mechanism is not bremsstrahlung of hot free electrons in the Γ valley involving momentum transfer to ionized impurities.

For the numerical values of the calculated and observed quantum efficiencies for two specific diodes the reader is referred to table 3C.

TABLE 3C

Comparison of experimental efficiency with results calculated for intra-valley transitions of hot electrons in the Γ_1 valley

DIODE No.	ASSUMED SCATTERING MECHANISM	QUANTUM EFFICIENCY 1.8 eV < E < 2.6eV		Measured quantum efficiency/calc. quantum efficiency
		Calculated	Measured	
23.9.71B	Ionized impurities	1.3×10^{-11}	7.6×10^{-6}	5.8×10^{5}
2.10.71B	"	1.3×10^{-11}	2.2×10^{-5}	1.7×10^{6}
23.9.71B	Acoustic phonon	4.6×10^{-8}	7.6×10^{-6}	1.6×10^{2}
2.10.71B	"	6.7×10^{-8}	2.2×10^{-5}	3.3×10^{2}
23.9.71B	Optical phonon	1.5×10^{-10}	7.6×10^{-6}	5.1×10^{4}

The following values were used in computing theoretical quantum efficiencies:

Symbol	Meaning	Value taken
C_l	Elastic constant	1.0×10^{12} dyne cm^{-2}
ε_s	Static dielectric constant	9.1
ε_∞	Optical dielectric constant	5.8
E^*	Deformation potential for Γ valley	7eV
$\hbar\omega_l$	Longitudinal optical phonon energy	0.031 eV
m^*	Effective mass for Γ valley electrons	0.2x free-electron mass
T	Lattice temperature	300K
T_e	Electron temperature	(Determined as described in text, but for each scattering mechanism $T_e \sim 7000K$).
v_d	Electron drift velocity in Γ_{1c} valley	4×10^{7} cm s^{-1}.

(ii) Acoustic phonon scattering.

For acoustic phonon scattering it is obvious that both the electron temperature (T_e) and the lattice temperature (T) must appear in the expression for the quantum efficiency. From fig. 3.12 it is seen that the lattice temperature does affect the measured quantum efficiency. A plausible argument for the shape of the curve in fig. 3.12 can be given as follows, for the model at present under consideration. A lattice temperature rise increases the density of acoustic phonons and is therefore expected to lead to a rise in the quantum efficiency. This could conceivably be the explanation of the form of fig. 3.12 for $T > 270K$. At a constant field, and possibly also at a constant current, a cooling of the diode would lead to an expected rise in the electron temperature on account of the reduced scattering probability. Since the quantum efficiency increases with a rise of electron temperature, there may be a temperature range in which, for lattice cooling, the quantum efficiency rises even though the phonon density falls. In fig. 3.12, for $T < 270K$, there is an observed increase of quantum efficiency for diode cooling.

No explicit formulae either for N(E) or for the quantum efficiency have been published, so far as the author is aware, for the case of acoustic phonon scattering of hot electrons within a single valley. However, Meyer[30] has published an expression giving the contribution to the free-carrier absorption due to acoustic phonon scattering and his result was used as the basis of a calculation for the emission efficiency, since this is a very much simpler procedure than a direct calculation from first principles. The method of inversion from the known absorption coefficient formula to the corresponding emission efficiency is as follows. A crystal of the material is imagined to be in an enclosure containing black-

body radiation of temperature T_e. Since the electrons and photons are, by hypothesis, at a common temperature there is equilibrium between them. This means that there is detailed balance for all electron-photon interactions so that between any arbitrary pair of electron states the rate of light absorption transitions is the same as the rate of radiative transitions in the reverse direction (when averaged over a time interval such that many transitions are made). Application of this condition enables the rate of photon emission to be obtained for the particular electron and lattice temperatures since the absorption rate can be found from the known absorption coefficient. This rate is the same under non-equilibrium conditions hence the diode efficiency can be calculated. Let the number of photons in black-body radiation of temperature T_e, per unit photon energy interval at the energy E, in unit volume of material of refractive index $\varepsilon_\infty^{\frac{1}{2}}$, be denoted by $B(E,T_e)$. Then equating rates of emission and absorption gives

$$N(E) = B(E,T_e) \cdot \frac{c}{\varepsilon_\infty^{1/2}} \cdot \alpha(E) \qquad \ldots(3.9)$$

where $\alpha(E)$ is the absorption coefficient for photons of energy E in a crystal of lattice temperature T containing free electrons at temperature T_e. Meyer's expression for the absorption coefficient[30] was derived for the case $T_e = T$ but it is easily generalized for the case $T_e \neq T$. The function $B(E,T_e)$ is greater by a factor $\varepsilon_\infty^{3/2}$ than the corresponding and well known result for an evacuated enclosure. Substitution for $B(E,T_e)$ and $\alpha(E)$ into 3.9 yields

$$N(E) = \left(\frac{8}{9}\right)^{1/2} \cdot \frac{1}{\pi^2} \cdot \frac{n e^2 \varepsilon_\infty^{1/2} m^{*1/2} (kT) E^{1/2} E^{*2}}{c^3 \hbar^5 C_l} \exp\left(\frac{-E}{kT_e}\right) \cdot \left[1 + \frac{1.875}{z} + \frac{0.82}{z^2} + \ldots\right]$$

$\ldots\ldots(3.10)$

where E^* is the deformation potential for acoustic phonon scattering,

C_l is a weighted average elastic constant.

and $z \equiv E/2kT_e$

From 3.6 and 3.10 the quantum efficiency is given by

$$\eta_{E_1}^{E_2} = \frac{0.27We^2\varepsilon_\infty^{1/2}m^{*1/2}(kT)(kT_e)^{3/2}E^{*2}}{V_d c^3 h^5 C_l} \cdot \int_{z_1}^{z_2} e^{-2z} z^{1/2}\left[1+\frac{1.875}{z}+\frac{0.82}{z^2}+..\right]dz \quad ....(3.11)$$

where $Z_1 \equiv E_1/2kT_e$ and $Z_2 \equiv E_2/2kT_e$

Following equation 3.10 a semilogarithmic plot of $E^{-1/2}N(E).\left[1+\frac{1.875}{z}+\frac{0.82}{z^2}+..\right]^{-1}$ against E was drawn using experimental data for N(E) and with an estimated T_e to evaluate the term in square brackets. From the slope the electron temperature was deduced and was close to the original estimate. As before, the plot was not straight, but a rough fit for $T_e = 7000^{\circ}K$ was obtained for $E > 1.8eV$. Taking this value for T_e, with $E^* = 7eV$ obtained by comparison with experimental measurements on semiconductors similar to ZnSe[31,32], and $C_l = 1.0 \times 10^{12}$ dyne cm^{-2}[33] the theoretical quantum efficiency per unit depletion width was calculated for $1.8eV < E < 2.8eV$. The result was $5 \times 10^{-8}\mu^{-1}$ which is less than the experimental value obtained for all diodes with $N_D < 10^{23}m^{-3}$ by a factor ~ 250. The maximum uncertainty in this ratio is estimated to be less than or about one order of magnitude so acoustic phonon scattering in a single valley is not the emission mechanism. For reference the numerical results obtained for the calculated and measured quantum efficiencies for two diodes are included in table 3C.

The electron temperatures, as deduced from spectra of a certain diode respectively at room temperature and at 125K, were not

distinguishably different. However, in discussing the possible cause for the experimentally observed temperature dependence of the relative quantum efficiency (as shown in fig. 3.12) it was necessary to assume that for cooling from a lattice temperature of 270K to 125K there should be an appreciable rise in the electron temperature.

(iii) Polar optical phonon scattering

The emission spectrum form and quantum efficiency were found in exactly the same manner as for acoustic phonon scattering. The absorption coefficient expression appropriate for polar optical phonon scattering has been derived by Visvanathan[34] and his result was used in the inversion procedure for finding the diode quantum efficiency. The expressions obtained for N(E) and $\eta_{E_1}^{E_2}$ are respectively:

$$N(E) = \frac{4}{\pi} \frac{n e^4 (\hbar\omega_l) \varepsilon_\infty^{3/2} (\varepsilon_\infty^{-1} - \varepsilon_s^{-1})}{\hbar^3 c^3 m^{*1/2} E^{1/2}} \cdot \coth\left(\frac{\hbar\omega_l}{2kT}\right) \cdot \exp\left(\frac{-E}{kT_e}\right)$$

and

....(3.12)

$$\eta_{E_1}^{E_2} = \frac{1.27 W e^4 (kT_e)^{1/2} (\hbar\omega_l) \varepsilon_\infty^{3/2} (\varepsilon_\infty^{-1} - \varepsilon_s^{-1})}{V_d \hbar^3 c^3 m^{*1/2}} \cdot \coth\left(\frac{\hbar\omega_l}{2kT}\right) \cdot \int_{u_1}^{u_2} e^{-u} u^{-1/2} du$$

....(3.13)

where $\hbar\omega_l$ is the longitudinal optical phonon energy,

$u_2 \equiv E_2/kT_e$ and $u_1 \equiv E_1/kT_e$.

The electron temperature was found from the spectrum of a typical diode in a similar way to that already discussed for the scattering mechanisms in sub-sections (i) and (ii). The quantum efficiency was then evaluated from equation 3.13, using the known value of 0.031eV[35] for the longitudinal optical phonon energy in ZnSe and with values for other required quantities as shown at the foot of

table 3C. For the photon energy range 1.8eV $<$ E $<$ 2.6eV the calculated quantum efficiency per unit depletion width is $2 \times 10^{-10}\ \mu^{-1}$ which is less than the corresponding mean experimental result for all measured diodes with $N_D < 10^{23} m^{-3}$ by a factor of 7×10^4. The conclusion drawn is that the light is not generated by polar optical phonon assisted transitions of hot electrons within the Γ valley of the conduction band.

For convenience of reference the calculated quantum efficiencies for certain typical diodes, based on the general model of intra-valley transitions of hot Γ-valley electrons, but with different scattering mechanisms, are collected together in table 3C. The experimental quantum efficiencies for the same diodes are also included in the table.

The ratio of the experimental quantum efficiency to that calculated for the hot electron intra-valley transition model with either ionized impurity scattering or optical phonon scattering is extremely large ($> 10^4$). For the case of scattering by the acoustic phonon modes the ratio is much smaller but it is nevertheless sufficiently large that there is very little probability that the model can be appropriate to ZnSe. Moreover, within the framework of the model, the calculated quantum efficiency for acoustic phonon scattering is liable to be a large overestimate because no regard was given to the selection rules governing phonon-assisted transitions and it is believed[36] that in the Γ valley of zinc-blende materials neither LA or TA phonon-assisted transitions are allowed to first order. Incidentally, the absorption coefficient equation used as a basis for the present author's calculation of the quantum efficiency for acoustic phonon assisted transitions was derived by Meyer[30] specifically for Ge. In this material the L_1 valleys have the lowest minima of

the conduction band and for L_1 valleys intra-valley transitions assisted by LA phonons are allowed by the selection rules[36].

For bremsstrahlen emission due to intra-valley transitions of hot electrons there would be a field dependence of the shape of the spectrum because an increase of the field would raise the electron temperature. With an increase of the field the spectrum would become relatively richer in photons of higher energy and the point of the high energy tail of the spectrum, marking the apparent upper photon limit, would shift, at least for fields up to a critical value, towards higher energies. No attempt has been made to put these ideas on a quantitative basis but spectra have been measured in individual diodes for the field range corresponding to currents from 100μA to 150mA and no change in the spectrum is observed. Similarly, spectra for currents of a few mA in diodes of widely different donor concentration and hence also widely different fields, are found to be identical (e.g. see fig. 3.8). The lack of a detectable variation of the spectral shape with field is further evidence that the model of intra-valley transitions of hot electrons is inappropriate.

3.4.3. Inter-valley transitions introduced as a possible light emission mechanism

From the discussion given up to this point the conclusion has been reached that light emission is due to electron transitions which occur wholly above the conduction band minimum (Γ_{1c}) and that the light is not due to electron transitions within the Γ valley. Bremsstrahlen due to electron transitions within another valley at least 2.65eV deep such as the X_3 valley is, and the L_1 valley probably is, might at first sight seem possible but a calculation of the quantum efficiency would fairly clearly not give a grossly different value to that computed for the Γ valley.

For the diodes under discussion it is proposed that the observed emission is due to electron transitions between valleys of the conduction band since this appears to be the only emission mechanism consistent with the conclusions outlined above. Further evidence cited in support of the proposition is as follows:-

(i) For reverse bias operation of a typical diode the field in the depletion layer is several times greater than the known Gunn threshold of 38kV cm^{-1} [37]. It therefore follows that in a typical reverse biassed diode electrons in the depletion layer are transferred from the Γ_1 valley to one or more higher valleys.

(ii) Structure is observed in the emission spectrum. This can be explained in terms of inter-valley radiative transitions. Moreover, the observed structure is consistent with knowledge of the band structure of ZnSe.

(iii) The quantum efficiency for diodes, as calculated assuming the emission to be due to inter-valley transitions, is of the same order as the observed quantum efficiency.

(iv) Measured characteristics of the light intensity as a function of voltage, obtained for many diodes and exemplified in figs. 3.5(a) and 3.5(b), are consistent with the absence of a threshold voltage for light emission. This is readily explained if the light is generated in inter-valley transitions because, for each studied diode, the built-in field exceeds the Gunn threshold and, therefore, even for zero bias the field is sufficient to populate a higher valley of the conduction band. As an illustration of this explanation the maximum built-in fields for the diodes corresponding to figs. 3.5(a) and 3.5(b) have been calculated, assuming a barrier height of 1.4V [16], as 160kVcm^{-1} and 83kVcm^{-1} respectively.

The truth of the above statements (ii) and (iii) has not yet been demonstrated but will be shown in sections 3.4.4 and 3.4.5 respectively.

The main reason for rejecting bremsstrahlung models

for a single valley was because the theoretical efficiency proved to be very much less than the measured efficiency. That the assumption of inter-valley transitions can yield a theoretical quantum efficiency very much greater than for the intra-valley transition model is readily seen as follows. The matrix element connecting initial and final electron states is of similar magnitude in the two models, for a similar photon energy, but the number of electrons in upper states for transitions yielding the spectrum high-energy tail is determined, in the single valley bremsstrahlung model, by the small probability of occupation of these upper states according to a Maxwellian distribution function. If, however, the field in the depletion layer exceeds the Gunn threshold all electrons are transferred from the lowest valley to a higher valley or to a set of higher valleys, which means that there is then a large reservoir of electrons in states from which downward transitions may be made.

3.4.4. Identification of spectral features in terms of inter-valley transitions.

In the last section reference was made to a paper[37] on the Gunn effect in n-type ZnSe. The authors of this paper did not identify the Gunn-active valleys so that this paper did not provide information on the population of particular upper valleys at high fields. It will be shown that such information is obtainable from an examination of the shape of the spectrum for reverse-biassed ZnSe diodes although for fields several times the Gunn threshold. From Table 3B it will be observed that there is general agreement that the conduction band minima above Γ, are, in ascending order, L_1, X_1 and X_3. (The subscripts 1 and 3 for the critical point X are interchangeable depending on the choice of either Zn or Se at the origin, but it remains valid that there

is agreement that, in the conduction band, the lowest L valley is lower than the lowest X valley). The high-energy limit of the spectrum for diodes operated at room temperature is 2.65eV which, even allowing for the large uncertainties in the band structure critical points, is too energetic to be likely to be due to transitions between the L_1 and Γ_1 minima. Photons of this energy could be generated in X_3-Γ_1 transitions, according to table 3B, although admittedly this would only be possible if the larger values computed for X_3 - Γ_1 gap are almost correct. The next higher minima above X_3 are Γ_{15} and W_3, both of which are too high to give a maximum photon energy of 2.65eV in transitions for which the Γ_1 valley forms the ground states. There does appear, therefore, some evidence from the spectrum that the X_3 valley is populated at diode working fields. It is not unreasonable that X_3 should be populated at these fields, even though X_3 is well above L_1, because the fields involved are several times the Gunn threshold and also because it is believed that for zinc-blende semiconductors the deformation potential linking Γ_1 to X valleys is larger than that linking Γ_1 to L_1 valleys[38]. From a close study of the spectrum it is thought that all of the valleys L_1, X_1 and X_3 are populated under diode operating conditions. This will be indicated below.

Let the upper and lower valleys involved in inter-valley transitions be designated [1] and [0] respectively and let their energy separation be ΔE_{10}. If only the states close to the bottom of [1] are populated then the spectrum shape is determined by the matrix element linking the bottom of [1] with the set of final states in [0] and the energy density of these final states. For a limited range of photon energies, corresponding to transitions to final states near the minimum of [0], the matrix element may

be considered constant, in which case the spectrum shape is wholly determined by the energy dependence of the density of states in [o] . If valley [o] is assumed to be parabolic in the vicinity of the valley minimum then the deduced form of the spectrum is

$$N(E) = K\left(\Delta E_{10} - E\right)^{1/2} \qquad \ldots.(3.14)$$

where K is a constant. According to this equation a plot of $N^2(E)$ against E is linear and the intercept on the photon energy axis is ΔE_{10}.

Using measurements of the high-energy tail region of the spectrum excited in ZnSe diodes at room temperature, a graph of $N^2(E)$ against E was drawn. Great care was taken to obtain accurate spectral data for this purpose. Measurements, using an S20 response photomultiplier, were made for three different diodes with several spectral scans for each diode. The diode chips were made as thin as conveniently possible to minimize spectral distortion due to absorption of light within the diodes and a correction was applied for the residual distortion. The $N^2(E)$ against E graph was based on the mean spectrum from these experiments. This graph is shown in fig. 3.15 in which it is observed that the points do not lie on a single line but instead lie on two intersecting lines.

The interpretation suggested for this result is that the observed spectrum is the superposition of two partially overlapping spectra, each due to inter-valley transitions. Referring to fig. 3.15 it is assumed that in the range AC the spectrum is due only to $X_3 - \Gamma_1$ transitions whilst for CD the spectrum is due to overlapping of individual spectra due to $X_3 - \Gamma_1$ transitions and $X_1 - \Gamma_1$ transitions. By extrapolating AC to find the contribution from $X_3 - \Gamma_1$ transitions the line EF for $X_1 - \Gamma_1$ transitions

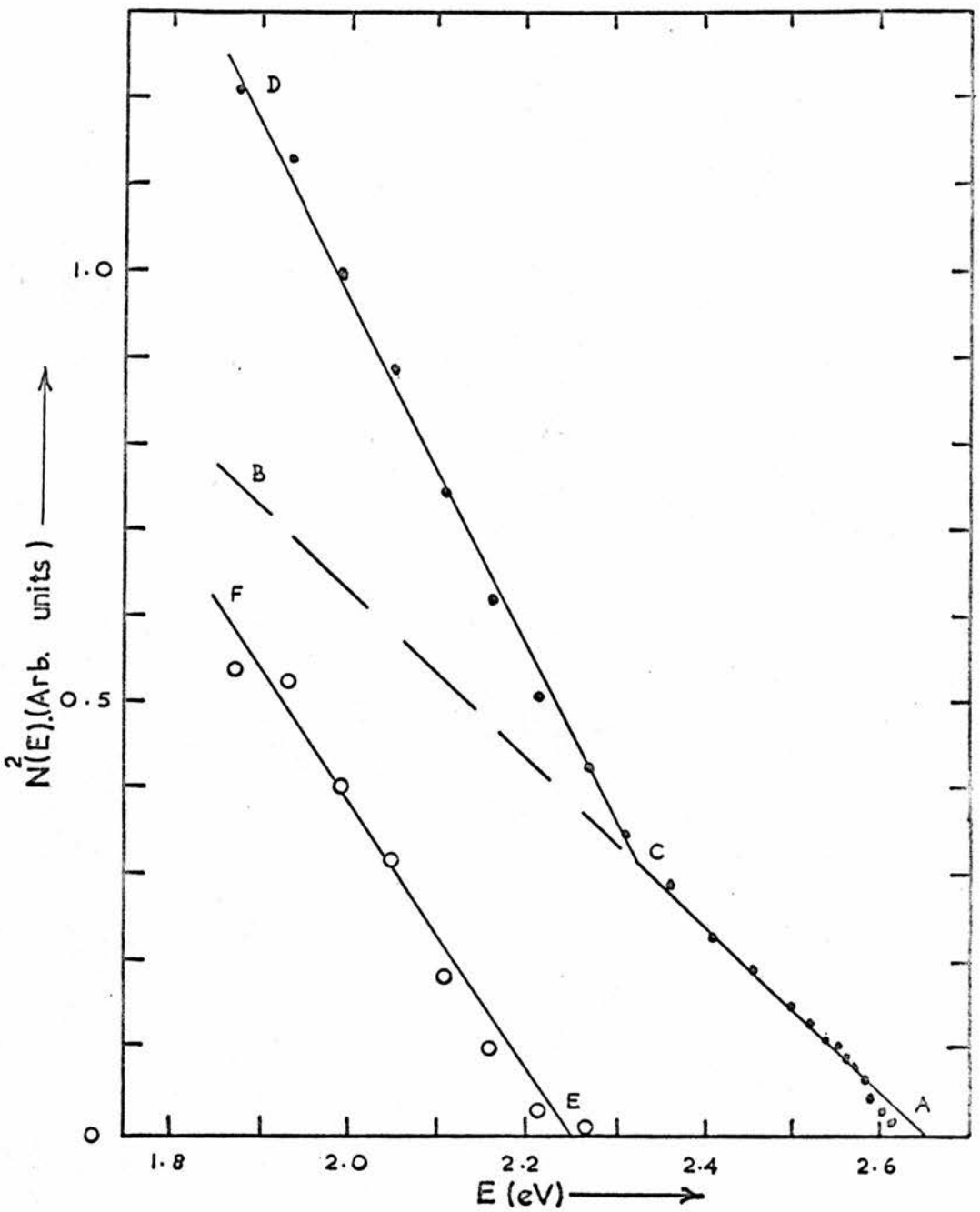

Fig. 3.15 Plots of $N^2(E)$ vs. E. See section 3.4.4 for an explanation of the figure.

was deduced. If this interpretation is correct the energy gap between Γ_1 and X_3 minima is 2.65eV and the gap between Γ_1 and X_1 minima is 2.25eV, both at room temperature. It should be noted that the scale of ordinates for EF is expanded by a factor of 10 relative to that for ACD, indicating that radiative coupling between X_3 and Γ_1 is stronger than between X_1 and Γ_1. The assigned values for the inter-valley spacings are plausible, given the data of table 3B.

Referring to fig. 3.8, in which a room temperature spectrum is shown for a wider spectral range than the spectra from which fig. 3.15 was drawn, a dip is seen at about 1.4eV. There is a similar feature in the room temperature spectrum taken with the PbS cell as detector (fig. 3.9) but it is somewhat less clear in this case on account of the wide error bars. It could possibly be argued that a dip is observed because of a band, associated with an impurity or other defect, having a maximum at an energy just above the dip and with this band superposed on the background of a broad spectrum. However, an explanation along these lines would require the superposed luminescence band to be improbably wide and, in order to explain the close agreement in the spectral shape at widely different fields, would require that the field dependence of the main broad band and the superposed band are very closely similar. Diodes from different batches of ZnSe preparations show identical spectra which forms evidence that there was no impurity band excited in the studied spectral range. It is believed that the rise in the spectrum with decreasing photon energy, which occurs at just below 1.4eV, is due to transitions from the L_1 valley to the Γ_1 valley. From the band structure critical point energies, obtained by calculation and listed in table 3B,

the gap between the L_1 and Γ_1 minima is ~1.4eV so the suggested cause of the spectral rise below 1.4eV is certainly in accord with the known band structure data. Selection rules[36,52,53], based on symmetry considerations do allow, for certain transition paths, radiative $L_1 - \Gamma_1$ transitions.

In the low temperature spectra, taken with a PbS cell as the detector, (fig 3.11) structure is clearly evident and the important features of the structure are reproducible, as is shown by the three spectra in the figure, each of which was obtained for a different diode. The shoulder, thought to be due to $L_1 - \Gamma_1$ transitions is observed and at slightly lower energy than at room temperature. There is a comparatively sharp peak at 0.55eV which may be due to $X_3 - X_1$ transitions. The spectrum presented in fig. 3.9 for room temperature diode operation shows little evidence of this peak but the displayed range extends slightly less far into the infra-red. There is some emission, from diodes near room temperature, at lower energy than that shown in fig. 3.9 but measurements in that range were not considered reliable on account of possible significant emission of temperature radiation. A sharp peak due to $X_3 - X_1$ transitions would be expected, since on the band structure diagram (fig 3.14), the curvature at the X_3 and X_1 minima are not very different. The X_3 valley is, however, slightly more strongly curved in the vicinity of its minimum than the X_1 valley is so the best estimate for the $X_1 - X_3$ gap is the low-energy cut-off for the part of the spectrum due to transitions between these two valleys. This gives 0.46eV for the gap at 117K, which is about 0.1eV higher than for the same gap estimated from a plot of $N^2(E)$ vs. E for the room temperature spectrum. Evidence is given below that the $X_3 - \Gamma_1$ gap increases by about 0.1eV for cooling from 300K to 117K and hence the observed

temperature dependence of the $X_1 - X_3$ gap would be explained if the $\Gamma_1 - X_1$ spacing is relatively temperature insensitive. In fig. 3.11 a small peak is seen at about 1.33eV for each spectrum. The transitions producing this peak have not been identified but could be $X_3 - L_1$ transitions. Apperson et al.[39] noted a photoluminescence peak at 1.24eV associated with defect centres in ZnSe free from deliberate doping, and the same centres could be the cause of the peak, measured at 1.33eV in the present work, but this is thought unlikely.

A spectrum for a diode at 125K, obtained using an S20 response photomultiplier, is shown in fig. 3.10. No correction has been applied for light absorption in the diode (light path length through ZnSe was 0.34mm) and the high energy limit of the externally observed spectrum is 2.74eV. For diodes with a light path length about twice that for the spectrum shown in fig. 3.10 the same upper energy limit was found for the externally observed spectrum, hence it is concluded that this limit would not be appreciably higher if determined for absorption-corrected spectra. The room temperature spectrum high energy limit, deduced from the intercept in fig 3.15, is 2.65eV and for this figure an absorption correction was applied. The band gap of ZnSe increases by about 0.1eV on cooling from room temperature to 125K but the increase in the high energy photon limit is not due to the corresponding change of the absorption edge because, as just stated, the room temperature spectrum had been corrected for absorption. The shift of the high energy limit of the spectrum on cooling has been frequently observed and checked by taking, for each of several specific diodes, successive spectral scans at room temperature and at about 125K.

The result for the temperature dependence of the maximum energy of the emitted photons, combined with the conclusion that the most energetic photons arise from transitions between the X_3 and Γ_1 minima, means that the separation of these minima increases by about 0.10eV for cooling from 300K to 125K. It would be a useful check on these ideas if there was independent experimental information available on the temperature dependence of the $X_3 - \Gamma_1$ gap in ZnSe but, unfortunately, no reports of suitable experiments are known. Similarly, no information on the temperature dependence of the corresponding gap for other zinc blende materials is known to the author. Measurements have been reported, however, which enable the temperature dependence of the $X_1 - \Gamma_1$ gap to be deduced for the zinc-blende ternary alloy $GaAs_xP_{1-x}$. Holonyak et al.[40] found, from measurements of the temperature dependence of both the photon energy and relative quantum efficiency of the light emission in forward biassed p-n junctions of the alloy, having composition close to the direct-indirect crossover point, that for cooling from 300K to 77K the $\Gamma_1 - X_1$ gap increased by 0.11eV. In ZnSe the $\Gamma_1 - X_3$ separation was concluded to increase by 0.10eV for cooling from 300K to 100K and the $\Gamma_1 - X_1$ separation was thought to be relatively temperature independent. It does appear, from the results for $GaAs_xP_{1-x}$ that there is, for some zinc-blende semiconductors, a temperature dependence of the separations of conduction band minima of the same sign and about the same magnitude as that suggested for ZnSe.

In table 3D the energy spacings between certain pairs of conduction band minima, as deduced from the spectra of ZnSe diodes, are given.

TABLE 3D

ENERGY SPACINGS BETWEEN ZnSe CONDUCTION BAND MINIMA AS ESTIMATED FROM SPECTRA OF REVERSE BIASSED SCHOTTKY DIODES

T (K)	Optical Detector	$\Gamma_1 - L_1$ (eV)	$\Gamma_1 - X_3$ (eV)	$X_1 - X_3$ (eV)
125	S20 photomult.		2.7_4 (a)	0.5_0 (c,d)
117	PbS cell	1.3-1.6 (a)		0.4_6 (b)
300	S1 photomult.	1.5 (a)	2.6_4 (a)	0.3_6 (c,d)
300	S20 photomult.		2.6_5 (a)	0.3_7 (c)
300	PbS cell	1.4-1.6 (a)		

Notes

(a) From the high energy limit of the relevant part of the spectrum.

(b) " " low " " " " " " " " " "

(c) From a plot of $N^2(E)$ vs. E.

(d) Graph from which the estimate made is not displayed in this thesis.

3.4.5. Theoretical calculation of the quantum efficiency for inter-valley transitions and comparison with experimental values.

It is clear that if it can be shown that the model of inter-valley transitions leads to a theoretical efficiency of the same order as measured efficiencies then considerable additional confidence will be gained that the proposed transitions do occur in ZnSe diodes. Also, since there is a change of electron wavevector in the transitions $X_3 - \Gamma_1$, $X_1 - \Gamma_1$ and $L_1 - \Gamma_1$, a theoretical quantum efficiency calculation should assist in elucidating the major scattering mechanisms involved in transfer of electrons between these respective pairs of valleys.

An expression for the quantum efficiency assuming inter-valley transitions has not, so far as the author is aware, appeared in the literature. However, Haga and Kimura[41] have derived expressions for the absorption coefficient contributions due to such transitions and, by application of a detailed balance argument similar to that employed in section 3.4.2, it is possible to invert these expressions to obtain theoretical estimates of the quantum efficiency for emission.

Referring to fig. 3.16, suppose it is desired to find the quantum efficiency due to transitions between an upper valley $[1]$ and a lower valley $[0]$. Let the concentration of electrons in valleys $[0]$ and $[1]$ be respectively n_0 and n_1. Further, let $R_{10}\, d\omega$ be the number of photons emitted per unit time in the range ω to $(\omega + d\omega)$ due to radiative transfer between $[1]$ and $[0]$ for unit volume of material and unit concentration of electrons in valley $[1]$. Then, if the absorption coefficient for $[0]$ - $[1]$ transitions is $\alpha(\omega)$, we have for equilibrium, from the detailed balance condition and from the fact that the radiation field will necessarily be black-body radiation, the equation

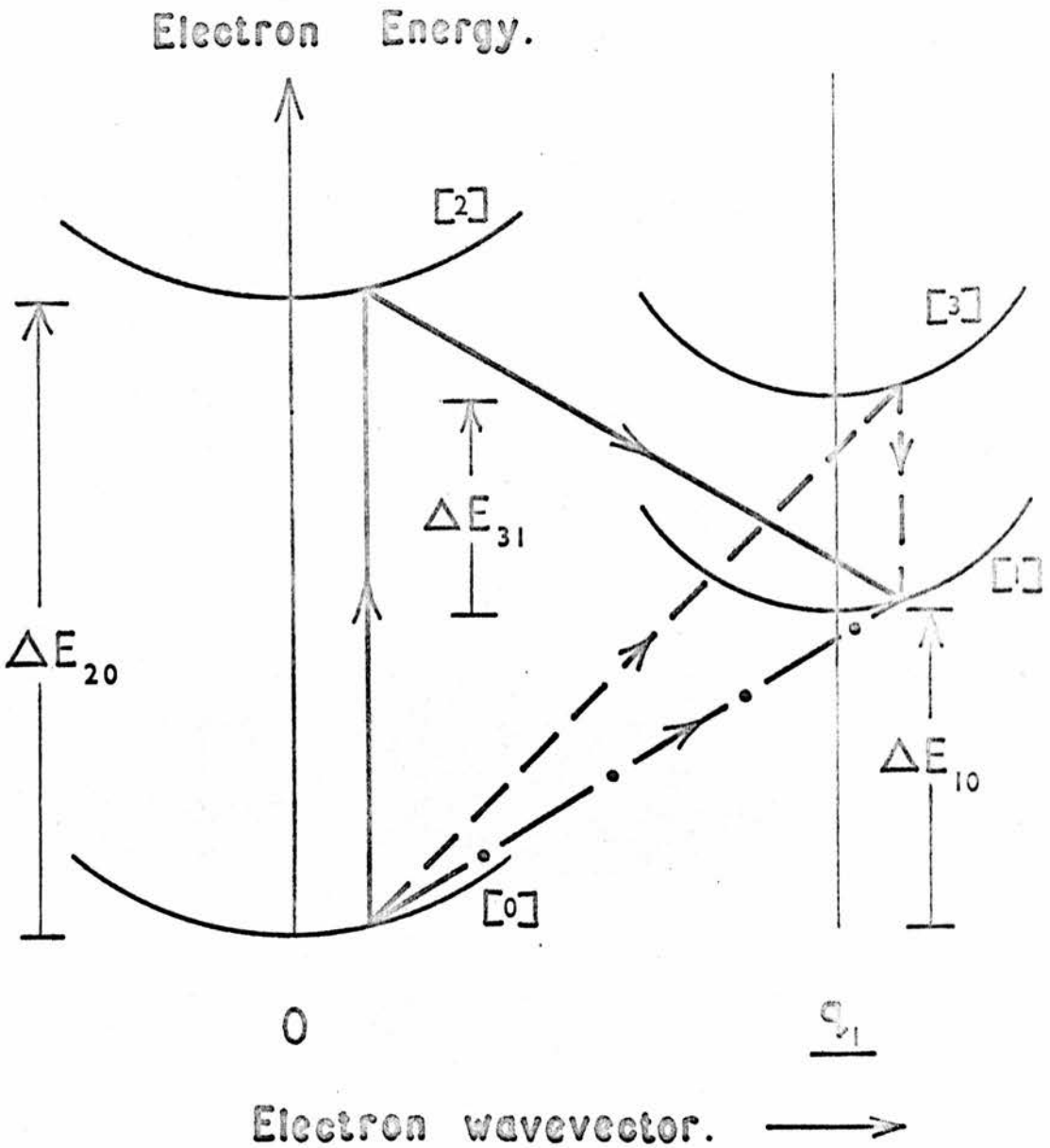

Fig. 3.16 Transition paths between valley [0] and an upper valley, [1].

——→—— I-type [0]–[2]–[1] path

— → — I-type [0]–[3]– [1] path

—·→·· D-type [0]–[1] path.

For emission transitions between [1] and [0] the arrows are reversed.

$$\alpha(\omega)\ \mathcal{B}(\omega)\ \frac{c}{\varepsilon_\infty^{1/2}} = n_1 R_{10} \qquad \ldots.(3.15)$$

Here $\mathcal{B}(\omega)$ is the number of photons in the range $\hbar\omega$ to $\hbar(\omega+d\omega)$ in unit volume of material of refractive index $\varepsilon_\infty^{1/2}$ for thermal radiation at equilibrium with the material. Since $\alpha(\omega)$ is proportional to n_o let us write $\alpha(\omega) = n_o \gamma(\omega)$. The expression, obtained from 3.15, for R_{10} then involves the ratio n_o/n_1 but, since we have assumed thermal equilibrium, this ratio is known in terms of the effective masses for the [0] and [1] valleys (each valley assumed parabolic) and the gap, ΔE_{10}, between the minima of these valleys. (It will be assumed $\Delta E_{10} \gg kT$ hence Boltzmann statistics may be employed). Making the substitution indicated for n_o/n_1 , together with a substitution for $\mathcal{B}(\omega)$, recalling that the latter is greater by a factor $\varepsilon_\infty^{3/2}$ than for black-body radiation in an evacuated enclosure, we have

$$R_{10} = \left(\frac{m_o^*}{m_1^*}\right)^{3/2} \cdot \exp\left(\Delta_{10} - \theta\right) \cdot \frac{\omega^2 \varepsilon_\infty}{\pi^2 c^2} \cdot \gamma(\omega) \qquad \ldots. (3.16)$$

where $\Delta_{10} \equiv \dfrac{\Delta E_{10}}{kT}$ and $\theta \equiv \dfrac{\hbar\omega}{kT}$.

The induced emission term of $\mathcal{B}(\omega)$ has been neglected in obtaining 3.16, this is justified because of the already made assumption that $\Delta E_{10} \gg kT$ and the fact that the interest is in photon emission with energies not small compared with ΔE_{10} . The value of n_1 taken up to this stage is that which is determined from thermal equilibrium but the form assumed for the rate of [1] - [0] transitions, involving a given emission energy, remains the same independently of the value of n_1 or of the processes which determine the value of n_1. Since the field in

the depletion layer of operating diodes is large compared with the Gunn threshold field all electrons are transferred from valley [0] and these electrons will be assumed to populate only valley [1] . The quantum efficiency may be calculated, for we find the rate of [1] - [0] transitions corresponding to a given infinitesimal photon energy interval in the spectrum of the emission, per electron in valley [1] , multiply by the number of electrons in this valley, divide by the rate at which electrons pass through the junction, and finally, integrate over the photon energy range of interest ie. $E_1 \leqslant E \leqslant E_2$. This gives for the quantum efficiency

$$\eta_{E_1}^{E_2} = \frac{W}{v_{d_1}} \int_{\omega_1}^{\omega_2} R_{10}\, d\omega \qquad \ldots\ (3.17)$$

$$\eta_{E_1}^{E_2} = \frac{WkT}{v_{d_1}\hbar} \int_{\theta_1}^{\theta_2} R_{10}(\theta)\, d\theta \qquad \ldots (3.17a)$$

where

$$\omega_2 \equiv E_2/\hbar\ ,\ \omega_1 \equiv E_1/\hbar\ ,\ \theta_2 \equiv E_2/kT\ ,\ \theta_1 \equiv E_1/kT$$

W = depletion width and v_{d_1} = electron drift velocity in valley [1] .

In these equations n_1 does not appear because both the photon emission rate and the rate of electron passage through the junction are proportional to n_1 which therefore cancels. It should be noted that if the current distribution is non-uniform, eg. if microplasmas are present, the results 3.17 and 3.17(a) are unchanged because the effective junction cross-section also cancelled out. For simplicity the multiplicity of upper valleys [1] was taken as unity but the final result is true for a general multiplicity.

The term $R_{10}(\theta)$ is found from the absorption coefficient equations of Haga and Kimura[41] by means of equation 3.16. It is necessary at this stage to digress in order to discuss the absorption processes for the theory developed by these authors. They considered two types of absorption transition which will be referred to as direct type (D) and indirect (I) type. These transitions differ in the nature of the intermediate states involved and are indicated in fig. 3.16. The two types of absorption are considered below for initial and final states respectively in valleys [0] and [1].

D-type There are two cases as follows.

(i) An electron in valley [0] first makes a virtual transition within the same valley by interaction with a photon then reaches the final state in valley [1] by interaction with a lattice imperfection.

(ii) An electron in valley [0] first makes a virtual transition to valley [1] by interaction with an imperfection then reaches the final state in valley [1] by interection with a photon.

I-type The intermediate states are either in valley [2] or valley [3]. Valleys [2] and [0] have minima at the same wavevector. Valleys [3] and [1] have minima at the same wavevector.

The two possible cases are as follows.

(i) An electron in valley [0] first makes a virtual transition to valley [2] by interaction with a photon then reaches the final state in valley [1] by interaction with an imperfection.

(ii) An electron in valley [0] first makes a virtual transition to valley [3] by interaction with an imperfection, then reaches the final state in valley [1] by interaction with a photon.

Haga and Kimura's results for the absorption coefficient (after some modification to make them more suitable for our purposes), for the case where $m_o^* \ll m_1^*$ are given below.

D-type. $[0] \rightarrow [1]$

$$\alpha_D = \left(\frac{128}{9\pi}\right)^{1/2} \cdot \frac{n_o V e^2 |T_{10} I_{10}|^2 m_1^{*3/2}}{\hbar^2 c \varepsilon_\infty^{1/2} m_o^* (kT)^{3/2} \theta^3} \int_u^\infty x^{3/2} e^{-x} \left[x - (\Delta_{10} - \theta)\right]^{1/2} dx \quad \ldots\ldots (3.18)$$

I-type $[0] - [2] - [1]$

$$\alpha_I = \left(\frac{32}{9\pi}\right)^{1/2} \cdot \frac{n_o V m_1^{*3/2} e^2 |P_{20}|^2 |T_{12} I_{12}|^2}{\hbar^2 c \varepsilon_\infty^{1/2} m^2 (\Delta E_{20} - \hbar\omega)^2 (kT)^{1/2} \theta} \int_u^\infty x^{1/2} e^{-x} \left[x - (\Delta_{10} - \theta)\right]^{1/2} dx \quad \ldots\ldots (3.19)$$

In these equations those symbols which have not been previously defined have the following meanings:-

m = free-electron mass

V = volume of crystal

P_{ij} = momentum operator connecting valleys i and j

T_{ij} = matrix element for the imperfection-induced transition between valleys i and j

I_{ij} = overlap integral (Normalized to unity for complete overlap)

$u = \Delta_{10} - \theta$ if $\hbar\omega < \Delta E_{10}$

$u = 0$ if $\hbar\omega > \Delta E_{10}$

In 3.18 and 3.19 the energies of the phonons participating in the transitions have been neglected. For I-type transitions via the path $[0] - [3] - [1]$ the changes shown below are made to equation 3.19.

$$P_{20} \longrightarrow P_{13}, \quad T_{12} \longrightarrow T_{30} \text{ and } (\Delta E_{20} - \hbar\omega) \longrightarrow (\Delta E_{31} + \hbar\omega)$$

The terms $(\Delta E_{20} - \hbar\omega)$ and $(\Delta E_{31} + \hbar\omega)$ are the energies associated with the intermediate states in [0] - [2] - [1] and [0] - [3] - [1] transitions respectively. The total absorption coefficient for I transitions is found by a summation of the contributions for all I-type paths. However, there is only a large contribution for those paths having small intermediate energies. This means that the important paths are through intermediate states such that the extrema for [0] and [3] or for [1] and [2] are of least energy separation.

For D transitions, with $\hbar\omega < \Delta E_{10}$, we have from 3.16 and 3.18

$$R_{10}(\theta) = \left(\frac{128}{9\pi^5}\right)^{1/2} \cdot \frac{V m_o^{*1/2} e^2 |T_{10} I_{10}|^2 (kT)^{1/2} \varepsilon_\infty^{1/2}}{c^3 \hbar^4 \theta} \cdot \int_0^\infty (x + \Delta_{10} - \theta)^{3/2} x^{1/2} e^{-x} dx \quad \ldots\ldots (3.20)$$

Similarly, from 3.16 and 3.19, for I-type [1] - [2] - [0] transitions, also with $\hbar\omega < \Delta E_{10}$, we have

$$R_{10}(\theta) = \left(\frac{32}{9\pi^5}\right)^{1/2} \frac{V m_o^{*3/2} e^2 |P_{20}|^2 |T_{12} I_{12}|^2 \varepsilon_\infty^{1/2} \theta}{c^3 \hbar^4 m^2 (\Delta_{20} - \theta)^2 (kT)^{1/2}} \int_0^\infty x^{1/2} \left(x + \Delta_{10} - \theta\right)^{1/2} e^{-x} dx \quad \ldots\ldots (3.21)$$

In obtaining these last two equations the integrals in 3.18 and 3.19 have been manipulated to make the lower limit of integration zero. This enabled exp $(\theta - \Delta_{10})$ to be brought outside each integral and to cancel with its reciprocal which appears in equation 3.16.

The theory leading to the equivalent of 3.21 for $\hbar\omega > \Delta E_{10}$ gives a small amount of emission in this range and it may be shown that

$$R_{10}(\Delta_{10} + \delta) = R_{10}(\Delta_{10} - \delta) \cdot \frac{\Delta_{10} + \delta}{\Delta_{10} - \delta} \cdot e^{-\delta} \quad \ldots\ldots (3.22)$$

where

$$\delta = \theta - \Delta_{10} \quad , \quad (\delta > 0)$$

For photon emission in the high energy tail the spectrum shape is mainly determined by the θ dependence of the integrals in 3.20 and 3.21. These integrals can be expanded as follows (not applicable for $\Delta_{10} = \theta$ but close to exact result for $\Delta - \theta > 2$, especially for 3.24.)

$$(D) \quad \int_0^\infty (x + \Delta_{10} - \theta)^{3/2} x^{1/2} e^{-x} dx = \frac{\sqrt{\pi}}{2} (\Delta_{10} - \theta)^{3/2} \left[1 + \frac{9}{4} (\Delta_{10} - \theta)^{-1} + \cdots \right] \quad \ldots\ldots (3.23)$$

$$(I) \quad \int_0^\infty (x + \Delta_{10} - \theta)^{1/2} x^{1/2} e^{-x} dx = \frac{\sqrt{\pi}}{2} (\Delta_{10} - \theta)^{1/2} \left[1 + \frac{3}{4} (\Delta_{10} - \theta)^{-1} + \cdots \right] \quad \ldots\ldots (3.24)$$

It will be observed that for I transitions this leads to a theoretical spectrum shape of the form 3.14 assumed in section 3.4.4. For D-transitions the spectrum does not reduce to this form which means that the overall transition probability is dependent on the photon energy to an extent comparable or greater than that for the density of final states in valley [0] .

Before the quantum efficiency can be calculated it is necessary to find the value for T_{ij}^2 in either 3.20 or 3.21 as appropriate. The relative probabilities for different scattering mechanisms are considered, firstly without regard to selection rules. The scattering mechanism corresponding to the largest probability, as calculated in this way, will then dominate unless this would violate a selection rule. Formulae as follows are given by Haga and Kimura[41] for $T_{ij}^2 V$. (The quantity T_{ij} is defined in a way which it gives it the

dimensions of energy and the crystal volume, V, does not appear in the final quantum efficiency result.

(i) Acoustical phonon (LA)

$$T_{ij}^2(q_1).V = \frac{\hbar q_1 E_1^{*2}}{2\rho s} \times \begin{cases} N(q_1) & \text{for phonon absorption} \\ N(q_1)+1 & \text{" " emission} \end{cases}$$

where $$N(q_1) = \left[\exp \frac{\hbar s q_1}{kT} - 1\right]^{-1} \qquad \ldots\ (3.25)$$

(ii) Optical phonon (LO)

$$T_{ij}^2(q_1).V = \frac{32\pi^2 e^4 \left(\frac{*}{e}\right)^2 \hbar}{M a^3 \omega_l} \cdot \left(\frac{q_1}{q_1^2 + l_D^{-2}}\right)^2 \times \begin{cases} N_l & \text{for phonon absorption} \\ N_l + 1 & \text{" " emission} \end{cases}$$

$$\ldots\ (3.26)$$

where $$N_l = \left[\exp \frac{\hbar \omega_l}{kT} - 1\right]^{-1}$$

(iii) Ionized impurity

$$T_{ij}^2(q_1).V = \frac{16\pi^2 Z^2 e^4}{\varepsilon_s^2} \cdot \left(\frac{1}{q_1^2 + l_D^{-2}}\right)^2 \qquad \ldots(3.27)$$

In these equations

V = volume of the crystal

E_1^* = deformation potential for the transition

q_1 = wavevector separation of the valleys.

l_D = Debye length

s = longitudinal sound velocity

$\hbar\omega_l$ = " optical phonon energy

a = lattice parameter.

M = reduced mass of a pair of ions

e^* = Callen effective charge of an ion

ρ = density of the crystal.

From equations 3.24 - 3.26, for T = 300K and $N_D = 10^{17} cm^{-3}$, the ratio of $X - \Gamma_1$ scattering probabilities by acoustic phonons, optical phonons and ionized impurity centres in ZnSe is 1:0.03 : 3 x 10^{-6}, hence unless there is a selection rule forbidding it, only acoustic phonon scattering is important. In calculating the values of $T_{ij}^2(V)$ s was taken as the mean value for the whole of the LA phonon branch ie. s = (LA zone edge energy[35])/($\hbar q_1$) , $\hbar\omega_L$ was taken as 0.031eV[35] and q_1 is $2\pi/a$. The effective ionic charge, e^* , appearing in 3.26 has been discussed by Ehrenreich[42] and is related, by an expression involving the optical and static dielectric constants, to the more commonly quoted Szigeti effective charge. Using the value 0.78e[35] for the latter charge, e^* was deduced to be 0.35e. E_1^* is not known for ZnSe but has been estimated[43] as 9eV for $X_1 - \Gamma_1$ coupling in GaAs and, in equation 3.25, this value was used. The L_1 valleys are believed to be more loosely coupled to Γ_1 than are the X_1 or X_3 valleys[38] and data for the $L_1 - \Gamma_1$ deformation potential have been given for several zinc-blende semiconductors[44-48] , not including ZnSe. These results showed a nearly linear dependence of the deformation potential with ionicity, from which the estimate 6eV has been obtained for ZnSe.

A further quantity which is required for calculating the quantum efficiency of diodes is the momentum operator, P_{ij} , which appears in equation 3.21. The subscripts i and j in P_{ij}

refer to the two valleys across which the vertical transition occurs in each I-type transition path. For the I-type transition paths which contribute significantly to the total quantum efficiency the appropriate values for P_{ij} are not known, either for ZnSe or for other zinc-blende materials. For the particular case of i and j respectively Γ_{15V} and Γ_{1C} it has been shown[40] from known effective masses at Γ_{1C}, that in many III-V and II-VI compounds $P_{ij}^2/2m$ is within 20% of 15eV. Similarly for the $L_{3V} - L_{1C}$ and $X_{4V} - X_{1C}$ interactions in Si[49] and Ge[50] respectively the values of $P_{ij}^2/2m$ are also within the above range. For the quantum efficiency calculation it has been assumed that for all momentum operators of interest $P_{ij}^2/2m = 15\text{eV}$. The overlap integral I_{ij} must be in the range of zero to unity and, from a published formula[51], I_{ij}^2 has been calculated as 0.7. The drift velocity (v_{d_i}) was taken as the Gunn domain drift velocity in ZnSe and this has the value $1 \times 10^7 \text{cm sec}^{-1}$[37].

In table 3E results are listed for the quantum efficiencies per micron depletion width, as calculated from equations 3.17(a) - 3.21, for different individual transition paths between initial and final valleys. The selection rules[52,53] for transitions in solids with zinc-blende structure have been taken into account to find the symmetries of the phonons which assist in the transitions. By reference to rules given by Birman et al.[36] it was possible to remove the ambiguity concerning the labelling scheme of phonon symmetries (the ambiguity arises from a choice of either Zn or Se at the origin) and then, from the allocated phonon symmetries, it was possible to identify the phonon types as LA, TA, LO or TO. It proved to be the case that the calculated quantum efficiency contribution from each path between

TABLE 3E

THEORETICAL RESULTS FOR DIODE QUANTUM EFFICIENCY PER UNIT DEPLETION WIDTH, BASED ON THE MODEL OF INTER-VALLEY TRANSITIONS.

Transition and Virtual path	Transition type (see text)	Selection rules applied			No selection rules applied
		Phonon symmetry	Phonon type	Calculated* $\frac{10^6}{W}\cdot\eta_{1.8eV}^{2.65eV}$ (μ^{-1})	Calculated* $\frac{10^6}{W}\cdot\eta_{1.8eV}^{2.65eV}$ (μ^{-1})
$X_{3c}-\Gamma_{1c}$					
$X_{3c}-\Gamma_{1c}$	1-0	X_3	LA	3.0	3.1
$X_{3c}-X_{1c}-\Gamma_{1c}$	1-3-0	X_1	LO	0.6	16.6
$X_{3c}-\Gamma_{15c}-\Gamma_{1c}$	1-2-0	X_1	LO	0.2	8.2
		X_5	TO,TA	0.0	
$X_{3c}-X_{5v}-\Gamma_{1c}$	1-3-0	X_5	TO,TA	0.0	2.3
$X_{1c}-\Gamma_{1c}$					
$X_{1c}-\Gamma_{1c}$	1-0	X_1	LO	0.04	1.3
$X_{1c}-X_{3c}-\Gamma_{1c}$	1-3-0	X_3	LA	3.1	3.1
$X_{1c}-\Gamma_{15c}-\Gamma_{1c}$	1-2-0	X_3	LA	2.3	2.4
		X_5	TO,TA	0.0	
$X_{1c}-X_{5v}-\Gamma_{1c}$	1-3-0	X_5	TO,TA	0.0	1.2
			TOTALS	9.2	38.2

EXPERIMENT : Mean $(10^6/W)\cdot\eta_{1.8eV}^{2.65eV}$ for 25 diodes, all with $N_D < 10^{17}$ cm^{-3}, is 14.3 μ^{-1} (84% of the diodes in this sample were within a factor 2 of the mean)

* See following page for meaning.

TABLE 3E (CONTINUED)

Transition and virtual path	Transition type (see text)	Selection rules applied			No selection rules applied
		Phonon symmetry	Phonon type	Calculated* $\frac{10^6}{W} \cdot \eta_{0.6eV}^{1.4eV}$ (μ^{-1})	Calculated* $\frac{10^6}{W} \cdot \eta_{0.6eV}^{1.4eV}$ (μ^{-1})
$L_{1c}-\Gamma_{1c}$					
$L_{1c}-\Gamma_{1c}$	1-0	L_1	LO	0.11	2.01
			LA	1.90	
$L_{1c}-\Gamma_{15c}-\Gamma_{1c}$	1-2-0	L_1	LO	0.04	0.73
			LA	0.69	
		L_3	TO,TA	0.00	
$L_{1c}-L_{3c}-\Gamma_{1c}$	1-3-0	L_3	TO,TA	0.00	0.41
$L_{1c}-\Gamma_{15v}-\Gamma_{1c}$	1-2-0	L_1	LO	0.04	0.76
			LA	0.72	
		L_3	TO,TA	0.00	
$L_{1c}-L_{3v}-\Gamma_{1c}$	1-3-0	L_3	TO,TA	0.00	0.79
			TOTALS	3.5	4.7

EXPERIMENT : Mean $(10^6/W) \cdot \eta_{0.6eV}^{1.4eV}$ for 25 diodes, all with $N_D < 10^{17}$ cm^{-3}, is 22 μ^{-1} (84% of the diodes in this sample were within a factor 2 of the mean).

* It has been assumed that all electrons are in the upper valley for each transition path. The calculated η/W values are therefore over-estimates. If electrons are assumed to distribute with equal numbers in the X_3, X_1 and L_1 valleys then all calculated η/W values should be divided by 3.

L_1 and Γ_1, with the selection rules applied, would be unaffected if the origin was identified incorrectly. For the total emission attributable to $X_3 - \Gamma_1$ and $X_1 - \Gamma_1$ there would only be a small error in the calculated quantum efficiency (again with application of the selection rules) by an incorrect identification of the origin but the calculated relative contributions of each path would be significantly changed. In addition to the transitions $X_3 - \Gamma_1$, $X_1 - \Gamma_1$ and $L_1 - \Gamma_1$ given in table 3E the transition $X_3 - X_1$ is also allowed[52,53] but no attempt was made to calculate the quantum efficiency corresponding to this latter transition.

The results for the computed quantum efficiencies, which can only be expected to be accurate to within about one order of magnitude, are similar to experimentally determined values and the latter are shown at the foot of each part of table 3E. For the calculation of the contribution to the total quantum efficiency from each transition path it was assumed that all free electrons were in the initial valley for that path. Since the free electrons are distributed into several upper valleys the calculated quantum efficiency is, to this extent, an overestimate. The quantum efficiencies, calculated as described, would however be too low if there is strong departure from the selection rules for transitions not between the minima of the initial and final valleys. In table 3E the result of a recalculation of the quantum efficiencies are given assuming total breakdown of the selection rules and, with this assumption, LA phonon scattering is dominant in all transition paths.

As regards the theoretical spectrum shapes, for all I-type transitions these are similar to the experimental results

and for each path there is a spectral maximum. D-type transition spectra, as calculated, show monotonic increase with reduction of the photon energy, E. However, for $E \ll \Delta E_{10}$ the assumption of constant T_{ij}^2 will become erroneous, and it is for this reason that the quantum efficiencies have only been calculated corresponding to a limited photon energy range below ΔE_{1c}.

Considerable use has been made here of the absorption coefficient expressions derived by Haga and Kimura. It is therefore of value to check these expressions by direct reference to experimental absorption coefficient data. The excess absorption in n-GaAs due to inter-valley transitions has been measured by Spitzer and Whelan[54]. Haga and Kimura[41] showed that their own expression for I-type absorption correctly described these results for n-GaAs in respect of the dependence on the wavelength, temperature and on the concentration of free electrons. They did not however calculate the absolute magnitude of the absorption coefficient for comparison with experiment. The fit of the theoretical expression to the experimental results required the assumption of an inter-valley gap of 0.44eV and this is within the limits of uncertainty for $\Gamma_{1C} - X_{1C}$ but not for $\Gamma_{1C} - X_{3C}$ or $\Gamma_{1C} - L_{1C}$. The present author has calculated the absolute magnitude of the absorption coefficient (α_I) as given by the theoretical equation. Taking P_{ij} and E_1^* to have the values assumed previously for ZnSe together with $\Delta E_{10} = 0.44eV$, $m_1^* = 1.2m$[55] and $m_o^* = 0.07m$[55] then, for the conditions $n = 1.3 \times 10^{17} cm^{-3}$, $T = 300^oK$ and a photon energy of 0.44eV, the calculated α_I is $1.2cm^{-1}$. The corresponding experimental result is $0.4cm^{-1}$[54]. In the absence of restrictions imposed by the selection rules LA phonon

scattering would be dominant as in ZnSe and the major indirect path contributing to $\Gamma_{1C} - X_{1C}$ absorption would be $\Gamma_{1C} - X_{3C} - X_{1C}$. With the selection rules applied the above path remains dominant and still involves LA phonon scattering. It was for this path that α_I was calculated. The quantities inserted in the α_I equation were necessarily only rough estimates so that the experimental and theoretical values for the absorption coefficient are satisfactorily close. The calculated D-absorption coefficient (α_D) for the conditions specified above is only $0.01cm^{-1}$ if account is taken of the selection rules. A relaxation of these rules to permit LA phonon scattering in the D-absorption then leads to the result $\alpha_D \sim 0.7cm^{-1}$ for the above conditions.

A check similar to that made for the I-type absorption formula has also been made for the D-type absorption formula. Haga and Kimura[41] showed that their formula for α_D was consistent with the measured[56] wavelength dependence of the absorption coefficient in n-GaSb over the wavelength range $1.5\mu - 4.5\mu$. The gap between the minima of the two valleys forming the initial and final states for the absorption transitions was deduced, from the value required to fit the theoretical dependence of α on wavelength, to be 0.30eV. The lowest valley in n-GaSb is the Γ_1 valley and the next higher but one is the X_1 valley with the $\Gamma_1 - X_1$ gap estimated to lie in the range 0.3 - 0.4eV[57]. The L_1 valley is only 0.1eV[57] above Γ_1 so Haga and Kimura believed that D-transitions occurred between the Γ_1 and X_1 valleys. Estimating necessary quantities in the way used for ZnSe and taking the values $m_o^* = 0.047m$,[57] $m_1^* \sim m$ and $\Delta E_{10} = 0.3eV$ for GaSb the calculated value of α_D for the conditions $n = 4.8 \times 10^{16}cm^{-3}$, $T = 77^\circ K$ and $\hbar\omega = 0.41eV$ is $0.2cm^{-1}$. The measured[56] absorption coefficient for these

conditions is $2.2cm^{-1}$. The quoted theoretical value of α_s was obtained under the assumption that LA phonon scattering is allowed but this in violation of the selection rules[36] for $\Gamma_1 - X_1$ direct transitions. If account is taken of the selection rules then essentially only LO phonon assisted transitions are allowed and the calculated α_s would be reduced to 3% of the value found by disregarding these rules. There is some, admittedly small, evidence therefore that a strict application of the selection rules is excessively stringent and, in support of this view, the calculated quantum efficiency for ZnSe diodes is closer to the measured value if the selection rules are ignored.

To summarize this section it has been shown that the theoretical estimates of the quantum efficiency in ZnSe diodes, as based on the model of inter-valley transitions, are not greatly different to the experimental observations.

3.4.6. Diode response time

The radiative lifetime for inter-valley transitions, τ_R, is simply related to the quantum efficiency (η) because η is the ratio of rates of inter-valley transitions $(n_1 A W/\tau_R)$ to the rate of electron passage through the diode $(n_1 A v_{d_1})$ giving

$$\eta = \frac{W}{\tau_R v_{d_1}} \qquad \ldots\ (3.28)$$

This equation gives, for each of the diodes in which the response time was measured, a radiative lifetime of about 300ns if v_{d_1} is taken as 10^7 cm sec^{-1} and with substitution of measured values for η and W. The observed response time was less then 5.5ns for each diode. The rapidity

of response is therefore determined by non-radiative transitions. An expression for the lifetime, τ_{NR}, for non-radiative transitions has been given by Conwell[58] and in deriving her result it was assumed that electron scattering is by longitudinal acoustic phonons. For other scattering mechanisms the non-radiative lifetimes can be obtained by scaling τ_{NR}^{-1} in the ratios of the appropriate squares of matrix elements found in the last section. The results for $X - \Gamma_{1C}$ transitions are $\tau_{NR} \sim 3 \times 10^{-13}$s for LA phonon scattering and $\tau_{NR} \sim 10^{-11}$s for LO phonon scattering. A weighted average τ_{NR} for $X_{3C} - \Gamma_{1C}$ transitions and $X_{1C} - \Gamma_{1C}$ transitions is close to the shorter of these times. For $\eta \ll 1$ the quantum efficiency is given by

$$\eta = \frac{\tau_{NR}}{\tau_R} \qquad \ldots\ldots (3.29)$$

Substituting $\tau_R = 3 \times 10^{-7}$s and $\tau_{NR} = 3 \times 10^{-13}$s in equation 3.29 gives an estimated value of 10^{-6} for the quantum efficiency attributable to the combined effects of X_{3C} / $X_{1C} - \Gamma_{1C}$ transitions. This is lower than the experimental result for typical diodes by a factor of about 20 but the calculation of τ_{NR} could possibly be in error by that amount.

3.4.7. Temperature dependence of quantum efficiency.

The quantum efficiency, as calculated from the theory of section 3.4.5, may be shown to have a temperature dependence which arises mainly through the temperature dependence of the scattering matrix elements. This is true for the separate D-type and the I-type contributions with their only other temperature dependence attributable to the weak variation of terms higher than the first in the respective expansions given by equations 3.23 and 3.24. Since the theory pointed to the conclusion that almost all of the

radiation from diodes results from electron transitions which are assisted by acoustic phonons the theoretical temperature dependence of the quantum efficiency is deduced to be of the form

$$\eta \propto 2N(q_1) + 1 \qquad \ldots\ldots (3.30)$$

where $N(q_1)$ was defined in connection with equation 3.25. The function on the right-hand side of equation 3.30 has been plotted against temperature in fig. 3.17 and should be compared with the experimentally observed temperature dependence of the relative quantum efficiency as shown in fig. 3.12. At temperatures below 280K there is obviously wide disagreement between theory and experiment, since for cooling theory predicts a decrease in quantum efficiency whilst experiment shows that cooling produces an increase. At temperatures above 280K experiment shows that the quantum efficiency increases with rise of temperature in qualitative agreement with the theory. However, in this latter temperature range, the experimentally observed dependence of the quantum efficiency on temperature is stronger than the nearly linear dependence which is predicted by the theory.

A possible cause for the rise of efficiency with cooling below 280K is as follows. For a given electric field cooling increases the probability of electron transfer from the Γ_{1C} valley to the X_{1C} and X_{3C} valleys. This is because cooling reduces the extent of electron scattering and therefore enhances excitation to higher valleys. Since the Gunn effect has been observed in ZnSe at room temperature[37] and at fields less than those typical of reverse-biassed diodes, electrons in the depletion layer of reverse-

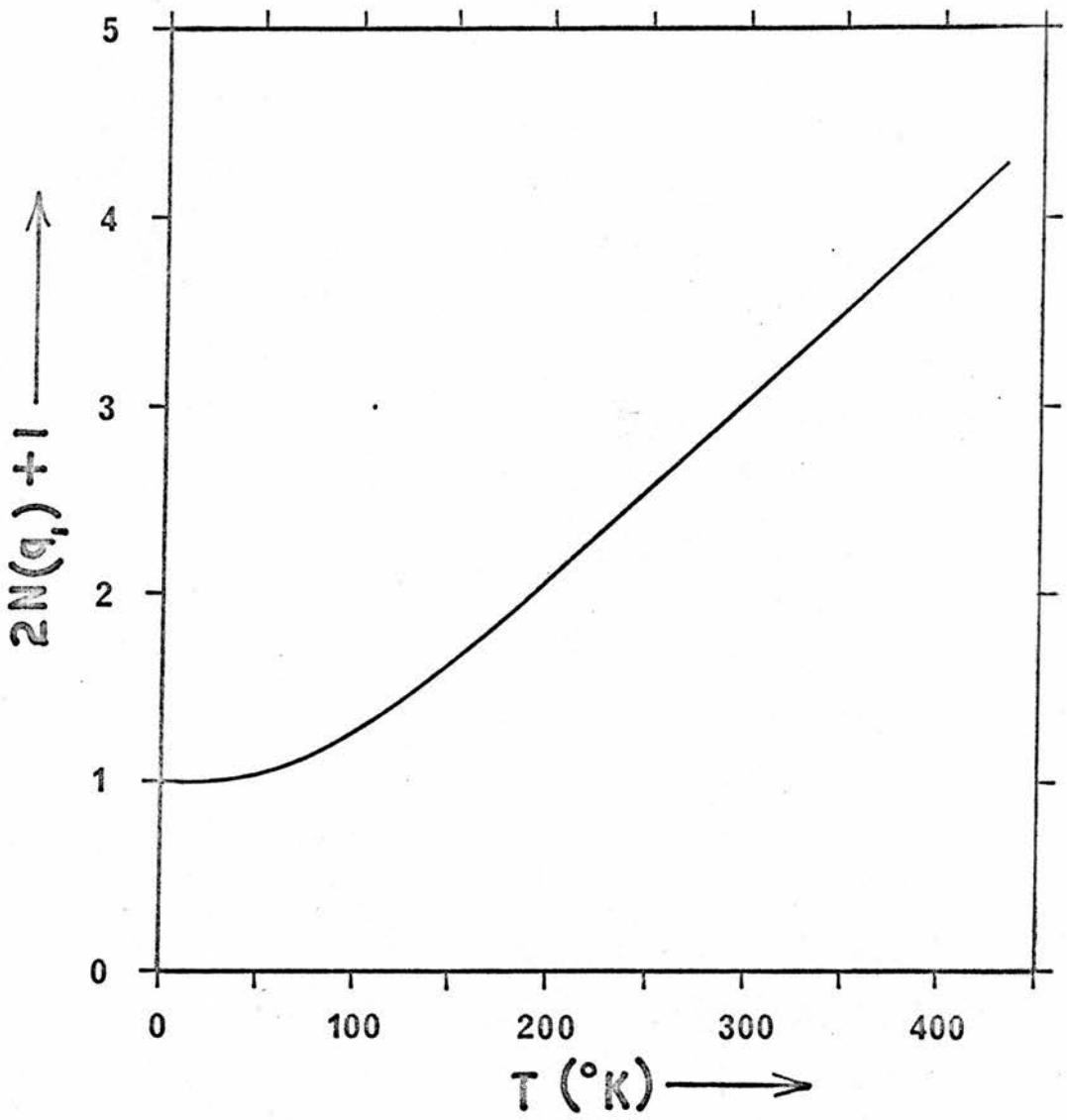

Fig. 3.17 The function $2N(q_1)+1$ which describes the theoretical temperature dependence of the relative quantum efficiency.

$$N(q_1) = \left[\exp\frac{0.0185\ eV}{kT} - 1\right]^{-1}$$

biassed diodes operating at room temperature are almost totally transferred from the Γ_{1C} valley. In view of the knowledge that L_{1C} is lower than X_{1C}, it may be that at room temperature electrons are freely transferred to L_{1C} but that considerable scattering in this valley leads to ineffecient transfer in the next stage up to X_{3C} and X_{1C}. It is suggested that a lowering of the lattice temperature facilitates electron transfer, for a given applied electric field, from L_{1C} to the higher lying X valleys by reason of the reduced electron scattering in the L_1 valley. A combination of the temperature dependence just postulated for the excitation to the X valleys, together with that for the rate of X to Γ_1 transitions for those electrons which reach X, could give a temperature dependence of quantum efficiency for the high energy part of the spectrum qualitatively similar to the experimental observations. Since the wave-vector separation for the L_{1C} and Γ_{1C} points is nearly the same as that for the X_{3C} and Γ_{1C} points (ratio of former to latter is $\sqrt{3}/2:1$) then, if the explanation given above for the temperature dependence of the quantum efficiency is correct, it follows that spectra at high temperatures should be relatively richer in $L_{1C} - \Gamma_{1C}$ transitions compared with those at low temperatures. Unfortunately, this temperature dependence of the spectrum shape cannot be unequivocally tested with the available measurements because these involve large uncertainties in the spectral range of interest. The ratio of the height of the peak due to $L_1 - \Gamma_1$ transitions (at about 0.9eV) to the height of the peak due to the sum of $X_3 - \Gamma_1$ and $X_1 - \Gamma_1$ transitions (at about 1.7eV) is, at room

temperature, greater than 1.5 according to fig. 3.8 and equal to 1.27 according to fig. 3.9. The same ratio for 125K is, for the three individual plots of fig. 3.11, respectively 1.3_2, 1.1_0 and 1.0_6. There is, therefore, some evidence in support of the suggested mechanism. It would be preferable, if possible, to compare areas under the parts of the spectrum curves due $X_3 - \Gamma_1$, $X_1 - \Gamma_1$ and $L_1 - \Gamma_1$ transitions rather than the peak heights. It appears that a larger difference would then be discerned between 125K and 300K spectra but comparison of areas for each contribution to the spectrum is a difficult operation because of overlapping of the $X - \Gamma_1$ and $L_1 - \Gamma_1$ parts of the spectra.

Pilkuhn and Schul[12] noted, for the broad emission spectrum in reverse-biassed GaAs p - n junction diodes, a temperature dependence of the quantum efficiency which, between 300K and 100K (the entire range of their measurements), is very similar qualitatively and quantitatively to the results for ZnSe. The authors suggested that in their diodes both Zener breakdown and avalanche breakdown occurred simultaneously but that radiation was due only to the avalanche component of the current and that this component increased relative to the Zener current on lowering the temperature. The evidence for this was that, in another diode which exhibited pure avalanche breakdown, there was no temperature dependence of quantum efficiency. The argument is not very convincing and is not applicable to the ZnSe diodes of this chapter because it is known that the multiplication is usually small.

In p - n diodes of GaP it has been observed[10]

that the radiation for reverse bias, in the broad band part of the spectrum, has a temperature independent quantum efficiency in the temperature range 80K - 300K. This supported the proposition, made by the authors, that the scattering mechanism was by ionized impurities.

3.5. SUMMARY

The reverse bias electrical behaviour of the diodes shows that the current does not flow by thermal excitation of electrons from the metal contact into the ZnSe. The qualitative behaviour is consistent with electron tunnelling from metal to ZnSe and the discrepancy from the quantitative results is thought to be due to a thin layer of insulating material which prevents intimate metal-semiconductor contact.

The light emission has been shown to result from electron transitions within the conduction band. The evidence is very heavily in support of the postulate that these transitions are between valleys of the conduction band since this enables the general spectrum shape to be explained and leads to a theoretical quantum efficiency of a similar magnitude to the measured values.

There are a few experimental observations which have not been satisfactorily explained. One such experimental observation is that the quantum efficiency per unit barrier width varies with donor density as $\eta/_W \propto N_D^{0.6}$ for a wide range of donor density. Since it is thought, from other evidence, that the principal scattering mechanism is by acoustic phonons, η/W is expected to be independent of N_D. Even if ionized impurity scattering

was important there would still be a discrepancy because then the expected variation of η/W with N_D is $\eta/W \propto N_D$. It cannot be that ionized impurities and another imperfection type act together with about equal scattering efficiency to produce the observed η/W vs. N_D dependence because then a law of the form $\eta/W \propto N_D^{0.6}$ would only hold over a very limited range of N_D. The observed temperature dependence of the relative quantum efficiency has not been explained in a fully satisfactory way. A further cause of concern is that, from fig. 3.15, the spectrum appears to be of the form for I-transitions but the considerations that led to the data of table 3E suggest that in the range covered by fig 3.15 the major part of the light is due to D-transitions. A relaxation of the selection rules would, however, largely remove this difficulty.

Apart from the above noted deficiencies there has been a large measure of success in explaining the behaviour of the diodes forming the subject of this chapter. An analysis of spectra observed in reverse biassed diodes, of material with a sufficiently low density of luminescence centres, is a potentially valuable method for checking band structure calculations and should be applicable in many semiconductors. This method of probing band structure has not been previously discussed in the literature.

4. REVERSE BIAS ELECTROLUMINESCENCE IN Mn-DOPED ZnSe SCHOTTKY DIODES.

4.1. INTRODUCTION

In chapter 3 results were presented and discussed for the reverse bias behaviour of Schottky diodes prepared from ZnSe with no luminescence centres deliberately added. The inclusion of suitable luminescence centres greatly enhances the reverse bias electroluminescence efficiency and modifies the spectrum to a form characteristic of the added centres. Since ZnS is very similar in its properties to ZnSe and the yellow luminescence band in the ZnS:Mn system has been extensively studied it was natural to consider adding Mn as a luminescence centre in ZnSe.

One aim of the work described in this chapter was to gain a greater understanding of the mechanism of reverse bias electroluminescence in ZnSe:Mn with a view to using the knowledge in improving the diode performance as a practical device. The colour of the light from reversed-biassed ZnSe:Mn diodes is yellow and is much more nearly monochromatic than for the diodes discussed in chapter 3.

4.2. EXPERIMENTAL RESULTS

Several different batches of ZnSe, which were doped both with Al donors and Mn centres were available for the experimental measurements. In materials designated by MAI and DM the proportion of manganese compound added at the material preparation stage was calculated to give 0.5 atom % of Mn in the final product. For 26Cl and 36Bl materials the manganese concentration is substantially less than for the above batches but neither the concentration in the product nor the proportion of manganese compound added in the preparation are known.

The experimental information collected for the reverse bias operation of these Mn-doped diodes includes the current-voltage characteristics, the relative light intensity as a function of current and as a function of voltage, the emission spectrum, the time response of the light emission for step changes in the applied voltage and the external quantum efficiency.

The majority of diodes were prepared with Au as the metal of the rectifying barrier and, unless otherwise stated, it may be assumed that this metal was used.

4.2.1. Electrical properties

The differential capacitance (C) was measured as a function of applied bias (V) at several frequencies in the range 200Hz to 100kHz for a large number of diodes. Plots of C^{-2} against V were linear with an intercept on the voltage axis, for the measurements made at 100kHz, which ranged from 1.45 volts to 5.1 volts. A few Al-contact diodes were measured and these also gave linear plots with intercepts on the voltage axis towards the lower end of the range stated above. Most diodes exhibited less than 30% change in dC^{-2}/dV over the frequency range 200Hz - 100kHz but a few showed a change, for the same frequency range, of about an order of magnitude. For diodes in which there was a detectable frequency dependence of dC^{-2}/dV this derivative had lower absolute value as the frequency was reduced as for the diodes of chapter 3.

The donor concentration, deduced from the slopes of C^{-2} against V plots, for measurements made at 100kHz, varied between diodes from $7 \times 10^{20} m^{-3}$ to $3.5 \times 10^{24} m^{-3}$.

Typical current-voltage characteristics for an MAl diode at room temperature are shown in fig. 4.1 together with the light-voltage characteristics for the same diode. The behaviour of diodes made from other batches of Mn-doped ZnSe are similar. Referring to the figure, the current is seen to vary exponentially with the applied voltage for a range of about four decades of the current above 1μA. At a current of about 10mA, which is beyond the range of the figure, curvature develops for typical diodes in semilogarithmic plots of current against voltage and this curvature is due to the series resistance of the diode chip. A departure from exponential variation of the current with the applied voltage at low currents such as exists below 1μA for the diode of fig.4.1 is often, but not always, observed in Mn-doped ZnSe diodes. For some diodes the curvature at low currents is in the opposite sense to that shown in fig 4.1 and

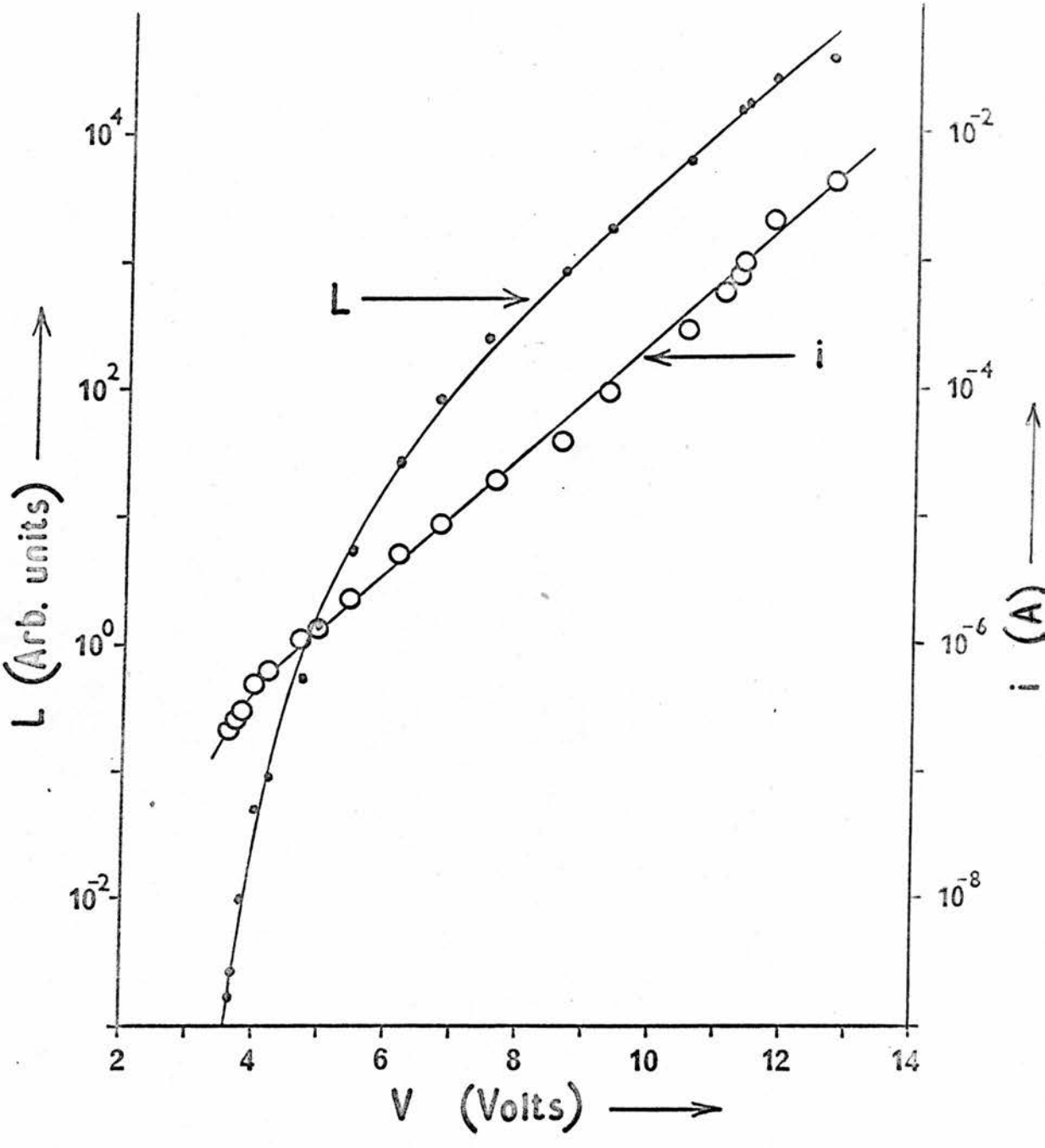

Fig. 4.1 L and i as functions of reverse bias in an MA1 diode at room temperature.

in those cases is attributed to shunt leakage.

The temperature dependence of the current-voltage characteristics is shown by the broken curves in fig 4.2. Lowering of the temperature at fixed voltage increases the reverse current as for diodes without deliberately added luminescence centres. At fixed current the voltage changes with temperature at a rate, $\partial V/\partial T\Big|_i$, of 1.0×10^{-2} V K^{-1}. This is about half the value found for diode without intentionally added luminescence centres.

4.2.2 Light emission as a function of voltage and current

From fig 4.1 it will be observed that after an initial steep rise of the light emission (L) with increasing voltage (V), ln L varies linearly with V. The data given for the L-V characteristic of fig 4.1 were obtained by measuring the output of an S20 response photomultiplier placed with its photocathode close to the diode. Since, at sufficiently small values of L, the rate of increase of L with V is very strong it is meaningful to speak of a threshold voltage for light emission. In the case of the diode shown in fig 4.1 this threshold is approximately 3.5 volts and threshold voltages close to this value have always been found. The shape of the L-V characteristic of fig 4.1 is in marked contrast to the results for diodes without intentionally added luminescence centres where it was found that ln L was linear with voltage down to the lowest measurable emissions. The same apparatus and geometry were used for both types of diode and the lowest light emission measurements represented in figs 3.5(a) and 3.5(b) for non-intentionally doped diodes were of similar magnitude to the equivalent lowest measurement shown in fig 4.1. For Mn-doped diodes, at voltages above the threshold region, there is a linear dependence of ln L on V and in this linear region L is approximately proportional to the current. This last mentioned result is shown by the approximate parallelism of the L-V and i-V characteristics in the appropriate voltage range in fig 4.1 and corresponds to a current range from 10μA to at least 5mA. At currents in excess of about 10mA the light emission varies less rapidly than linearly with the current and this result remains valid for diodes suitably pulsed to avoid heating effects. Fig 4.3 shows, for a certain

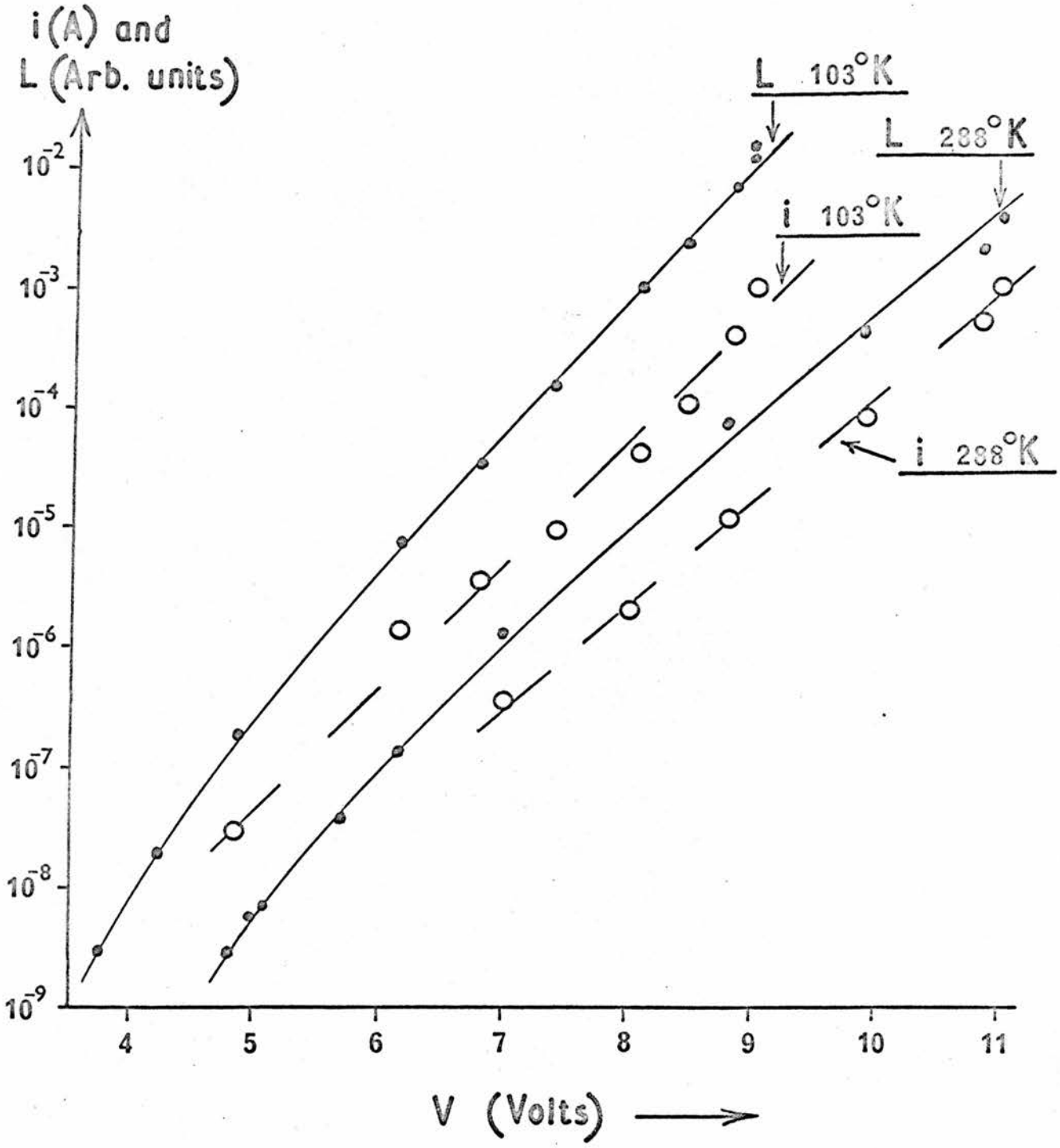

Fig. 4.2 L and i as functions of V for two temperatures of a Mn—doped diode

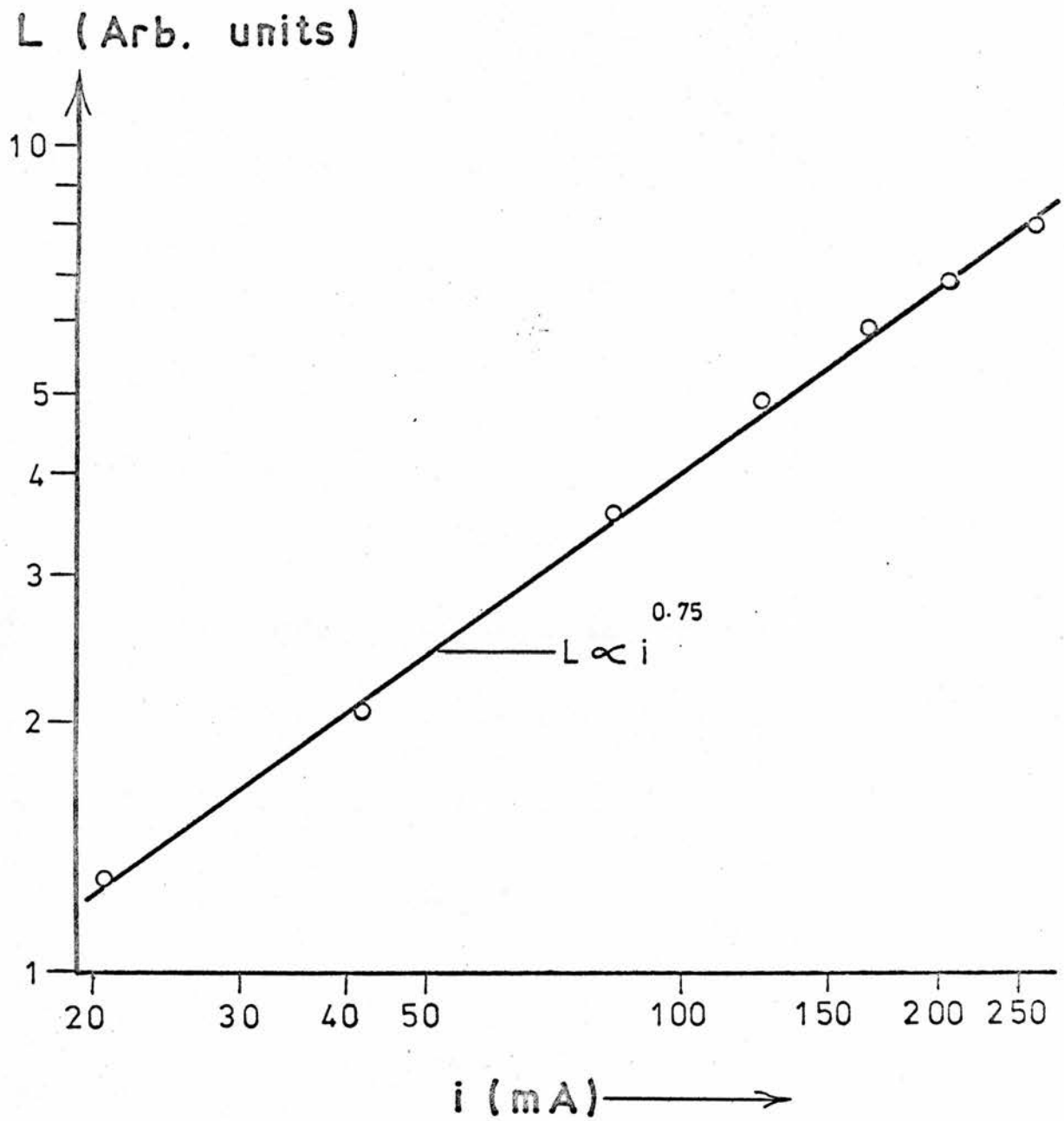

Fig 4.3 Variation of L with i. Measured for a pulsed 36B1 diode [P.W. = 10 μs , duty cycle = 6 %]
L was measured only for 2.1 eV photons.

36B1 diode, the observed variation of light emission with current for pulse currents (10μs pulse width, 6% duty cycle) in the range 20mA to 260mA. The relative light emission was measured after passage of the light through a spectrometer set to pass a band narrow compared with the spectral width and centred at the wavelength corresponding to the low current spectrum peak. From the figure the relationship $L \propto i^{0.75}$ is seen to be a good description of the results.

Referring to the light-voltage characteristics of fig 4.2 it appears that the threshold voltage for light emission shifts to lower voltages with cooling of the diode. The result is not entirely clear since a very steep rise of L with V was not observed, due partly to the diode characteristics and also because very low light emission levels were not explored as a consequence of the apparatus limitations.

From fig 4.2 it is seen that lowering of the temperature at fixed current increases the light emission. Since cooling also lowers the voltage for a fixed current, there is a larger increase in power efficiency on cooling than there is for the quantum efficiency.

4.2.3. Spectrum for reverse bias emission

Spectra for reverse bias in an MA1 diode are shown in fig 4.4. The peak of the spectrum is at 2.10eV for room temperature and shifts to 2.12eV on cooling of the diode to 118K. The spectra, which have been normalized to the same peak height, were for currents of about 2mA. As always, throughout this thesis, the spectra have been corrected for the response of the measuring apparatus. The width of the spectrum at half-height is reduced from 0.19eV to 0.13eV by cooling from room temperature to 118K. The result reported here for the shift in peak position is not much more than the uncertainty in the energy of the peak, but since the same shift has been observed several times and in different diodes it is believed that there is a genuine small shift on cooling.

Diodes made from all of the material batches tested (ie. MA1, DM, 36B1 and 26C1) consistently exhibited a room temperature peak in reverse bias at

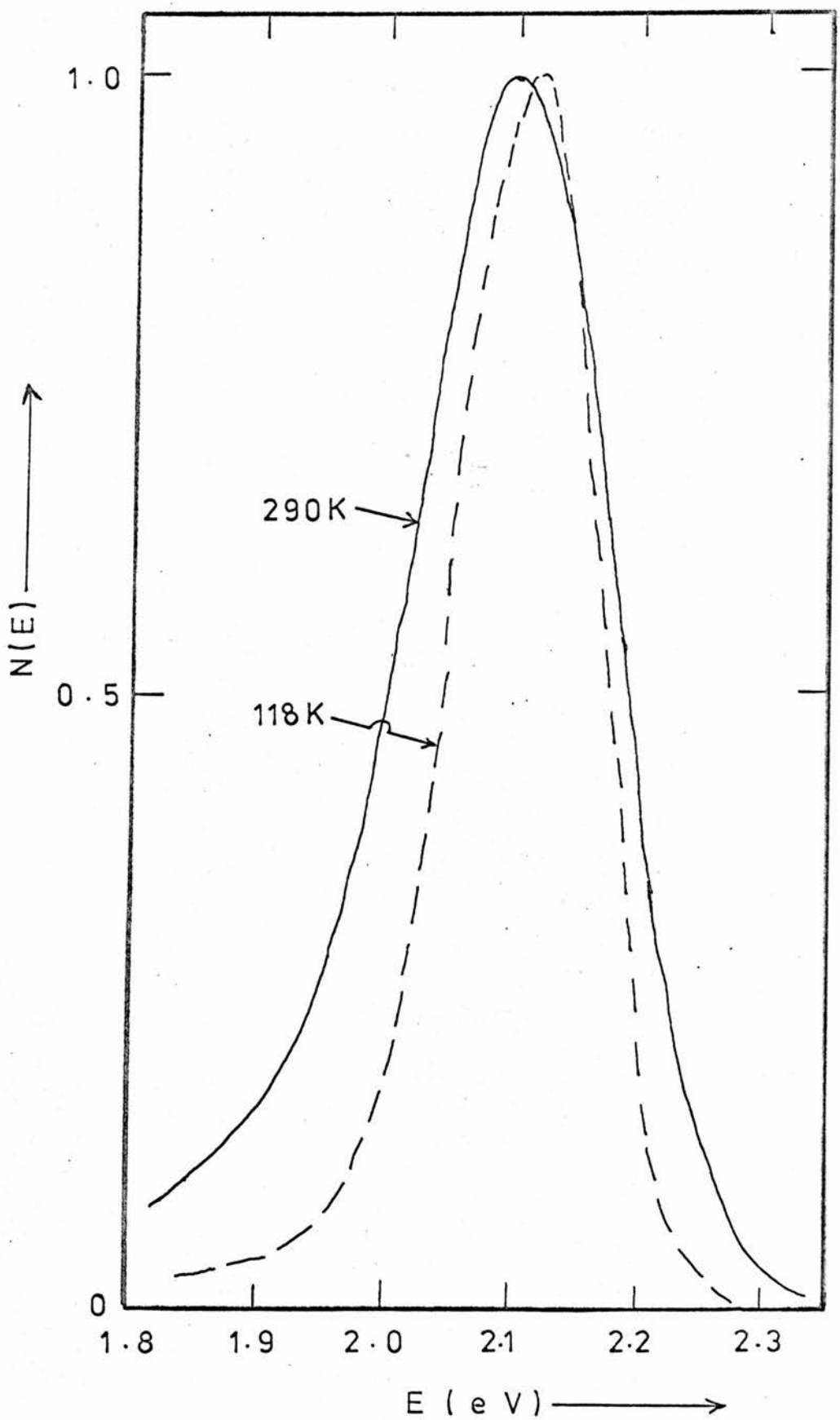

Fig. 4·4 Reverse-bias spectra, normalized to a common peak height, for two temperatures of an MA1 diode.

2.11±0.01eV and a width at half-height of 0.20±0.02eV, where the width is given for a current of about 1mA. The integrated luminosity of the room temperature spectrum, as excited with a reverse current of about 1mA, is 450 lumen watt^{-1}. Diodes with Al contacts give identical spectra to Au-contact diodes when both are measured at room temperature and this is the only temperature for which spectra of Al-contact diodes have been measured. There is no observable change in the spectrum for currents between 40μA and 1mA. The lower current limit quoted is the current at which the light output from typical diodes is just sufficient to obtain useful spectrum measurements with the apparatus that was available.

For currents greater than a few mA, in the diodes of lower Mn concentration, some asymmetry develops in the shape of the emission spectrum. This is illustrated in fig. 4.5 where it is shown that with increase of current the spectrum becomes relatively richer in the lower energy tail of the spectrum. By making spectrum measurements at lower energies than those shown in the figure it has been concluded that the increase in the low energy tail of the spectrum is due to transitions of electrons within the conduction band as discussed in the preceeding chapter. From time-resolved spectrum measurements of pulse operated diodes it was found that the spectrum, corresponding to a time of a few micro-seconds after the last current falling edge, did not contain the additional low energy contribution although the spectrum excited whilst pulses were on did contain this contribution.

The photoluminescence spectrum for Mn-doped ZnSe at room temperature and excited by 365nm light is shown in fig. 4.6. The peak of the spectrum is at 2.00eV and the width at half-height is 0.44eV. A very similar spectrum is also excited in forward bias. For reasons to be given in the discussion it is believed that the photoluminescence and forward bias spectra are not due to transitions involving Mn but that the observed reverse bias spectrum is due to the presence of Mn. In appendix I data for luminescence bands excited by various means in ZnSe with various dopants, including Mn, are given.

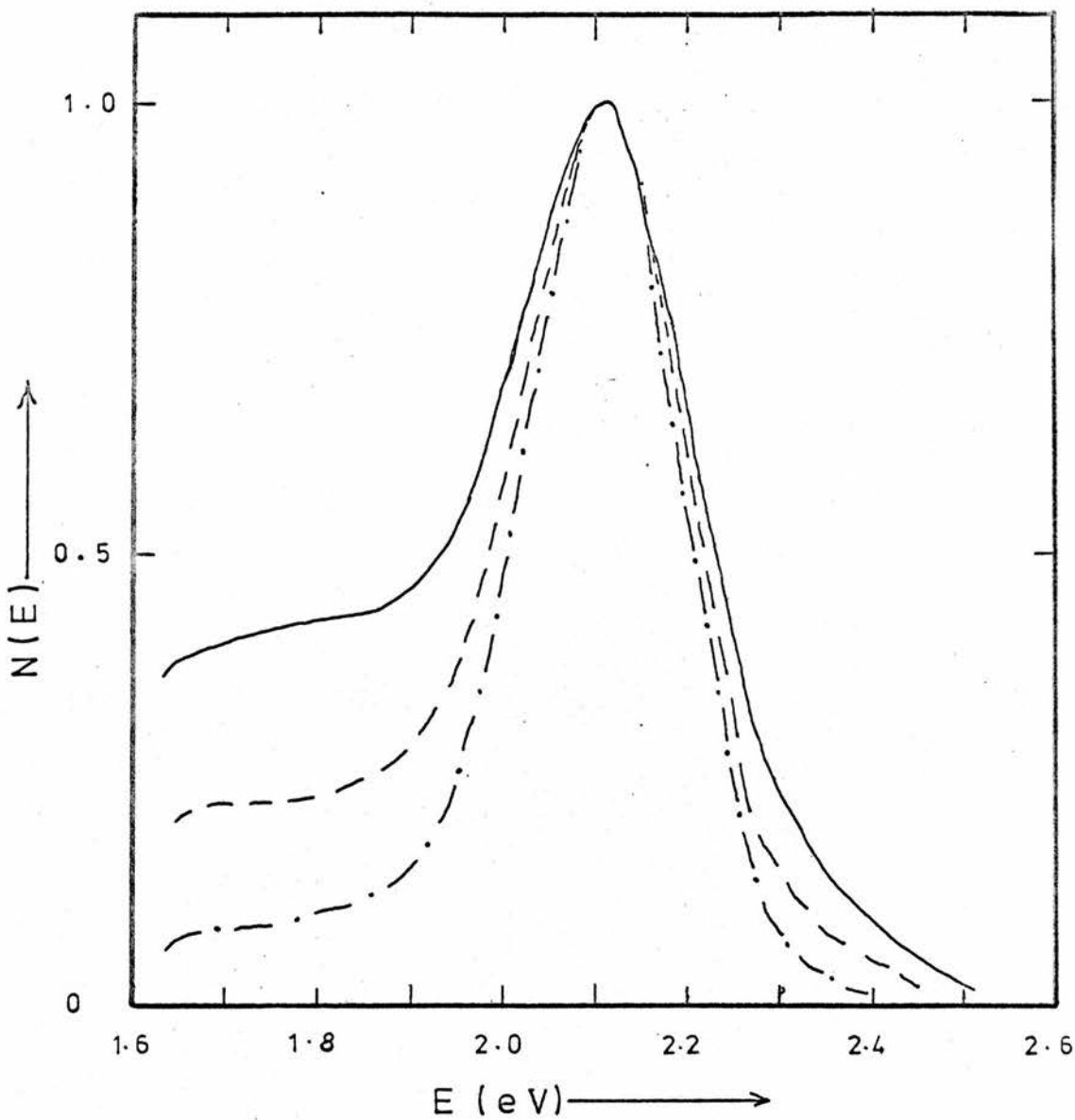

Fig. 4.5 Spectra for 3 currents in a 36B1 diode. The spectra are normalized to a common peak height.

——— i = 25.5 mA

— — — i = 9.6 mA

— • — i = 1.5 mA

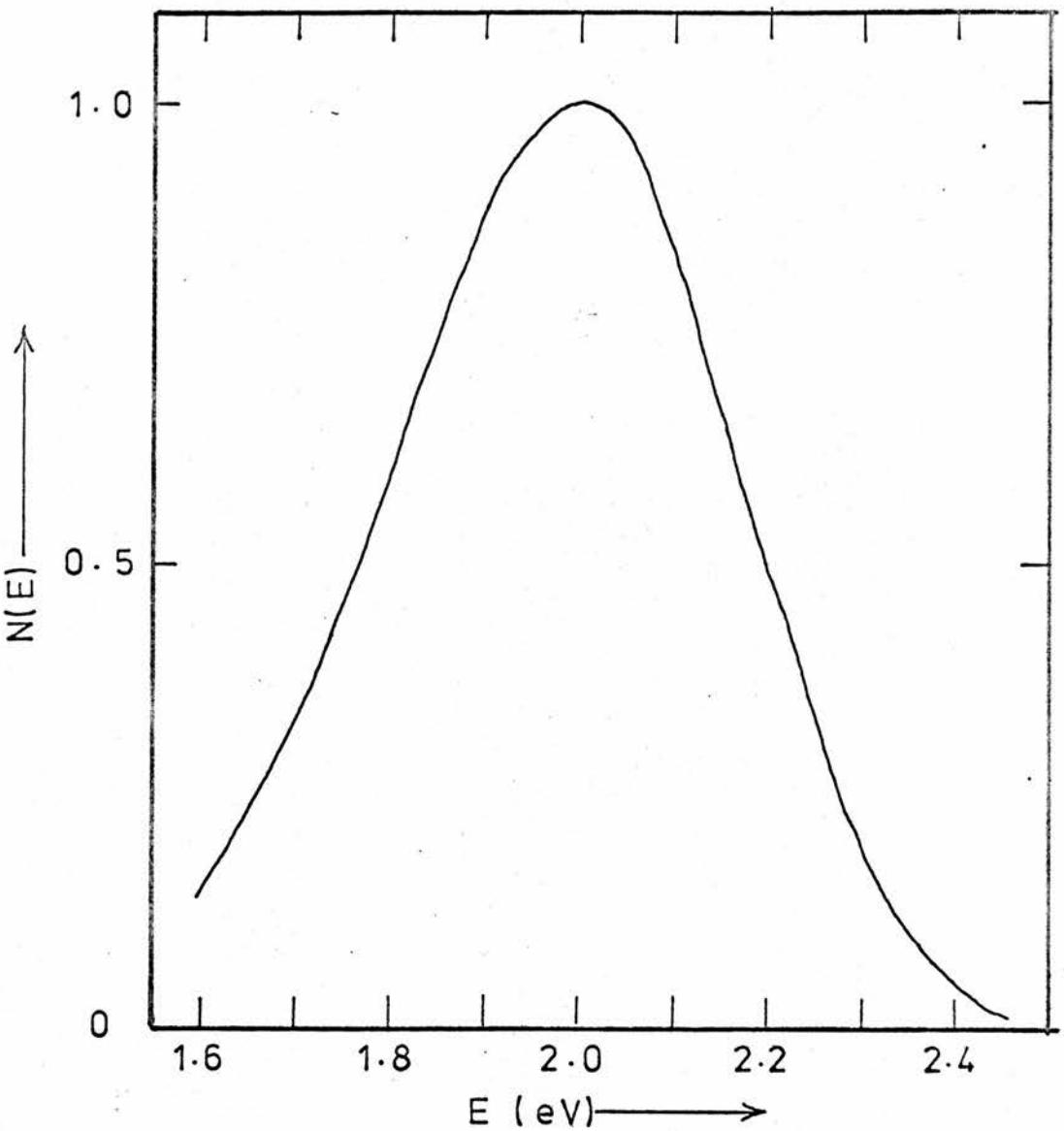

Fig. 4.6 Photoluminescence spectrum in 36B1 material.
[T = 290K , $\lambda_{exciting}$ = 365nm]

4.2.4. External quantum efficiency and external power efficiency

The current-voltage characteristics for reverse bias are sufficiently hard, that to a good approximation, the current for which any given diode exhibits a maximum quantum efficiency is also the current for a maximum power efficiency. The largest measured quantum efficiency in the diodes tested was 8.0×10^{-4}. This was for an MA1 diode at a current of 4.0mA. The power efficiency, expressed in photometric terms, for this diode and at the same current was 52 millilumens watt^{-1}. The largest observed power efficiency in any diode was 56 millilumens watt^{-1} and this was for a DM diode at a current of 10.0mA. For this DM diode the quantum efficiency at 10.0mA was 4.0×10^{-4}. The reason why the MA1 and DM diodes referred to differ by a factor of two in their maximum quantum efficiency and yet have almost the same power efficiency was because the DM diode reached its optimum performance at very nearly half the voltage for the optimum performance of the MA1 diode. The highest power efficiency observed in any 36B1 diode was 13 millilumens watt^{-1}. This was for a current of only 0.4mA although the maximum in a plot of light output as a function of current was broad and at 4mA the power efficiency was 10 millilumens watt^{-1}.

4.2.5. Relative quantum efficiency as a function of temperature

It has already been noted in section 4.2.2 that cooling of a diode increases its quantum efficiency. In this section more detailed results for the temperature dependence of the relative quantum efficiency are given.

The variation of the light emission with temperature for fixed current in a diode of MA1 material is shown in fig. 4.7. Qualitatively similar results have been found for a diode of 36B1 material. From fig 4.7 the ratio of the maximum relative quantum efficiency to the room temperature value was 1.6. The corresponding ratio for the only tested 36B1 diode was 3.3.

4.2.6. Light rise and decay times

For step application of a reverse bias to typical MA1 diodes at room temperature the light rises to 25% of its final height in 3μs and to 90% in about 80μs. No components of the light rise were present with time constants

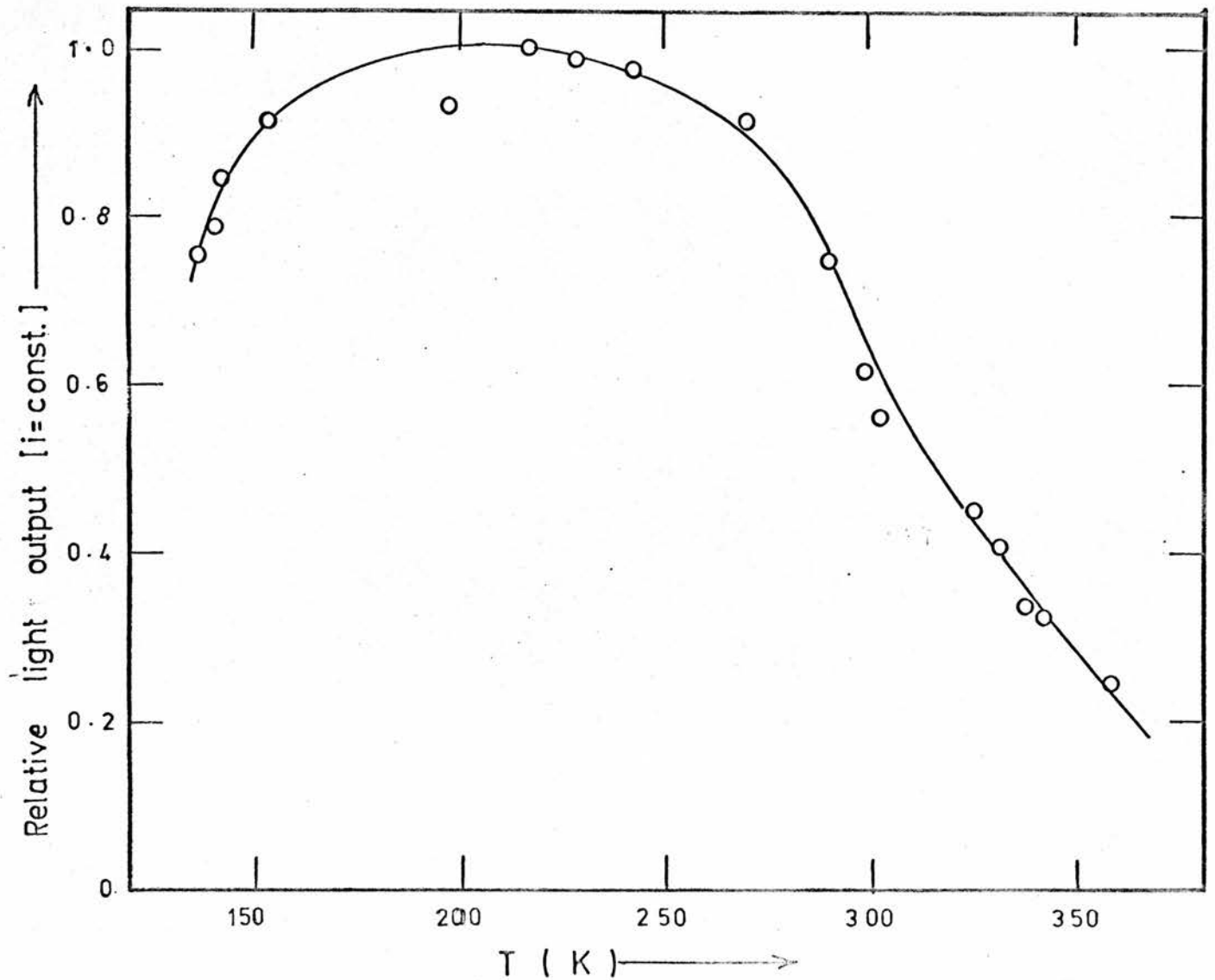

Fig. 4. 7 Relative light output as a function of temperature.[MA1 diode ; i=4mA]

of less than 1μs. On the falling edge of a light pulse similar time constants as in the rise were evident with a typical fall time (100% - 90%) of 50μs. The luminescence emission during the whole of the decay remained in the same spectral band as for D.C. diode operation. The current response time on both rising and falling edges was less than 6ns.

Diodes of 36B1 material have been similarly tested and had a current rise and fall time also each less than 6ns. The majority of these diodes exhibited, for an applied voltage pulse, a light rise to about 20% of the final level in a time less than 20ns. This was followed by much slower components, having time constant of a few μs. On the falling edge the light decayed to about 25% in a time of less than 50ns and was followed by a decay which took a few μs to reach essential completion. As mentioned in section 4.2.3, the spectrum during the decay is similar in peak energy to a D.C. spectrum but after a decay time of 1μs, and possibly also after a much shorter decay time, the low energy tail contribution, such as is seen in the D.C. spectra of fig 4.5, is absent. From spectrum measurements it has been shown that the spectrum excited in the relatively sharp initial rise is richer in this low energy contribution than a D.C. spectrum for the same current.

A few 36B1 diodes exhibited a rise of light which was complete in 20ns and the spectrum excited immediately at the end of this time was shown to be identical to that found for steady excitation in all 36B1 diodes.

It was discovered that the light decay time, following pulse excitation in MA1 diodes, was increased if the diode temperature was reduced. The light rise was similarly affected by temperature change and these results were also true of those 36B1 diodes which showed time constants of more than about 1μs. In fig 4.8 results are shown for the temperature dependence of the decay time in a certain MA1 diode for a constant pulse current. The semilogarithmic plot in the figure has for the ordinate the reciprocal of the time taken for the light to decay to 20% of its initial intensity, and for the abcissa, the reciprocal of the absolute temperature. This form of plot was chosen since qualitatively the results

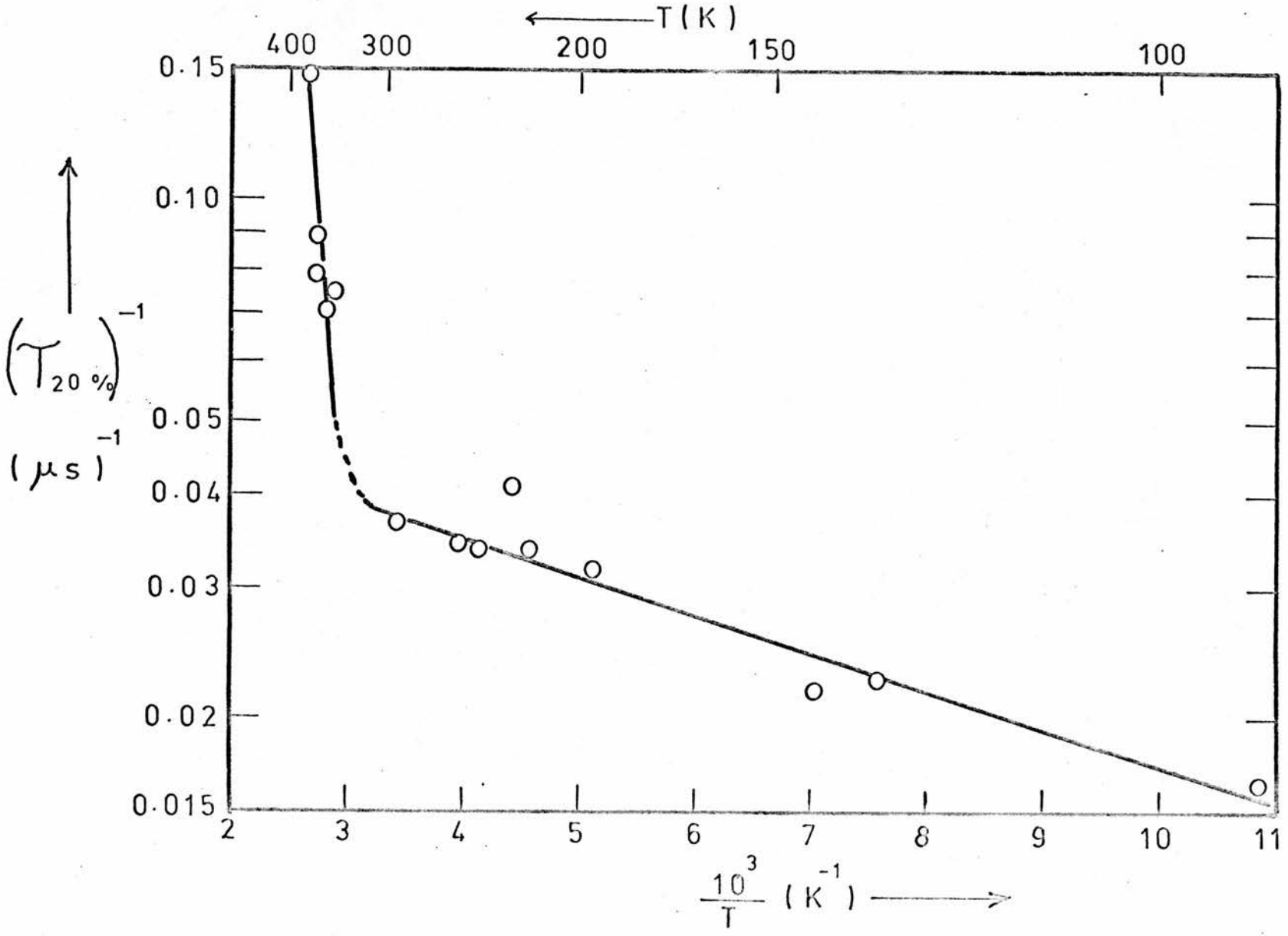

Fig. 4.8 Temperature dependence of time, $\tau_{20\%}$, for light to decay to 20%. [MA1 diode, i=const.]

were consistent with a thermally activated trap-emptying mechanism. If this interpretation is correct, then from the figure, the principal activation energies involved are 0.40eV and 0.010eV.

4.3. DISCUSSION

4.3.1. Properties of a predominantly electrical character.

It has been shown by Livingstone[59] and by Allen et al.[60] that, in n-type ZnSe doped with Mn, the necessary field for the onset of multiplication is lower than in n-type ZnSe of the same donor concentration but without deliberate luminescence centre doping. At approximately the field corresponding to the onset of multiplication in the latter material a second threshold is observed in the Mn-doped ZnSe. These results show that the minimum field necessary for impact ionization of the Mn centres is lower than that necessary for impact ionization of the ZnSe lattice. With a steady increase of the applied field in Mn-doped material the first multiplication threshold is due to impact ionization of the Mn centres and the second threshold is due to impact ionization of the host lattice. The multiplication measurements were made in n-ZnSe:Mn Schottky barrier structures and the lower multiplication threshold voltage was coincident with the light emission threshold voltage as deduced from a plot of the form of fig. 4.1. Light emission is evidently connected with impact ionization of Mn centres but, for reasons to be given later, the radiative transitions are not thought to be de-ionization transitions. It was shown in the preceding chapter that in fields similar to those pertaining in operating Mn-doped diodes, but in the absence of intentionally added luminescence centres, electrons reach an energy as high as 2.65eV above the conduction band edge. In the presence of a sufficient concentration of Mn centres it is expected that electrons in the Γ valley will have a high probability of interacting with these centres before acquiring the necessary energy to transfer to higher valleys. In 36B1 and 26C1 diodes an appreciable fraction of the free electrons do reach the higher conduction band valleys, certainly up to X_1 and probably also to X_3 as is shown by spectra for

currents in excess of a few mA. In the more heavily Mn-doped MAl and DM materials the emission is almost entirely restricted to the band centred on 2.11eV, at least for currents up to 10mA.

From fig. 4.2, the temperature dependence of the current in Mn doped diodes at a constant applied reverse voltage is weak, but from figs. 4.1 and 4.2, the voltage dependence of the current at constant temperature is strong. This behaviour is similar to that observed in diodes without the intentional incorporation of luminescence centres and therefore, by the same reasoning as presented for this latter type of diode, the injection current for reverse bias in Mn-doped diodes is also a tunnel current.

Referring again to fig. 4.2, it appears that the threshold voltage for light emission shifts to lower voltages as the diode temperature is reduced. This dependence is expected, for as the temperature is reduced the electron scattering in the Γ valley of the conduction band is also reduced and, therefore, a smaller applied voltage is necessary for the electrons to attain sufficient energy to interact with the Mn centres.

According to the model discussed here the incorporation of Mn as luminescence centres enhances the multiplication for a given field. It is therefore expected that for a given current density and a given donor concentration the applied reverse bias would be smaller for diodes containing Mn than for those essentially free of luminescence centres. In fig. 4.9 the necessary applied reverse voltage for a fixed reverse current density of $2mA/mm^2$ is plotted against the donor concentration for diodes with Mn addition and also for those without any deliberately added centres. The points shown for the latter type of diode are reproduced directly from fig. 3.4 of the last chapter. Although, in fig. 4.9, the points for any particular batch of material are scattered about a curve which would give the best fit, the addition of Mn does have the

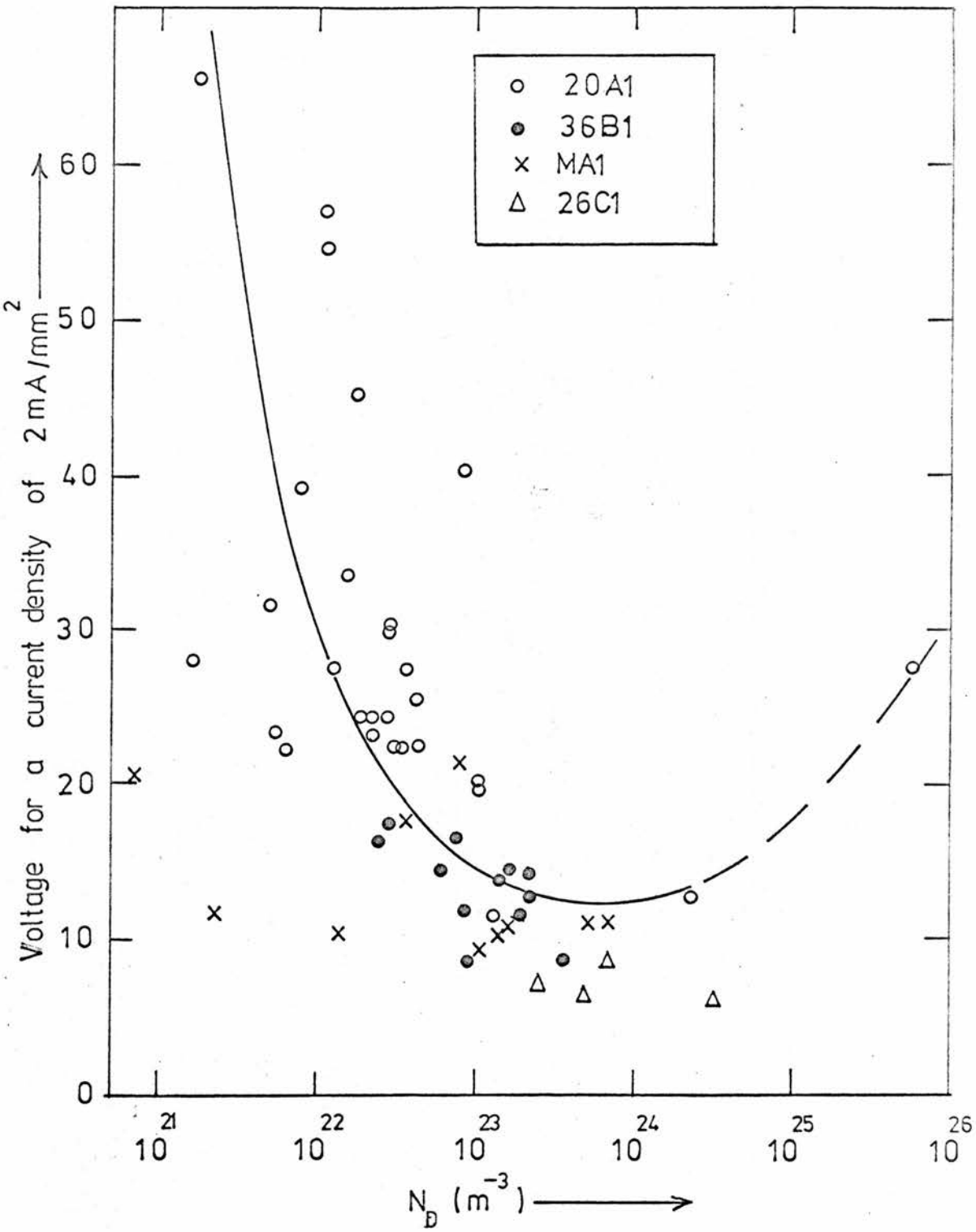

Fig. 4.9 Voltage for a current density of 2 mA/mm^2 as a function of N_D in diodes of different ZnSe preparations. A curve has only been drawn in for 20A1 diodes. 20A1 contains no deliberately added luminescence centres. 36B1, 26C1 and MA1 contain Mn.

predicted effect. Within the range of scatter for different types of points in fig. 4.9, the points representing diodes of the highest Mn concentration (MA1) lie along the same curve as for the diodes made from the less strongly Mn-doped 26C1 and 36B1 materials. This last result is surprising because it is to be expected that an increase of Mn concentration at fixed donor concentration would lead to a reduction in the voltage necessary for a given current density.

4.3.2. Comparison of the reverse bias electroluminescence spectrum with the spectrum in photoluminescence and with luminescence spectra obtained by other workers

In all of the batches of Mn-doped ZnSe the peak of the reverse bias spectrum for room temperature is at 2.11 ± 0.01eV.

The photoluminescence peak in ZnSe:Mn:Al, measured only for 36B1 material, is at 2.00eV and the spectrum is shown in fig. 4.6. In obtaining this spectrum the phosphor was at room temperature and excitation was by light of wavelength 365nm. A band peaking at 2.02eV has been observed in forward bias of both 36B1 and DM diodes at room temperature, but for the same excitation conditions in MA1 diodes, a different spectrum is excited. The forward bias electroluminescence band in 36B1 and DM diodes, together with the photoluminescence band of 36B1, are, apart from their similarity in peak position, also very similar in width. The widths of these bands are greater than for the spectrum excited in reverse bias electroluminescence of Mn-doped ZnSe diodes. Ryall[61] has observed a band, excited in forward biassed ZnSe diodes without deliberate luminescence centre doping, which has a peak at 1.99eV. A tabulation of all these results is given in appendix I. Several authors[62-67] have described a photoluminescence band which they have observed near 2.00eV and which they have attributed to a self-activated process, possibly involving Zn vacancies as the luminescence centres. There is thus some evidence that the observations, in the present work, of bands near 2.00eV are

due to a common transition and that Mn is not involved in this transition.

A band at 1.90eV is observed in forward bias of MA1 diodes. A spectrum which is, to within experimental accuracy, the same as this both as regards the width and the peak energy, has been observed in the present work for room temperature photoluminescence of Mn doped ZnSe (36B1') which had not been subjected to a normally given treatment in molten Zn and not rendered conducting. The treatment in Zn is known[68] to be effective in removing Cu impurity and, in the course of the work described in chapter 6, a band at 1.90eV was noted in Cu-doped ZnSe excited either in reverse bias electroluminescence, forward bias electroluminescence or photoluminescence. For each of these methods of excitation in ZnSe:Cu the 1.90eV band had a width roughly the same as the described 1.90eV bands in ZnSe:Mn. There is thus some evidence that the 1.90eV bands in Mn-doped ZnSe are due to Cu impurity. A weak point in the argument, however, is that MA1 material was subjected to Zn treatment. The concentration of Cl in MA1 was higher than in the other Mn-doped ZnSe preparations hence it is possible that the 1.90eV band observed in forward bias of MA1 diodes is due to Cl.

There is a wide spread in published reports for the photon energy corresponding to the peak of the luminescence band in ZnSe:Mn. Langer and Richter[69] observed a photoluminescence band with a peak at 2.13eV for ZnSe:Mn at 4.2K. In cathodoluminescence, Larach[70] reported a band with a peak at 2.09eV in ZnSe:Mn at room temperature. These two results are close to the reverse bias electroluminescence peak in the present work but other reports for the peak, as excited by 365nm light at room temperature, include 1.95eV[71], 1.92eV[67] and 1.91[72]eV, with the band in all cases attributed to Mn. For none of the references(62) - (72) is it known if corrections for the measuring system response were applied.

The results for the luminescence band in cubic ZnS:Mn are much less ambiguous than in cubic ZnSe:Mn and hence, in an attempt to identify which, if any, of the luminescence bands observed in ZnSe:Mn are due to Mn, analogies will be made with ZnS:Mn. Absorption measurements for ZnS:Mn at 4.2K show three absorption bands with peaks at 2.34eV, 2.48eV and 2.68eV[73]. To within $\pm$0.01eV the same absorption energies are found for ZnSe:Mn at 4.2K[69]. It is emphasised, for future reference, that in neither material is there evidence of an absorption band at a photon energy less than 2.34eV. Since the absorption bands in ZnSe:Mn and ZnS:Mn are very similar then it is expected that the emission bands in the two materials would be similar. In ZnS:Mn Asano et al[67] observed, in photoluminescence, a band which peaked at 2.11eV, both for 80 K and for 300K. Leverenz[72] found the emission peak in ZnS:Mn at 300K for both photoluminescence and cathodo-luminescence to be at 2.11eV. The emission peak for ZnS:Mn is, therefore, very close in energy to that observed in the present work for reverse bias electroluminescence in ZnSe:Mn. This suggests that the reverse bias electroluminescence peak is indeed due to Mn.

Emission peaks in phosphors are at a slightly lower energy than the corresponding absorption peaks, hence the emission observed in reverse bias electroluminescence is probably the reverse transition to that involved in the 2.34eV absorption. If this is correct, then since 2.34eV is the lowest absorption peak, the emission peaks observed in the present work at 1.90eV and 2.00eV do not have an absorption counterpart attributable to Mn and these emission bands are then concluded to be not due to Mn.

4.3.3. Transitions involved in ZnSe:Mn reverse bias electroluminescence

The absorption band near 2.34eV in both ZnS:Mn and ZnSe:Mn has been identified[69,73,74] as due to the $^6A_1 - {}^4T_1$ internal transition characteristic of Mn in tetrahedral co-ordination. Similarly, the

2.11eV emission[69] in ZnSe:Mn has been identified as the $^4T_1$-$^6A_1$ transition. It follows from the discussion of the last section that the reverse bias electroluminescence band in ZnSe:Mn is due to Mn internal $^4T_1$-$^6A_1$ transitions.

From photocapacitance measurements it has been shown[75] that there is a level due to Mn in ZnSe:Mn at 0.6eV above the valence band edge. If this level is the ground state ($^6A_1$) for the reverse bias electroluminescence emission, then, since the band gap of ZnSe is 2.7eV, the upper state for this emission is close to the conduction band edge and the states populated in the 2.34eV and 2.68eV absorption transitions from the Mn $^6A_1$ state would be degenerate with states in the conduction band.

For the $^6A_1$ - $^4T_2$ (2.34eV) and $^6A_1$ - $^4A_1$ (2.68eV) absorptions in ZnSe:Mn at 4.2K Langer and Richter [69] observed zero phonon lines of about 1Å width. Closely similar results have also been observed by Wray[76]. Langer and Richter[69] observed zero phonon lines of 2Å width for $^4T_1$ - $^6A_1$ emission transitions at 4.2K but neither they or Wray observed zero phonon absorption lines for the reverse transition, almost certainly because these were too weak to detect. Absorption lines as sharp as 1Å for transitions to states degenerate with the conduction band would only be observed if there is a barrier to autoionization, since without such a barrier the absorption lines would be strongly lifetime broadened. A line width of 1Å corresponds to a lifetime in the excited state exceeding 2×10^{-12}s. Two possible forms of auto-ionization barriers are shown in figs 4.10(a) and 4.10(b). In the barrier of the former figure the Mn ground state and the excited states are within a potential well, whilst the barrier of fig.4.10(b) arises through the large disturbance of the lattice necessary to release an electron from an excited state (only the lowest such state is shown) into the conduction band.

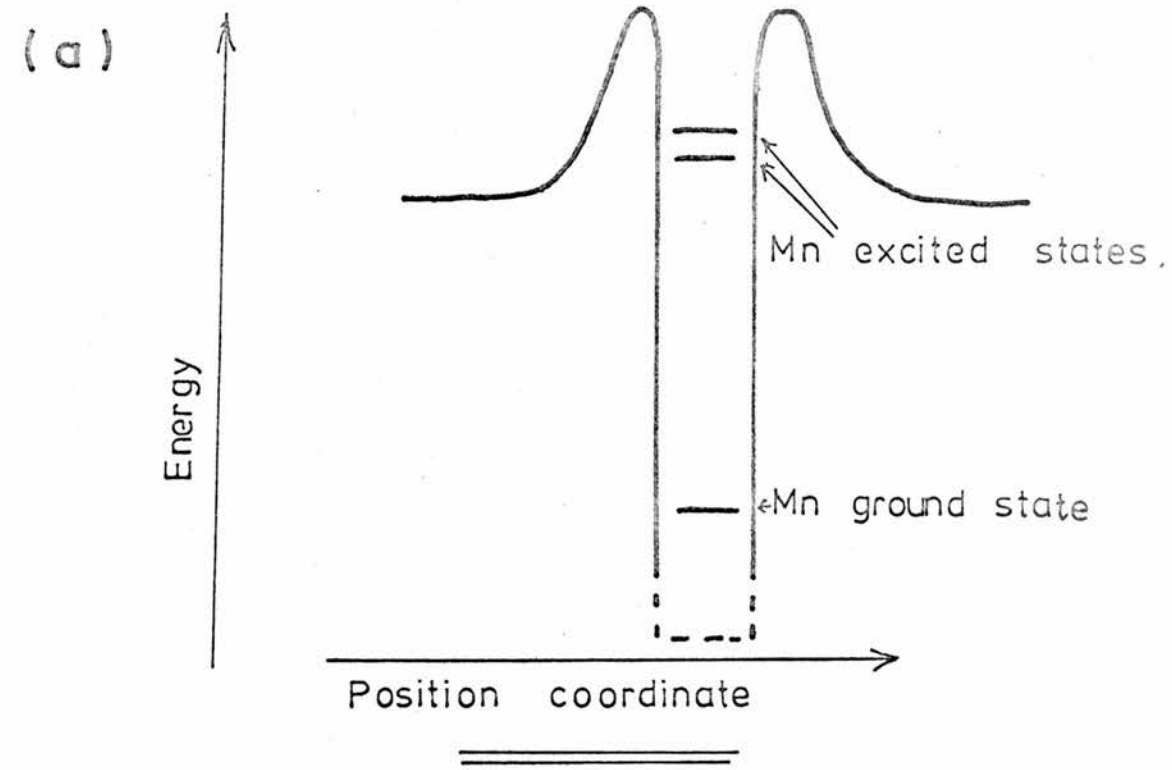

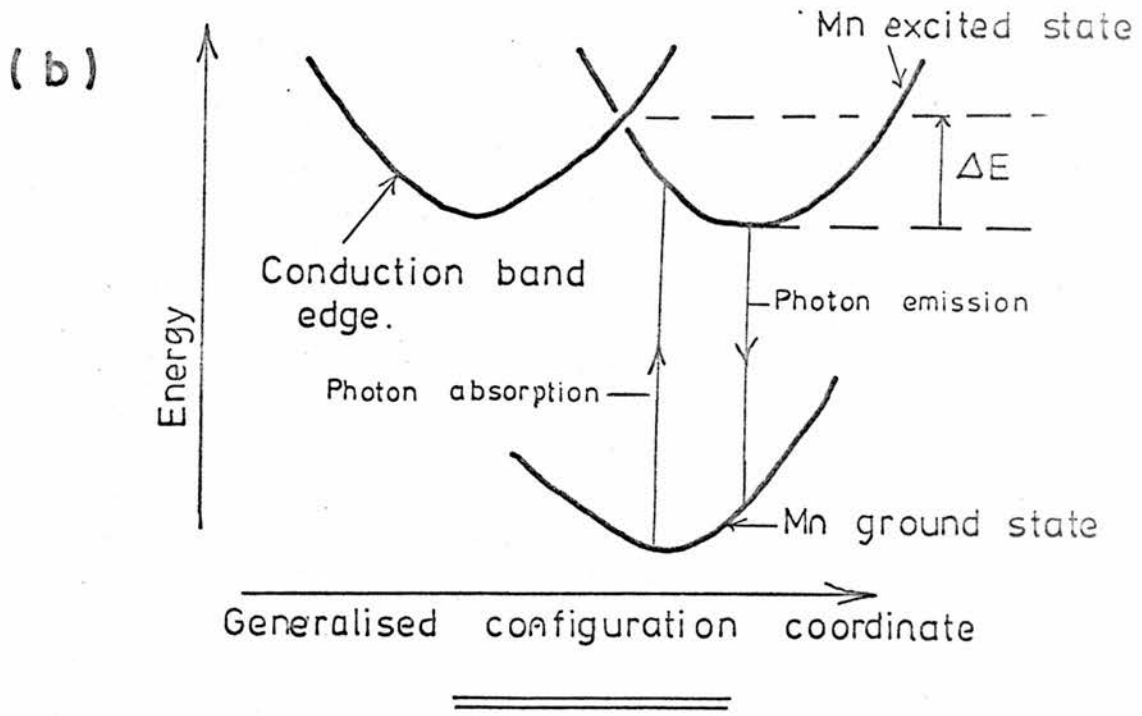

Fig 4.10 Two possible forms of barrier to auto-ionization from Mn excited states. In (a) the Mn system is within a potential well. There is a barrier, of height ΔE, in (b), due to the lattice disturbance necessary to release electrons from the excited state into the conduction band.

It was noted in section 4.3.1 that if a reverse bias, which exceeds the light emission threshold, is applied in ZnSe-Mn diodes then there is multiplication, and for a certain range of applied bias above the threshold value the multiplication is entirely due to the presence of Mn centres. This result requires for its explanation that some electrons take a path from the Mn ground state to the conduction band. The simultaneous population of the conduction band and the Mn $^4T_1$ state with electrons from the Mn ground state, necessary to respectively explain the observed multiplication and spectrum, may be due to both excitation and ionization occurring together. Alternatively, some electrons which are first excited to the Mn $^4T_1$ state, may tunnel from this state into states of the conduction band.

4.3.4. Response time for reverse bias electroluminescence

It was of interest to compare the measured rise and fall times of the light emission with the radiative lifetime for the Mn internal $^4T_1 - {}^6A_1$ transitions. This radiative lifetime was calculated from measurements of the absorption coefficient for the Mn $^6A_1 - {}^4T_1$ transition in ZnS:Mn given by Mc.Clure[73] with absorption data for ZnS:Mn used because similar information for ZnSe:Mn was not available. The result obtained for the radiative lifetime is 10^{-4}s with an uncertainty range of a factor of two.

The fastest components in the rise and fall of light in most 36B1 diodes have characteristic times of less than 5×10^{-8}s and only about 20% of the total decay of light takes place with time constant of a few μs or longer. In some 36B1 diodes essentially all optical response occurred in less than 5×10^{-8}s and the spectrum excited was due to Mn. Since the response time in all 36B1 diodes was much less than the radiative lifetime it is concluded that the radiative recombination efficiency is small. The response time in MA1 diodes was longer than in 36B1 diodes but this was due to the effect of traps, as shown from the

temperature dependence of the response time (fig. 4.8) rather than to an appreciably higher radiative recombination efficiency. Traps also caused the last 20% of the decay in 36B1 diodes to be much longer than would be the case in their absence.

4.3.5. Temperature dependence of the relative quantum efficiency

The temperature dependence of the reverse bias emission at constant current was mentioned in section 4.2.5 and shown in fig 4.7. If the assumptions are made that the radiative lifetime is temperature independent, but that the radiative recombination involves a thermal activation energy, ΔE, then the light emission L for a constant excitation rate varies as

$$L = \frac{L_o}{1 + A \exp\left(\frac{-\Delta E}{kT}\right)} \quad \ldots\ldots (4.1)$$

where A and L_o are constants. By suitable choice of A and ΔE this equation could be made to fit the results for fig. 4.7 in the temperature range above 220K. In obtaining this fit L_o was taken as the value of L corresponding to the approximate plateau of fig. 4.7 and ΔE was found to be 0.32eV. For a 36B1 diode a similar treatment of the results yielded $\Delta E = 0.21$eV.

The fact that equation 4.1 can be fitted to the results does not imply the validity of the assumptions which lead to the equation. Since a change of temperature alters the diode voltage at constant current the excitation efficiency under the experimental conditions would probably have been dependent on the temperature. From the remarks of section 4.4.3 the radiative recombination efficiency at room temperature is small, yet in fitting equation 4.1 it is assumed that the radiative recombination is approximately unity at the plateau of fig 4.7. According to the figure steady cooling eventually produces a reduction in the light output and this is not predicted by equation 4.1.

A possible mechanism for temperature quenching of electroluminescence is the excitation of electrons from the Mn excited state ($^4T_1$) to the conduction band as indicated on fig. 4.10(b). The activation energy shown is expected to be of the order of a few tenths of an eV.

4.3.6. Mn-doped ZnSe diodes as practical devices.

The largest measured photometric power efficiency in any Mn-doped ZnSe diode was 56 millilumens watt^{-1} and this occurred at a current of 10mA in an MAl diode. Red-light sources using GaP:Zn:O are commercially available with photometric power efficiencies of 800 millilumens watt^{-1}. For some applications red lamps are unsuitable so that Mn-doped ZnSe should, more properly, be compared with other available electroluminescent sources of yellow light. $GaAs_x P_{1-x}$ diodes are, at present, the most important such sources of yellow light and the commercially available lamps have been found, from a survey of the specifications of several manufacturers, to have photometric power efficiencies in the range 45-70 millilumens watt^{-1}. Green light sources mainly use GaP and these have typical power efficiencies of 100 millilumens watt^{-1}.

ZnSe:Mn diodes are still in a very early stage of development but the results obtained are encouraging. The basic materials cost for ZnSe:Mn lamps is much less than for GaP or $GaAs_x P_{1-x}$ lamps so that a possible application for ZnSe:Mn could be in large area displays. The fabrication of Schottky diodes as used in the ZnSe:Mn diodes is also a much cheaper procedure than the preparation of p - n junctions.

4.4. SUMMARY

The injection current in reverse bias is a tunnel current. In the high field of reverse biassed diodes ($\sim 10^5 V cm^{-1}$) impact excitation of Mn centres occurs and this populates the Mn $^4T_1$ state.

Light emission is associated with the de-excitation $^4T_1 - {}^6A_1$ transition for Mn in the crystal field of the ZnSe lattice. The photometric power efficiencies of diodes made to date, combined with the cheapness both of the materials and the device fabrication, gives some encouragement that ZnSe:Mn diodes, may, with further development, have commercial value.

5. FORWARD BIAS ELECTROLUMINESCENCE IN ZnSe SCHOTTKY DIODES

5.1. INTRODUCTION

It was noticed that ZnSe Schottky diodes emit visible light in forward bias although in any given diode the quantum efficiency was usually very much less than for reverse bias. In this chapter observations concerned with the forward bias emission are presented and discussed. A more detailed discussion has been given elsewhere[77].

5.2. EXPERIMENTAL RESULTS

5.2.1. Current-voltage characteristics

Typical current-voltage characteristics are shown for two temperatures of a Au contact diode on ZnSe in fig. 5.1. The figure is drawn for a diode which contains Mn centres but closely similar characteristics have always been found for diodes containing no deliberately added luminescence centres and for diodes containing Cu centres. The following is a summary of the experimental results regarding the current-voltage characteristics and is based on an examination of the data of fig. 5.1 together with similar data obtained for other diodes.

(i) On a semilogarithmic plot as in fig 5.1 the current-voltage characteristics at constant temperature are nearly straight lines over a wide range of current. Departure from linearity occurs at sufficiently high currents and is due to the series resistance of the diode chip.

(ii) The semilogarithmic current-voltage lines corresponding to different temperatures for a given diode are parallel to one another. An increase of temperature at a

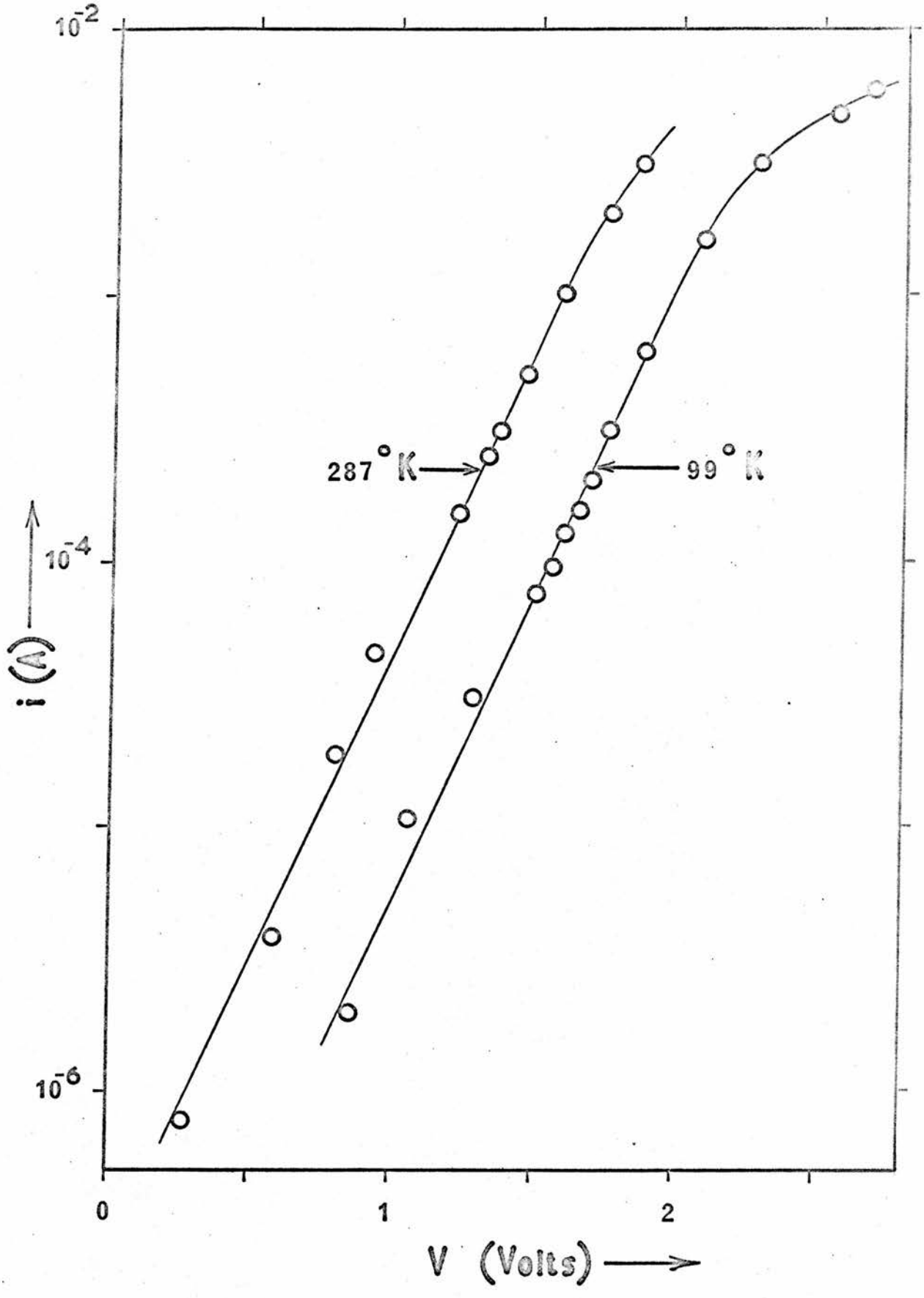

Fig. 5.1 Forward bias i vs. V characteristics for a Au - contact MA1 diode.

fixed voltage increases the current and an increase of temperature at a fixed current reduces the voltage. For the diode of fig. 5.1 the latter dependence, corresponds to a value of -2.2×10^{-3} volts K^{-1} for the partial derivative $\partial V/\partial T\big|_i$ (averaged over the temperature range of the figure). For all other suitably studied diodes, including those both with and without deliberate luminescence centre incorporation, it was found that $\partial V/\partial T\big|_i$ was within 30% of the value quoted above. It has been shown also that V varies approximately linearly with T at fixed i.

(iii) The slopes of the forward bias semilogarithmic plots of current against voltage are much steeper than for reverse bias of the same diode. Typically the ratio of these slopes is 5.5 with this same value for the ratio valid for diodes free and not free from deliberately added luminescence centres.

5.2.2. The dependence of light emission on current and voltage

Both the current and the light intensity increase as the forward bias is increased. There is a range of applied forward bias in which the light intensity is relatively much more strongly dependent on the bias than is the case for the current. At higher voltages the light emission and the current rise at equal relative rates as the voltage is raised. This result is illustrated in fig 5.2 where curves are plotted which display the light per unit current (L/i), in arbitrary units, as a function of the applied forward voltage (V) for each of three Au-contact diodes at room temperature. From the figure it is seen that with increasing V there is a voltage range in which L/i rises

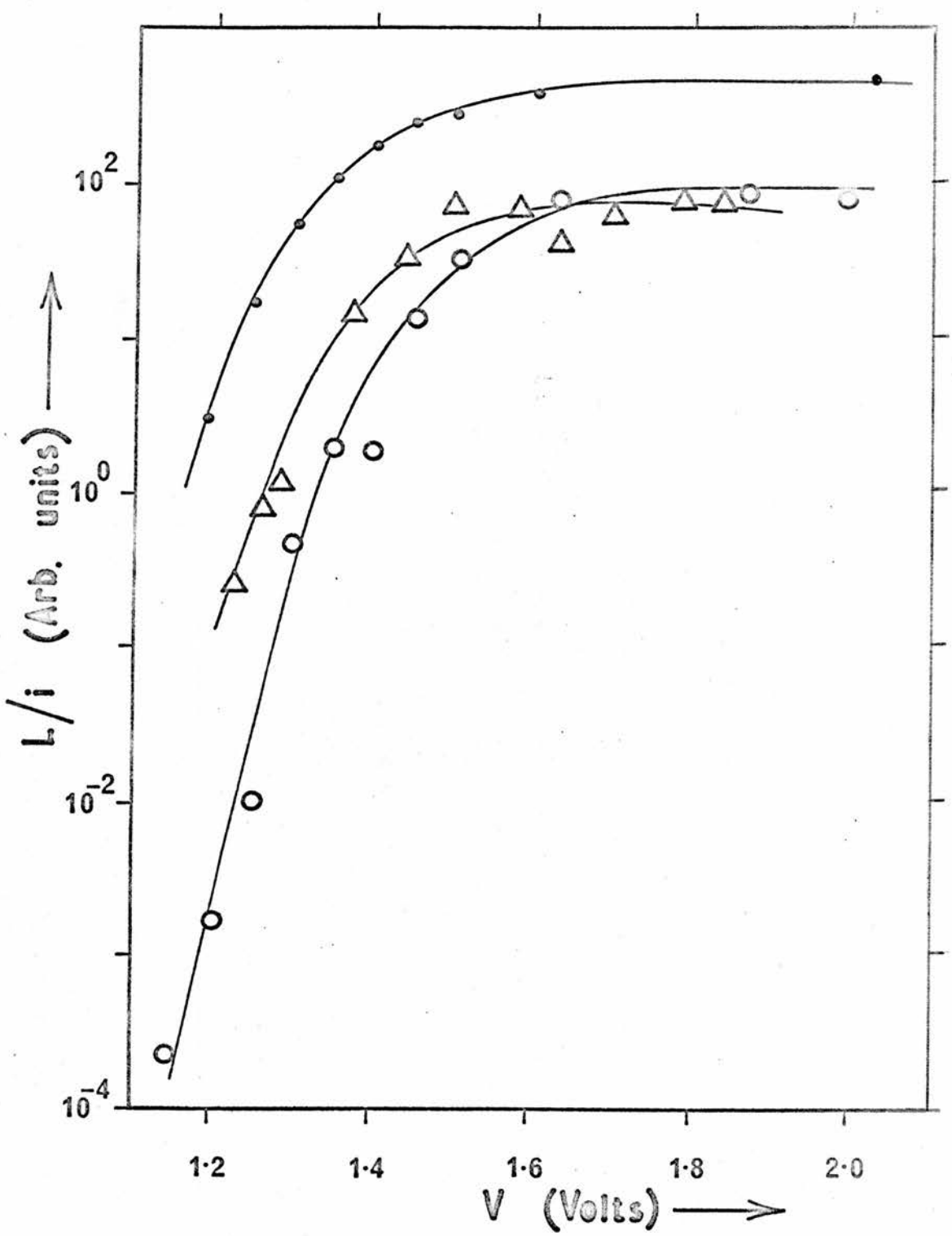

Fig. 5.2 Forward bias L/i vs. V curves for 3 Au-contact diodes at ~290 K.

sharply, and this range is followed, for voltages greater than 1.3 - 1.5 volts, by voltage independence of $L/_i$. The curves of fig 5.2 were drawn for three diodes which all contained Mn centres although not all to approximately equal concentrations. Curves of similar shape and with the same voltage for the onset of the constant $L/_i$ region as those of fig. 5.2, have been obtained for the room temperature emission properties of Au contacts on ZnSe containing Cu centres and on ZnSe with no deliberately added luminescence centres. The measurements on which the data of fig. 5.2 are based have been presented in fig. 5.3 as plots showing the variation of light emission with forward current. It will be observed from fig. 5.3 that, for currents sufficiently below the onset of proportionality between the light emission (L) and the current (i), there is a very strong dependence of L on i. The diodes, for which the measurements forming the basis of figs. 5.2 and 5.3 were made, emitted light only in a yellow band (see next section).

The radiation for forward bias originates from the vicinity of the rectifying contact. A few diodes have been prepared with Al as the rectifying contact metal, and for these diodes, it is known that the $L/_i$ vs. V characteristics are qualitatively similar to those shown in fig. 5.2 for Au-contact diodes. No detailed information has been gained concerning the threshold voltage for the approximate proportionality between L and i in Al-contact diodes.

5.2.3. Electroluminescence spectra for forward biassed ZnSe diodes

For the MAI batch of Mn-doped ZnSe the forward

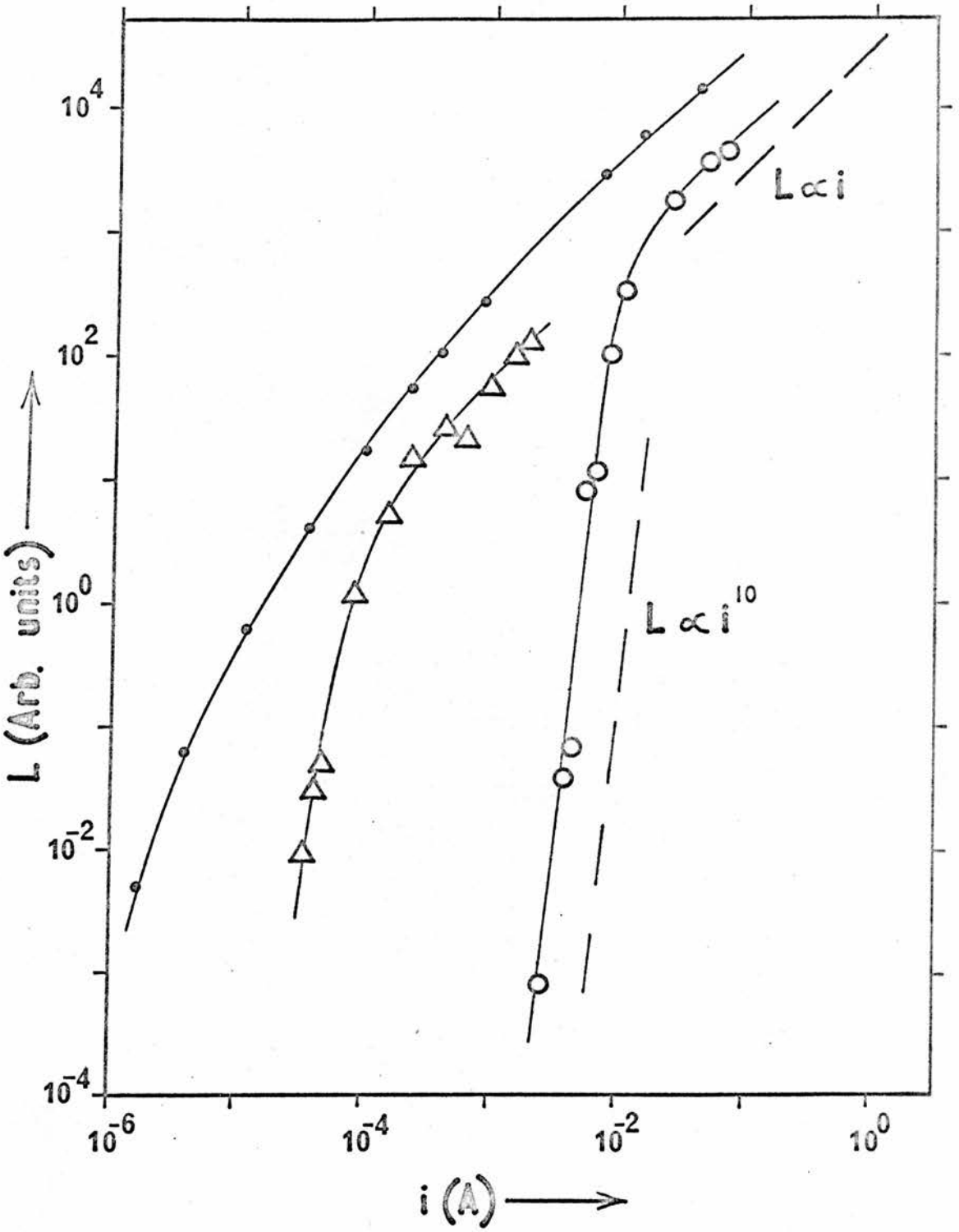

Fig. 5.3 Forward bias L vs. i for 3 diodes. The data are for the same measurements as used in drawing fig. 5.2. Symbols in the figs. 5.2 and 5.3 correspond.

bias spectrum peaks at 1.90eV for diodes at room temperature. The spectrum is identical for Au and Al as the rectifying contact metal. In the 36B1 and DM batches of Mn-doped ZnSe the forward bias spectrum, measured only for Au contacts, is a band peaking at 2.00eV. An apparently identical band has also been observed[61] for the same excitation conditions in ZnSe free from deliberately added luminescence centres. In photoluminescence, as excited by 365nm light, conducting specimens of 36B1 material exhibited at room temperature a band with a peak at 2.00eV (e.g. see fig. 4.6). Cu-doped ZnSe will receive attention in the next chapter but it is mentioned here that in forward bias, this material at room temperature, exhibits a spectrum peaking at 1.90eV and this spectrum is closely similar to the corresponding spectra for photoluminescence and reverse bias electroluminescence, also at room temperature. The above results for spectra observed in variously doped ZnSe under different excitation conditions, are summarized, along with other results, in appendix 1.

Some diodes, made of ZnSe free of deliberately added luminescence centres, exhibit a forward bias spectrum at room temperature which peaks at 2.676 $\pm$ 0.005eV and has a width at half peak height of 0.052eV. This sharp band of blue emission is shown in fig. 5.4.

A range of colours, including green, has been observed in different diodes which were prepared without taking precautions to minimize surface contamination. The reverse bias spectra for the same diodes are, however, indistinguishable from those of diodes prepared from corresponding materials but under clean conditions.

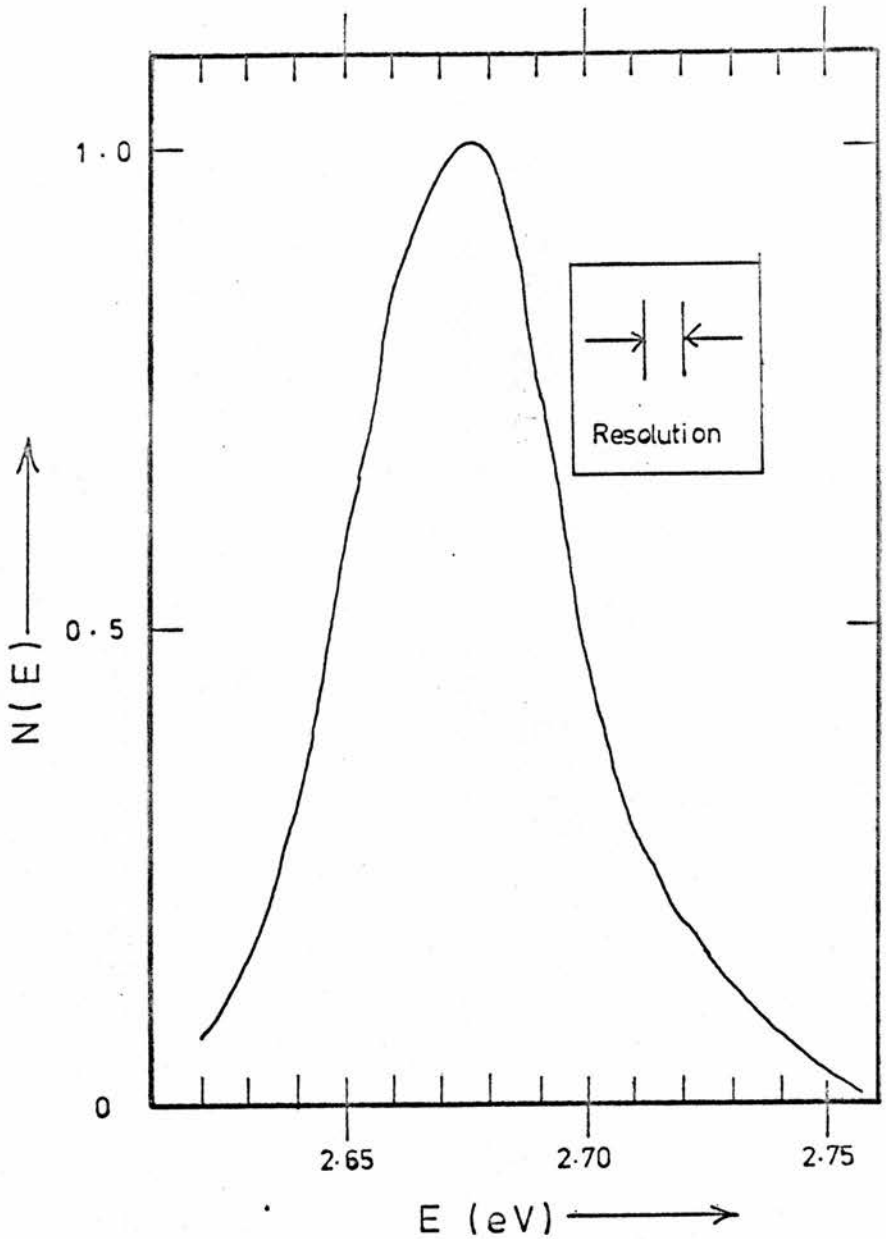

Fig. 5.4 Blue emission band for forward bias of a ZnSe diode at room temperature.

5.2.4. Temperature dependence of forward bias relative quantum efficiency

The yellow band observed in forward bias of Mn doped ZnSe increases in intensity for a fixed current when the diode is cooled. This temperature dependence is shown in figs 5.5(a) and 5.5(b). From the former figure, the relative quantum efficiency of the diode concerned is independent of temperature for a large temperature range below 265K. A range of temperature independence of the relative quantum efficiency was not observed for the majority of tested diodes and more typical results are shown in fig. 5.5(b). The activation energy for temperature quenching of forward bias electroluminescence, as determined from the slopes of the steepest linear sections in plots of the form of figs. 5.5.(a) and 5.5(b) for different diodes, was always in the range 0.25 - 0.50eV.

The quantum efficiency associated with emission into the blue spectral band which was mentioned in section 5.2.3 also increases for cooling of the source diode. The temperature dependence for this band is apparently stronger than for the yellow band because diodes have been prepared which, in forward bias, emit predominantly yellow light at room temperature whilst, for the same diode at liquid nitrogen temperature, the light is predominantly blue.

5.2.5. External quantum efficiency

In the voltage range in which for individual diodes the ratio $L/_i$ is independent of current, the external quantum efficiency, measured at room temperature for diodes with Mn centres or with no intentionally added luminescence centres, ranged from 6×10^{-8} to 2×10^{-5}. This range refers to diodes having room

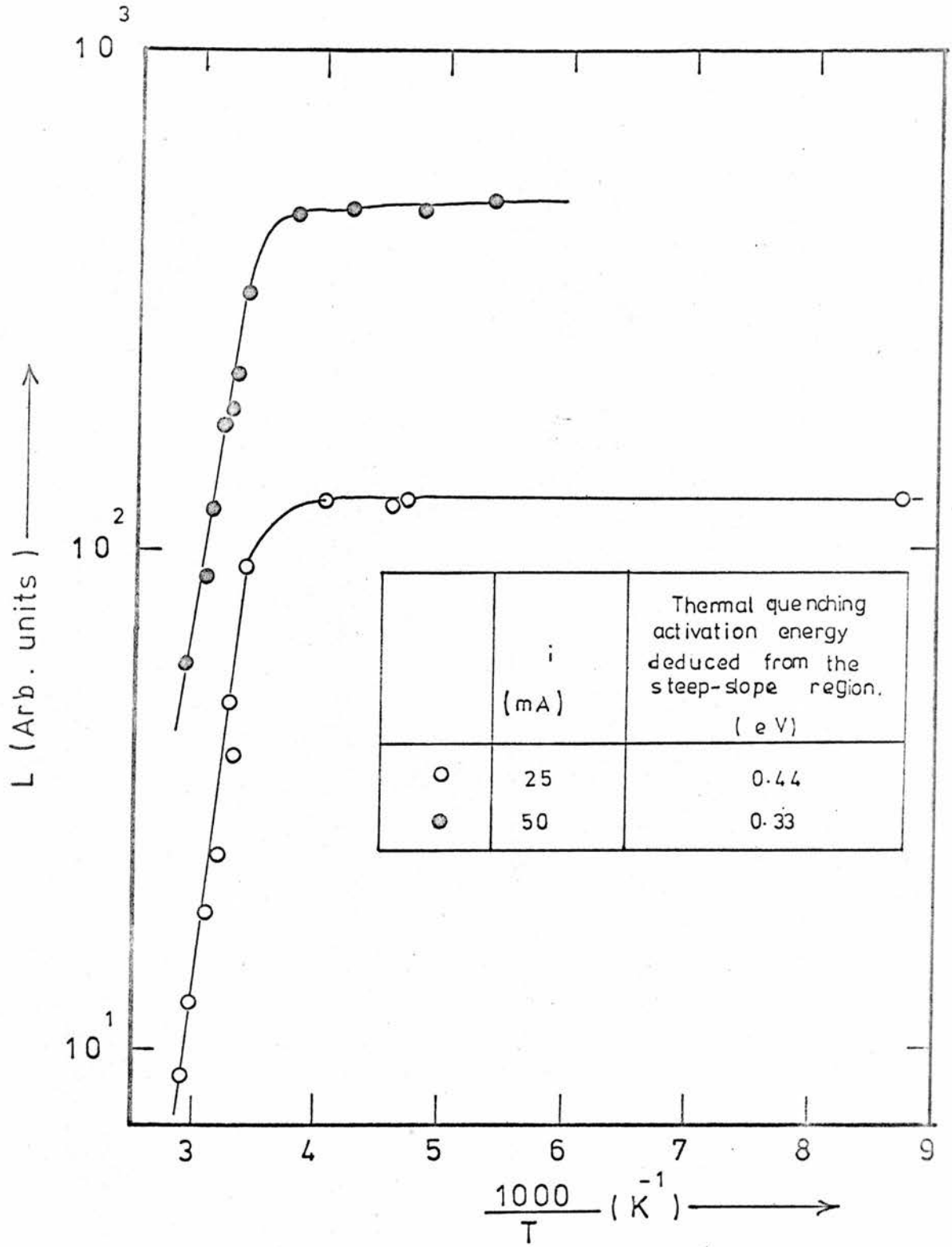

Fig. 5.5 (a) Temperature dependence of L for forward bias. [Measured for a 26C1 diode.]

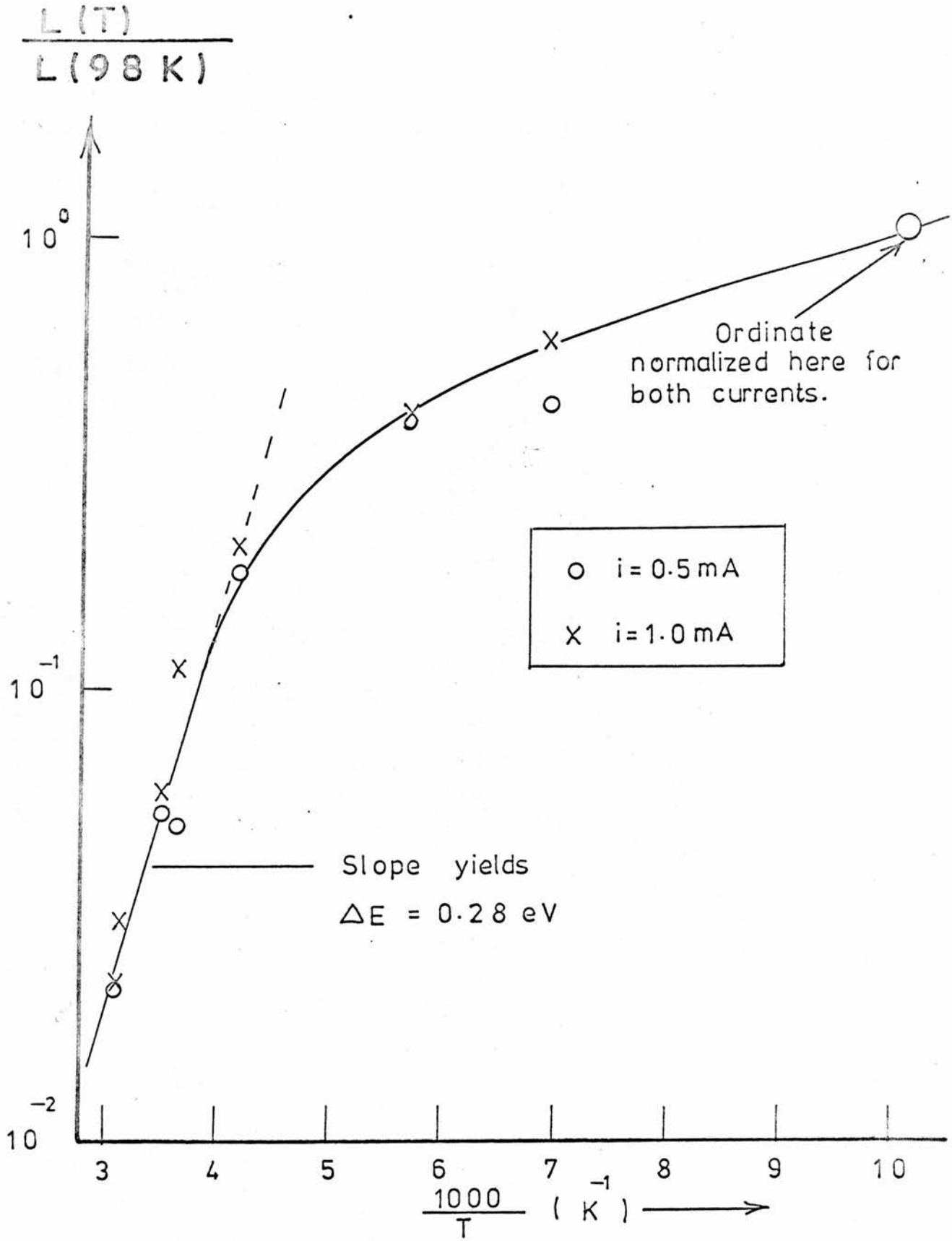

Fig . 5·5(b) Temperature dependence of forward bias light emission for an MA1 diode .

temperature emission at 1.9eV or 2.0eV. Amongst diodes prepared from any given batch of material there is a much wider spread of quantum efficiency in forward bias than for reverse bias. Apparently the Mn concentration has no effect on the forward bias quantum efficiency because diodes made from the materials MAI (thought to contain about 0.5 atom % Mn), 36B1 (Mn concentration believed less than 0.1 atom %) or 20A1 (no deliberately added luminescence centres) yielded quantum efficiencies with similar spreads of values. For the few Cu - doped diodes which have been experimentally studied the largest forward bias external quantum efficiency, measured in a current range where this is independent of current and at room temperature, is 7.7×10^{-5}. There is often a rapid deterioration of forward bias quantum efficiency with ageing time for all of the studied ZnSe materials and this change in diode properties was not necessarily associated with a significant change in the forward current-voltage characteristics.

No measurements have been made of the quantum efficiency for the blue band emission. Since, at room temperature and at a forward current of 26mA, blue light is seen by a dark-adapted eye for some diodes whilst for other diodes operated and viewed under corresponding conditions, either no light or blue light is observed, it is concluded that the quantum efficiency range range for the blue emission is wide.

5.2.6. Diode response time

The 1.90eV band observed in forward bias of MAI Mn doped ZnSe diodes has a rise time of a few microseconds but a fall time to essential completion (2% of the intensity before the start of the decay) of less than 60ns. There are no components in the rising edge with time constant less than 100ns.

The forward bias light in 36B1 diodes (band at 2.00eV)

has a rise time, to 75% of the final height, of about 1μs and has a fall which appears to involve the same time constants as the rise. In the 36B1 diodes both the rise and the fall of the light showed components of less than 50ns characteristic time.

For MA1 and 36B1 diodes the current rise and fall time is less than 10ns.

Cu-doped diodes are to be discussed separately in the next chapter.

5.3 DISCUSSION

5.3.1. Forward current-voltage characteristics

It is evident from fig 5.1 that the mode of current injection in forward bias is not by thermal activation of carriers over a barrier because, in complete contrast to the figure, this would give a slope $\left.\frac{\partial \ln i}{\partial V}\right|_T$ proportional to T^{-1}. The injection mechanism is presumed to be tunnelling of electrons from the conduction band of the n-type ZnSe into unoccupied levels of the metal above the metal quasi Fermi energy. Although it is not apparent from the current-voltage characteristics, there is other evidence, which will be given later, that some minority carrier injection into the semiconductor occurs.

5.3.2. The emission spectrum

It follows from the discussion of spectra given in the last chapter that the bands observed at 1.90eV and 2.00eV in different types of Mn-doped ZnSe diodes for forward bias are not due to the presence of Mn. The 1.90eV band may be due to Cu or to Cl impurity whilst the 2.00eV band is probably the ZnSe self-activated band. The reasons for the asserted probable identity of the 2.00eV band have already been given in chapter 4 and included the facts that many authors have observed a luminescence band in ZnSe in the vicinity of 2.00eV which they attributed to self-activation and

that the forward bias spectrum of ZnSe diodes free from deliberately added luminescence centres has been shown,[61] from work conducted in this laboratory, to be closely similar to that for diodes with Mn incorporation. Fischer[66] has also reported a yellow emission for forward bias of Schottky diodes on ZnSe with no deliberately added luminescence centres. This band is very similar to the 2.00eV of the present work since, by reference to Fischer's results for the room temperature spectrum, it peaks at 1.98eV and has half-height width of 0.36eV. The rectifying contacts used in Fischer's work were Pt, Ir, colloidal graphite and certain organic semiconductors, with the forward bias spectrum the same for all of these.

The sharp 2.676eV band observed at room temperature in forward bias of some diodes is close in energy to the fundamental gap of ZnSe and this is evidence that the radiative transition is from an excitonic state. Room temperature luminescence emission involving exciton levels has not been observed for many materials but has been reported for CdS[78].

5.3.3. The mechanism of forward bias emission

In reverse bias electroluminescence of luminescence centre-doped ZnSe these centres are impact excited or ionized by carriers and in the return of electrons to the centres radiation is produced. In forward bias the electric field is too weak for impact excitation or ionization to occur. If holes are injected into the n-type ZnSe radiation results when electrons from the conduction band recombine with these holes via luminescence centres. In an ideal metal to n-type semiconductor contact if the electron barrier height for emission of electrons from the metal into the semiconductor is $e\phi$, then the barrier which holes must surmount to reach the semiconductor valence band from the metal is $E_g - e\phi$

where E_g is the band gap of the semiconductor. From measurements of ϕ for Au contacts[16,17] on ZnSe the hole barrier is deduced to be about 1.2eV. At room temperature the probability of thermal excitation of carriers over a barrier of this height is negligible.

Injection of holes from Au into n-type ZnSe is also negligible, for intimate Au-ZnSe contact, if the holes are assumed to tunnel through the barrier. This is because the density of empty states in the Au at 1.2eV below the Au Fermi level is negligible. Fischer and Moss [79] have pointed out that if an insulating layer of suitable thickness is interposed between metal and n-type semiconductor, thus forming a metal-insulator-semiconductor structure, then hole injection into the semiconductor can be much enhanced compared with the case of intimate metal-semiconductor contact. This is shown by reference to fig. 5.6. In fig. 5.6(a) a metal-insulator-semiconductor (n-type) contact is drawn for zero applied bias. On application of a forward bias the semiconductor valence band edge is raised relative to the metal Fermi energy by an energy equal to the electronic charge multiplied by the potential drop across the insulator. For a certain applied forward bias, V_T, the valence band edge of the semiconductor at the insulator-semiconductor junction just becomes level with the metal Fermi energy E_{fm}. This condition is shown in fig. 5.6(b) for the case (with given materials forming the contact structure) of the minimum possible V_T, denoted by V_{TO}, when all of the applied bias is dropped across the insulator and none across the depletion layer of the semiconductor. For applied voltages greater than V_T holes from the empty states above E_{fm} in the metal can travel across the insulating layer into the semiconductor without change of energy. One such method of hole transport is by tunnelling. For an applied forward bias range just below V_T the hole injection efficiency is a steep

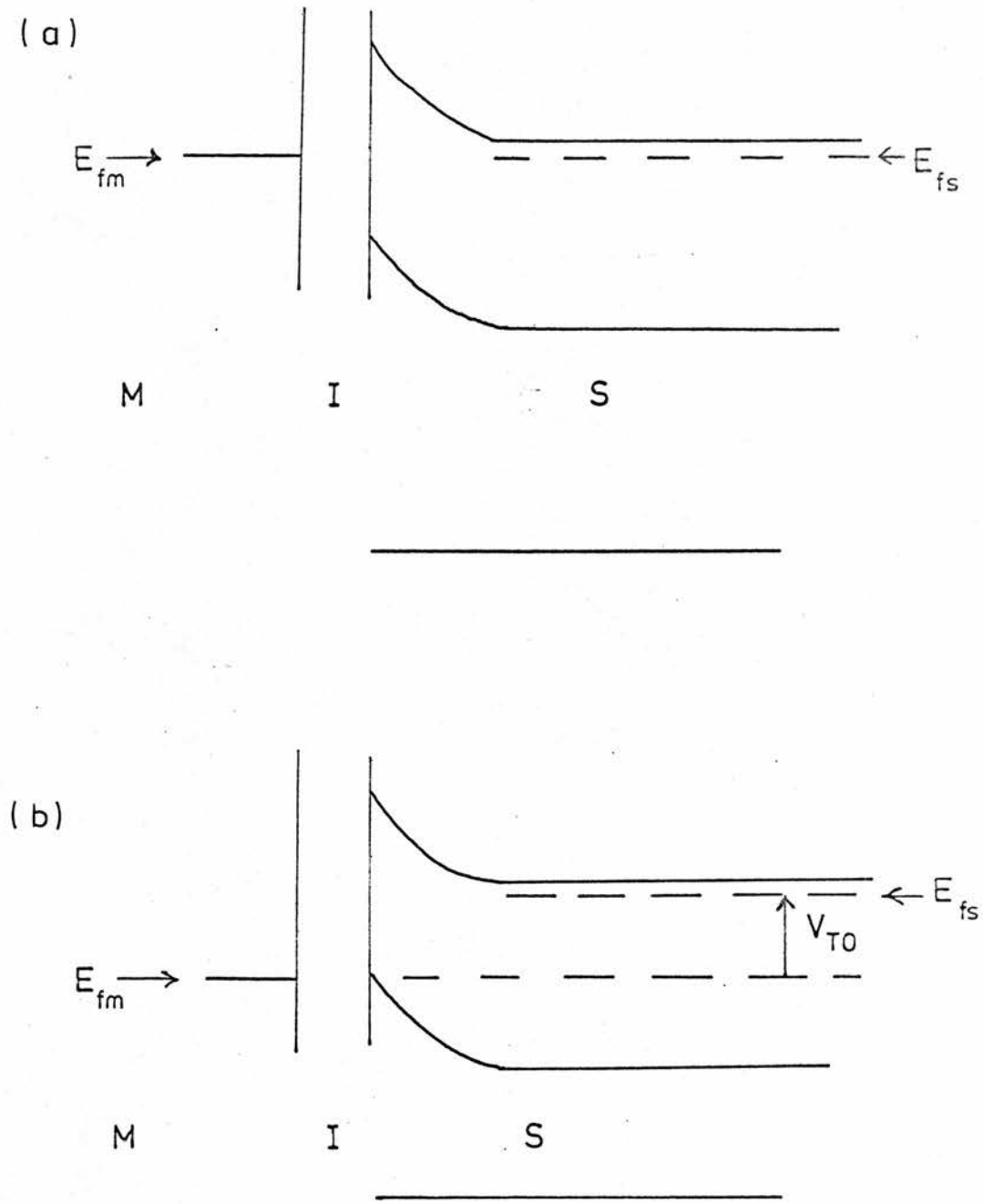

Fig 5 6 Energy band diagrams for metal (M) - insulator (I) - semiconductor (S) structure.

(a) —— Zero applied bias.

(b) —— Threshold condition in the case of all applied bias dropped across I of the same diode as in (a).

function of the bias because the density of empty states in the metal and immediately below the metal Fermi level, is very strongly energy dependent.

In the Au on ZnSe contacts prepared in this work there is believed to be a layer of ZnO between the Au and the ZnSe. This layer facilitates hole injection into the ZnSe for an applied forward bias by the mechanism just described. Assuming the radiative recombination efficiency to be independent of the excitation intensity, the light per unit current in any given diode is a direct measure of the relative fraction of the current conveyed across the depletion layer by holes, and the previously defined voltage V_T may be identified with the threshold bias for a constant quantum efficiency. Referring to fig. 5.2 the value of V_T, for each of the diodes of the figure, is in the range 1.3 - 1.5 volts. From fig. 5.3 the diode current at the onset of the constant relative quantum efficiency regime, is small for the diodes with the lower threshold voltages and hence it follows that for these diodes V_T is a close approximation to V_{TO}. In this way V_{TO} is estimated as 1.3 volts. The electron barrier height for Au on ZnSe is approximately 1.5eV[17] independently of surface preparation and, by subtracting this barrier height from the ZnSe band gap, eV_{TO} is deduced to be 1.2eV. Within the limits of experimental error this is in agreement with the estimate made above for V_{TO}, thus confirming that the Au and ZnSe bands in a diode biassed at the constant quantum efficiency threshold do align as shown in fig 5.6(b) or to within $\pm$ 0.1eV of that alignment.

If the holes tunnelled directly across the insulating layer then an optimum thickness of the layer for maximum quantum efficiency would exist. It has been shown by Livingstone[59] and by Livingstone et al.[77] that the quantum efficiency is not de-

pendent on the insulating layer thickness if this is more than 400Å and up to at least 1800Å. This result indicates that the holes, for most and probably for all of this thickness range, do not tunnel directly across the insulating layer. The same V_{TO} is found independently of thickness[77] so holes, for all tested ZnO thicknesses, are transported without energy change. A possible method of hole transport across the ZnO layer is by impurity band conduction. For consistency with experimental observations it would be necessary, for this suggested transport mechanism, to assume that in the forbidden gap of the ZnO layer there is a wide energy distribution of impurity levels.

It has been assumed in discussing the shape of fig. 5.2 that the radiative recombination efficiency is independent of the intensity of the excitation. Dr. Wight[80] of S.E.R.L. has verified this assumption by showing that the quantum efficiency for photoluminescence, in the same 2.0eV band as for forward bias electroluminescence, is over the emission intensity range of fig. 5.2, constant to within a factor of two. Since cooling of the diodes to 100K increases the quantum efficiency by only a factor of about an order of magnitude the main reason for the very low observed quantum efficiencies is that the hole injection efficiency is low.

5.4 SUMMARY

In forward bias of the studied Schottky barriers the main carriers of current are electrons and these, of course, travel from the n-type ZnSe towards the metal. The electrons are definitely not thermally activated over the potential barrier which remains in the depletion layer when a forward bias is applied and there is little doubt that the electron transport mechanism is by tunnelling through this barrier. The radiative transitions

resulting in light emission are, in certain cases, characteristic of added impurities and in other cases are believed to be due to self-activation. Light emission associated with the presence of excitons has been observed at room temperature. Hole injection into the ZnSe is necessary for forward bias light emission and this injection is possible if the diodes have a metal-insulator-semiconductor structure.

6. ELECTROLUMINESCENCE IN Cu-DOPED ZnSe.

6.1. INTRODUCTION

As a minor part of the work of this thesis electroluminescence in Schottky diodes of Cu-doped ZnSe was studied for both polarities of bias. The results obtained are compared with those given in earlier chapters for diodes containing Mn centres. Diodes were prepared from two batches of Cu-doped ZnSe, referred to as 46A1 and CA1. The Cu concentration is not known for either batch but it is higher in the CA1 material. Since Cu forms acceptor centres in ZnSe and both batches exhibited n-type behaviour it is concluded that the Cu concentration is, for each batch, less than the concentration of donor centres and this latter concentration is similar to that for the diodes discussed in the preceding chapters.

6.2. EXPERIMENTAL RESULTS

6.2.1. Relationships between light emission, current and voltage

In reverse bias of Cu-doped ZnSe diodes measurements, which were only made for diodes at room temperature, show that the current-voltage characteristics are closely similar to those for Mn-doped ZnSe diodes. In each of the figs. 6.1(a) and 6.2 the current voltage characteristics are given for a different Cu-doped diode. A high leakage is evident in the diode for which the latter figure is drawn.

The dependence of the light emission (L) on the reverse bias (V) is shown in fig. 6.1(a) for the same diode as the current-voltage characteristics in that figure. For this diode the light emission is proportional to the current for a range of currents from 30μA up to at least 10mA. Referring to the reverse bias L-V characteristics in fig. 6.2 it appears that there are two different

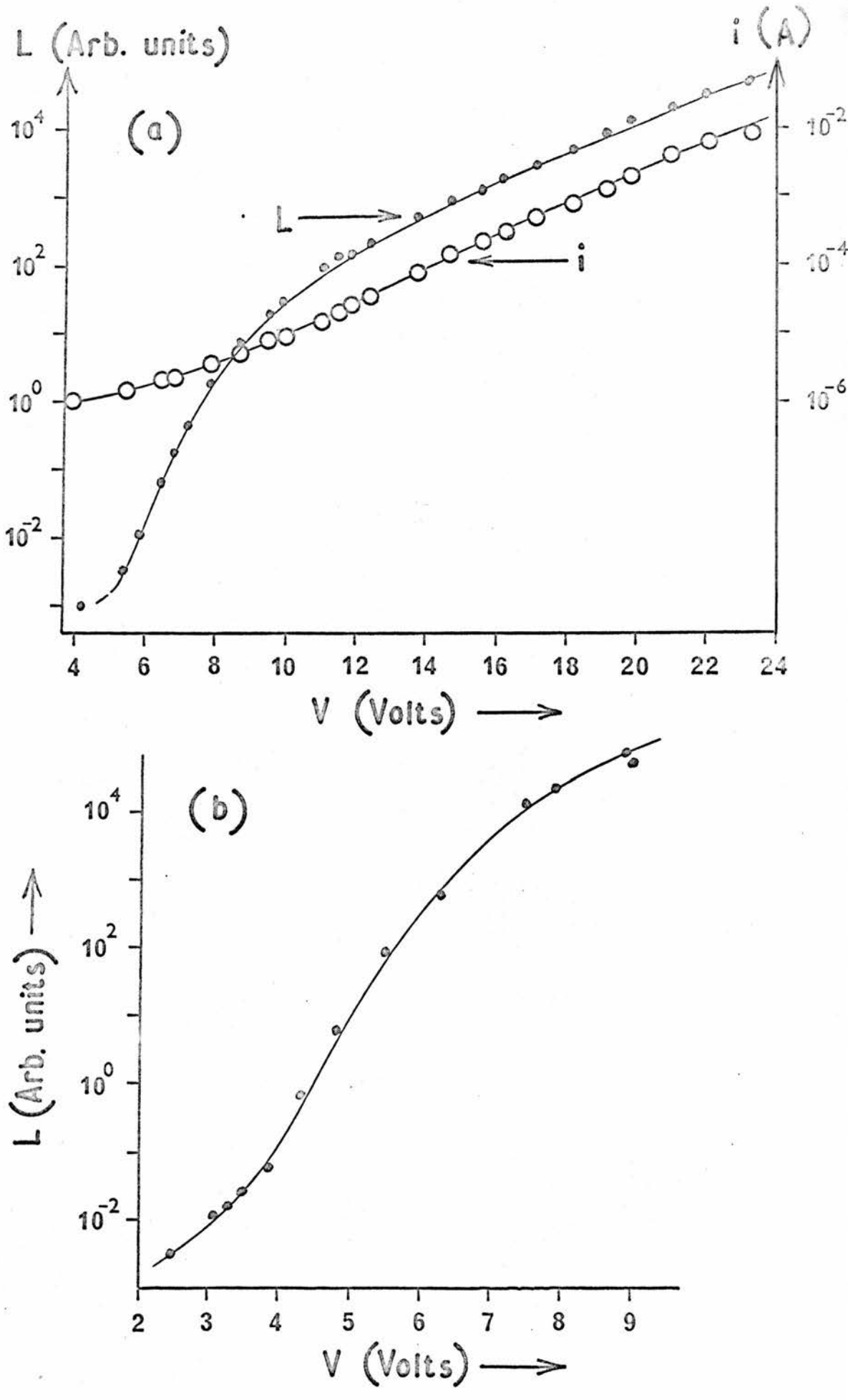

Fig. 6.1 Room temperature L-V and i-V curves for reverse bias of two ZnSe:Cu diodes. (a)-46Al ; (b)-CAl materials.

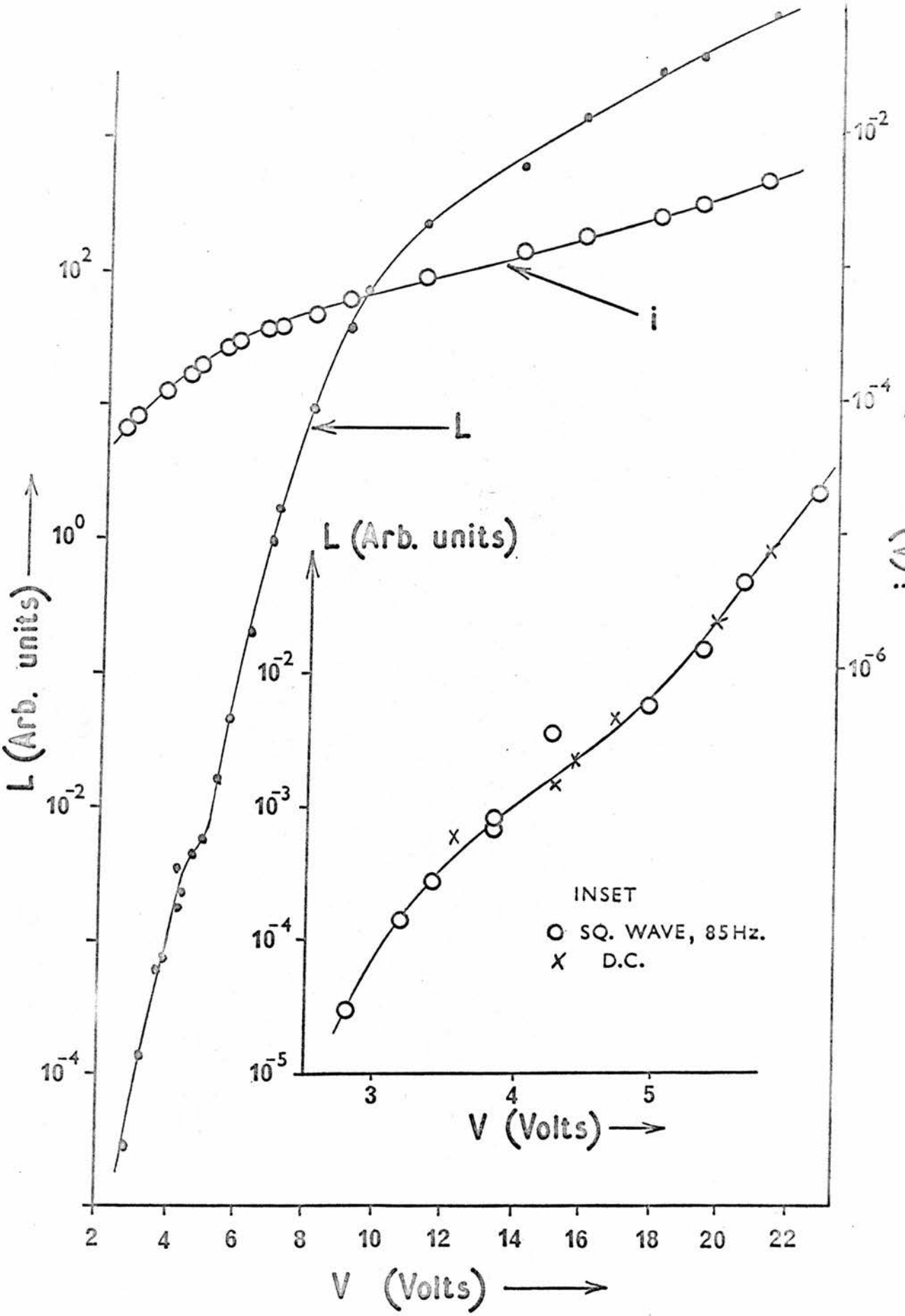

Fig. 6.2 Room temperature L-V and i-V characteristics for a 46Al diode. The inset shows the inflexion in the L-V curve on an expanded scale and also shows the reproducibility of this feature.

light excitation processes active within the range of bias shown since there are two voltage regions in which the light increases especially rapidly for a small increase in the voltage. The inset of the figure shows more clearly the existence of two threshold voltages for light excitation processes and there is no evidence to suggest that in the lower observed threshold region the light does not rise from a zero level. The L-V characteristics of figs. 6.1(a) and 6.1(b) are also consistent with two thresholds in the respective diodes to which they refer. Double thresholds have been independently observed by Livingstone[81] for other Cu-doped ZnSe diodes in reverse bias. There is apparently a genuine difference in the nature of the reverse bias behaviour of Cu-doped and Mn-doped ZnSe diodes since for the latter type the measured L-V characteristics, which were obtained in approximately the same light intensity range as for the former type, have always shown only one threshold in each diode.

In forward bias of Cu-doped ZnSe diodes the relationships between current, voltage and light intensity are closely similar in form to the corresponding results for diodes with no deliberately added luminescence centres and for diodes containing Mn centres. For all three diode types in forward bias the same minimum bias of about 1.3 volts is found for the voltage marking the transition from a strong voltage dependence to voltage independence of the quantum efficiency.

6.2.2. Spectrum of ZnSe : Cu

The room temperature emission spectrum for ZnSe : Cu (material 46A1) in reverse bias electroluminescence is shown in fig 6.3. Included in the figure, for purposes of comparison, is the photoluminescence spectrum for the same specimen, also at room temperature. A room temperature spectrum for a ZnSe : Cu diode

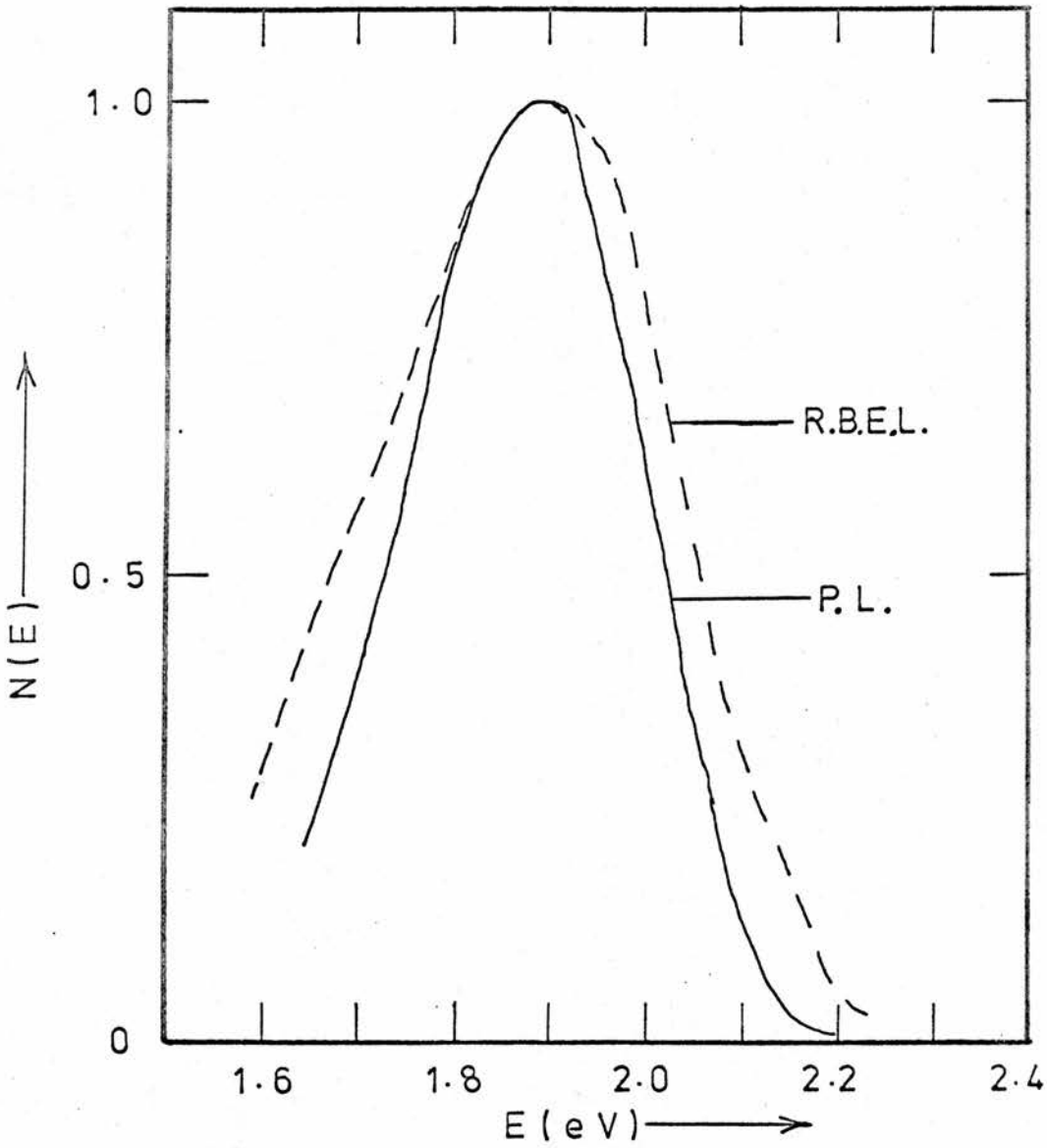

Fig. 6.3 Spectra excited in Cu-doped ZnSe [46A1] for reverse bias electroluminescence (R.B.E.L.) and photoluminescence (P.L.) The two spectra were obtained for the same specimen and at room temperature. The P.L. spectrum was excited by 365 nm light.

(46Al material) in forward bias is shown in fig. 6.4. The peak positions for the spectra obtained for the three methods of excitation are all the same to within experimental error and are 1.90eV. At room temperature the widths at half-height for the reverse-bias and forward bias spectra are similar, each being close to 0.38eV. The photoluminescence spectrum is somewhat sharper, having a width at half-height of 0.295eV, again stated for room temperature.

The reverse bias spectrum is identical for Au or Sn as the rectifying contact metal. These were the only metals used in preparing the rectifying contacts. For forward bias in ZnSe : Cu, measurements have only been made for diodes with Au rectifying contacts, but because for this metal the forward and reverse spectra are very similar, and the reverse bias spectrum is apparently independent of the choice of contact metal it is inferred that in forward bias the spectrum is also independent of which contact metal is used.

From the measured spectra and from the known relative response of the standard eye the integrated luminosity for both forward and reverse bias spectra in Cu-doped ZnSe has been evaluated as 130 lumen watt^{-1}.

6.2.3. External quantum and power efficiencies

The external quantum efficiency has only been measured for a very few diodes of Cu-doped ZnSe. In reverse bias the largest measured external quantum efficiency, for diodes at room temperature, was 3.3×10^{-4}. This was for a diode prepared from material batch CA1 and for a current of 2.5mA. The same diode exhibited the highest power efficiency for reverse bias; this was 9.4 millilumen watt^{-1} and also occurred at 2.5mA. In reverse bias electroluminescence of diodes prepared from the 46Al batch of Cu-doped ZnSe the highest

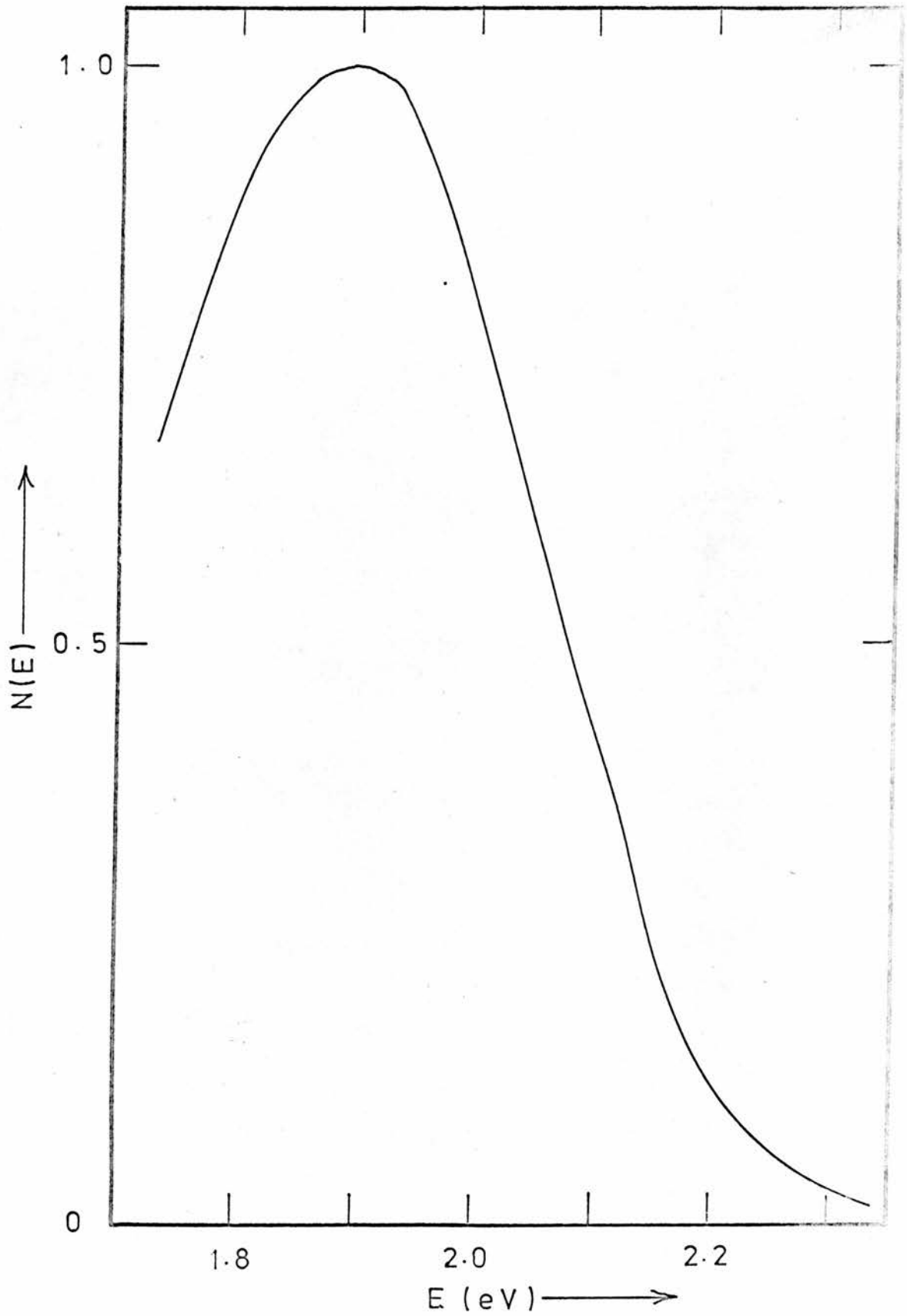

Fig. 6.4 Forward bias spectrum for a Cu-doped diode at room temperature. [46 A1 material]

observed room temperature quantum efficiency was 7.7×10^{-5}.

The largest measured quantum efficiency in forward bias for any Cu-doped ZnSe diode was obtained for the same CA1 diode as exhibited the largest measured reverse bias quantum efficiency. This diode had a forward bias quantum efficiency of 7.9×10^{-5} at 24mA and for this current the constant quantum efficiency regime was approached. In 46A1 diodes at room temperature external quantum efficiencies in forward bias were found to be in the range 3×10^{-8} to 10^{-6}. The measurements on forward bias quantum efficiencies in 46A1 material were made at a current of only a few mA and the maximum quantum efficiency for each diode may be about an order of magnitude larger than at such currents.

There is some evidence of correlation between forward bias and reverse bias quantum efficiencies with the diodes of highest reverse bias quantum efficiency tending to also show the highest forward bias quantum efficiency.

6.2.4. Diode response time

The rise of light for reverse bias electroluminescence has been measured for currents in the range 0.5mA to 12mA. For currents of less than 2mA the rise, following a step application of a steady voltage, is well described by an exponential form with a single time constant. This time constant is about 10μs for a current of 1mA and is approximately proportional to the inverse of the current in the current range 0.5mA to 2mA. The fall of the light after the passage of a reverse current pulse is also approximately of a simple exponential form, for currents in the range 0.5mA to 2mA, exhibiting a single time constant of similar magnitude to that in the rising edge for the same current.

At reverse currents greater than about 2mA more complicated behaviour is found in the temporal response since at least

two time constants are involved.

The rise time of light in forward bias is much less dependent on current than for reverse bias. At a forward current of 7mA the light from a typical diode rose to half its final level in 48μs. The rise was not of a single time constant exponential form but no components of the rise were present with time constant less than a few μs. On the falling edge the light decayed to about 20% in a time less than 100ns and was followed by a decay of about 30μs time constant.

In MAl Mn-doped diodes the forward bias electroluminescence peak is at 1.90eV and may be due to Cu impurity. For these diodes there is a more marked difference in the rise and fall times for forward bias than for the deliberately Cu-doped diodes. MAl diodes in forward bias typically have a rise time, to 75% of final height, of a few μs and a sharp fall down to 2% which takes place in less than 60ns.

All of the above results in this section refer to diodes at room temperature and the current response time was always less than 10ns.

6.3 DISCUSSION

6.3.1. The Current-voltage and light-current-voltage characteristics

For Mn-doped ZnSe diodes it had been concluded in earlier chapters that, for both polarities of bias, the electron transport across the depletion layer was by tunnelling. Since in each bias direction the current-voltage characteristics for Cu-doped diodes are closely similar to those for Mn-doped diodes, it appears that for Cu-doped diodes in either forward or reverse bias the electron current tunnels through the depletion layer. The conclusions regarding the electron transport mechanism in Mn-doped diodes were based, to a large extent, on the effect of temperature changes on the current-voltage characteristics and these characteristics for Cu-doped diodes have only been measured at room temperature. It is expected that Cu-doped diodes would behave similarly to Mn-doped diodes as regards the temperature dependence of the current-voltage characteristics.

It has been shown by Livingstone[59] and by Allen et al.[60] that if the applied reverse voltage in Cu-doped diodes is sufficient to produce appreciable light emission then impact ionization of Cu centres occurs. It was pointed out in section 6.2.1 that for many Cu-doped diodes in reverse bias two emission threshold voltages have been observed. No explanation is offered for the occurrence of these double thresholds.

In chapter 5 a discussion of the excitation of luminescence in forward bias of (non-ideal) Schottky diodes was given. This discussion is equally applicable for Cu-doped diodes, as for Mn-doped diodes and those without the deliberate incorporation of luminescence centres, since all these types of diode exhibit the same minimum bias (V_{TO}) at the lower end of the constant quantum efficiency range of voltage.

6.3.2. Comparison between spectra obtained under different excitation conditions in the present work and with the spectra observed by other authors

Since in the present work on Cu-doped ZnSe the spectral bands for photoluminescence, reverse bias electroluminescence and forward bias electroluminescence were all found to peak at very nearly the same energy (1.90eV) there is evidence that identical radiative transitions are involved in the three types of luminescence. The spectral width for the two polarities of electroluminescencent excitation are very similar but a somewhat sharper spectrum in obtained for photoluminescence. The peak positions and the widths of the observed luminescence bands in ZnSe : Cu are given in Appendix I.

Several authors have reported a red band in the luminescence spectrum of Cu-doped ZnSe and most of these have given the energy corresponding to the peak of this band as slightly higher than the value found by the present author. For example, the following results have been given for the peak of the red luminescence band in Cu-doped ZnSe at room temperature:- photoluminescence: 1.923eV[62]; cathodoluminescence: 1.915eV[70] and 1.922eV[82]; A.C. excitation of powders: 1.930eV[83] and 1.96 - 2.07eV[84]. In the spectra pertinent to each of these reports the width at half-height was 0.29 $\pm$ 0.02eV. At 77K the red luminescence band in ZnSe:Cu peaks, according to several authors[62,63,85-87] in the range 1.95 - 1.99eV and, also at 77K, each of these authors observed a green band in the emission. None of the authors referred to in this section state if their published spectral data were corrected for the response of the measuring system used. For spectra of the width and of the energy location of the red luminescence band in ZnSe:Cu this is not a negligible correction for many of the more commonly used photocathode surfaces in photomultipliers. As an illustration of this it is mentioned that the spectra for luminescence of Cu-doped ZnSe, as measured by the author

when using an S20 response photomultiplier as the detector, peak, in their uncorrected form, at 1.95eV. Corrected spectra obtained with the S20 response photomultiplier and with an S1 response photomultiplier were in good agreement.

6.3.3. The transitions involved in the luminescence of Cu-doped ZnSe.

Fujiwara and Fukai[85] observed that the peak of the red band of photoluminescence emission in ZnSe:Cu:In shifted to lower energies during the decay of the photoluminescence following pulse excitation. According to their measurements, which were made at 77K, there are spectral bands at 1.95eV and 2.24eV for steady excitation, but after a decay time of 100μs, only the red band remains, and its peak is then at 1.92eV. The authors interpreted the observed shift by postulating that the luminescence transitions are between donor-acceptor pairs with In centres as the donors and Cu centres as the acceptors. Coupling is strongest between relatively close donor-acceptor pairs and for these the emission energy is also greatest; hence, during the decay of the light, the emission band shifts to lower energies. The present work on Cu-doped ZnSe was performed on material in which Al was added as a donor but no time resolved spectra for the decay of either photoluminescence or electroluminescence were measured so that it is not known if there is a shift as in ZnSe:Cu:In. It has already been noted in section 6.3.1 that in reverse bias the multiplication for a given electric field strength and donor concentration is increased by the addition of Cu centres. This does not necessarily mean that the radiative transitions in reverse-biassed diodes are de-ionization transitions rather than donor-acceptor pair transitions.

The decay time of the red luminescence band in ZnSe:Cu:In at 77K is, from the experiments of Fujiwara and Fukai[85], about 50μs.

This decay time is of similar magnitude to the rise time found in the present work for forward bias electroluminescence at room temperature.

In the photoluminescence spectrum for the phosphor ZnS:Cu:Al at room temperature Shionoya et al.[88] found a green band at 2.42eV to be dominant and at 77K he found that in addition to this green band there is a blue band at approximately 2.75eV with the two bands of similar intensity. The authors showed that, during the decay of photoluminescence, the green band shifts to lower energies with the peak shifted from its steady excitation position by 0.04eV after a decay time of 1ms. The blue band, which decayed more rapidly, did not shift in position. Shionoya et al. interpreted the shift of the green band during the photoluminescence decay in terms of a model in which the green emission arises from transitions between donors and acceptors. There are many obvious similarities in the luminescence of ZnS and ZnSe, both doped with Cu, since each exhibits two bands separated by about 0.35eV with the lower energy band having the properties of the longer decay time, of dominance at room temperature and of exhibiting a shift to lower energy during its decay. Unfortunately, Shionoya et al. did not make it clear whether their measurements referred to ZnS:Cu:Al in the zinc blende or hexagonal form. At room temperature, for the cubic form of ZnS:Cu:Cl, Leverenz[82] found the photoluminescence spectrum to be dominated by a green band peaking at 2.34eV and, in numerous papers on the luminescence of Cu-doped ZnS of unspecified crystallographic form including one for A.C. electroluminescence in a powder phosphor[89], the existence of bands, in any given specimen, at about 2.4eV and 2.8eV has been described. The fact that the luminescence bands of Cu-doped ZnS are at substantially higher energy than for the corresponding bands

in Cu-doped ZnSe, whilst the bands due to the presence of Mn in ZnS and ZnSe are at very nearly identical energies, is further evidence that in the two Cu-doped phosphors the emission is not due to a Cu internal transition.

The fast decay of light relative to the speed of the rise of light in Cu-doped ZnSe diodes subjected to forward bias pulses may be due to field ionization of the upper levels involved in the radiative transitions between donor and acceptor pairs. For zero applied bias, which is the condition for which the light decay was observed, there is, in the depletion layer of diodes, a strong built-in field. This field is about 10^5 V cm^{-1} in typical diodes used in the present work and a field of this magnitude would cause ionization of levels at a few tenths of an eV below the conduction band edge in a time small compared to the probable radiative lifetime for these levels. In the rising edge of a light pulse field ionization does not occur because the field is reduced to a small value. As mentioned in section 4.2.4. the difference in the rise and fall times for the light emission associated with forward bias is more marked in MAl diodes, where it is thought that the emission may be due to Cu impurity, than for the diodes which were deliberately doped with Cu. Possibly the explanation given is essentially correct for MAl diodes except that some other transition between donor and acceptor pairs, not involving Cu, takes place.

6.4. SUMMARY

The similarity of the spectral peaks for photoluminescence, reverse bias electroluminescence and forward bias electroluminescence is evidence that in the three excitation methods the same respective upper and lower radiatively coupled levels are involved. The upper levels may be due to donor centres and the lower levels may be acceptor levels attributable to the presence of Cu.

7. CONCLUSIONS

The main advance resulting from the work described in this thesis is considered to be that a method has been devised for experimentally studying the band structure of semiconductors, based on an examination of the reverse bias electroluminescence spectra from Schottky diodes prepared from material free from intentionally added luminescence centres. In the present work only ZnSe has been studied but the method should be equally applicable to a wide range of semiconductors. Some preliminary work, as a check on the method, is currently progressing for GaP, with this material chosen because its band structure is more accurately known than is the case for ZnSe. The results obtained to date[90] give support to the viability of the method. It was found for ZnSe that in the absence of deliberately added luminescence centres and in the electric fields of the order of $10^5 V\ cm^{-1}$ which occur in reverse-biassed diodes electrons are raised to an energy 2.65eV above the lowest minimum of the conduction band causing population of the higher minima at L_1, X_1 and X_3.

The electroluminescence band for reverse bias of Mn-doped ZnSe arises from Mn internal $^4T_1 - {}^6A_1$ transitions. In these Mn-doped ZnSe diodes, sufficient photometric power efficiency has been achieved in reverse bias operation, which considered in conjunction with the cheapness of the diode materials and fabrication, makes further development worthwhile pursuing with the aim of producing practical light-emitting diodes.

The work on Cu-doped ZnSe was interesting from the point of view of gaining information on the behaviour of diodes with a luminescence centre other than Mn. It is not however probable that the performance of Cu-doped ZnSe diodes can be developed to a point where they match, as practical devices, the performance of other, already available, diodes which emit red light.

APPENDIX I

LUMINESCENCE BANDS OBSERVED* IN ZnSe WITH DIFFERENT DOPANTS AND EXCITATION METHODS

DOPANTS	MATERIAL CODE NO.	PHOTOLUMINESCENCE Excitation wavelength = 365nm Peak(eV)	Width(eV)	T(K)	REVERSE BIAS E.L. Peak(eV)	width(eV)	T(K)	FORWARD BIAS E.L. Peak(eV)	Width(eV)	T(K)
Zn:Al	20Al	(very weak)		290	(Inter-valley transitions)		290–120	1.99(61) 2.675	0.31 also 0.051	120 290
Mn:Zn:Al:Cl	MAl				2.10 2.12	0.19 0.13	290 118	1.91 1.94	0.33 0.29	290 117
Mn:Zn:Al:Cl	DM				2.12	0.19	290	2.02	0.42	290
Mn:Zn:Al:Cl	36Bl	2.00	0.44	290	2.11 2.12	0.20 0.18	290 120	2.01(61)	0.42	290
Mn:Zn:Al:Cl	26Cl				2.11	0.22	290			
Mn:Cl	36Bl'	1.90	0.34	290						
Cu:Zn:Al	46Al	1.89	0.30	290	1.90	0.39	290	1.90	0.37	290

Spectrum 'width' in this table refers to energy difference between $\frac{1}{2}$-height points.

* Observed by the author unless shown otherwise by a reference no.

REFERENCES

1. A. GOODMAN, J. Appl. Phys. 34, 329 (1963)

2. D. BERLINCOURT, H. JAFFE AND L.R. SHIOZAWA, Phys. Rev. 129, 1009 (1963)

3. J.C. DE VOS, Physica 20, 690 (1954)

4. 'Handbook of Chemistry and Physics', 46th edition, pE 147. The Chemical Rubber Co., Cleveland, Ohio (1965)

5. B.T. BARNES AND W.E. FORSYTHE, J. Opt. Soc. Am. 26, 313 (1936)

6. A.G. CHYNOWETH AND K.G. MC.KAY, J. Appl. Phys. 30, 1811 (1959)

7. R. NEWMAN, Phys. Rev. 100, 700 (1955)

8. A.G. CHYNOWETH AND K.G. MC.KAY. Phys. Rev. 102, 369 (1956)

9. A.G. CHYNOWETH AND H.K. GUMMEL, J. Phys. Chem. Solids 16, 191 (1960).

10. M.H. PILKUHN, J. Appl. Phys. 40, 3162 (1969)

11. M. GERSHENZON AND H.K. MIKULYAK, J. Appl. Phys. 32, 1338 (1961)

12. M.H. PILKUHN AND G. SCHUL, Proc. 2nd. Int. Symposium on GaAs, Dallas 1968, p.238, I.P.P.S.

13. M.H. PILKUHN AND H. RUPPRECHT, J. Appl. Phys. 36, 684 (1965)

14. G.F. KHOLUYANOV, Sov. Phys. - Solid State 3, 2405 (1962)

15. T. FIGIELSKI AND A. TORUN, Proc. Int. Conf. on the Physics of Semiconductors, Exeter 1962, p. 863, I.P.P.S.

16. C.A. MEAD, Phys. Lett. 18, 218 (1965)

17. R.K. SWANK, M. AVEN AND J.Z. DEVINE, J. Appl. Phys. 40, 89 (1969)

18. J.L. MOLL, 'Physics of Semiconductors', p.253, Mc.Graw-Hill, New York, (1964).

19. M.A. LAMPERT AND P. MARK, 'Current Injection in Solids' p. 189, Academic Press, New York, (1970).

20. R.H. GOOD AND W. MÜLLER in 'Handbuch der Physik', 21, p. 176, Springer, Berlin, (1956).

21. A.W. LIVINGSTONE AND J.W. ALLEN, J. Phys. C, 3, 2468 (1970)

22. J. SHEWCHUN AND L.Y. WEI, Solid State Electronics, 8, 485 (1965)

23. E. KAMIENIECKI, Phys. Stat. Sol. 6, 887 (1964)

24. D.J. STUKEL, R.N. EUWEMA, T.C. COLLINS, F. HERMAN AND R.L. KORTUM, Phys. Rev. 179, 740 (1969)

25. M.L. COHEN AND T.K. BERGSTRESSER, Phys. Rev. 141, 789 (1966)

26. P. ECKELT, Phys. Stat. Sol. 23, 307 (1967)

27. Y. PETROFF, M. BALKANSKI, J.P. WALTER AND M.L. COHEN, Solid State Comm. 7, 459 (1969)

28. F. HERMAN, R.L. KORTUM, C.D. KUGLIN AND J.L. SHAY, II-VI Semiconducting Compounds 1967 Conf., p. 503, Benjamin, N.Y. (1967)

29. S. VISVANATHAN, Phys. Rev. 120, 379 (1960)

30. H.J.G. MEYER, Phys. Rev. 112, 298 (1958)

31. W. PAUL, J. Appl. Phys. 32, 2082 (1961)

32. D.G. THOMAS, J. Appl. Phys. 32, 2298 (1961)

33. R.M. MARTIN, Phys. Rev. 1B, 4005 (1970)

34. S. VISVANATHAN, Phys. Rev. 120, 376 (1960)

35. A. HADNI, J. CLAUDEL AND P. STRIMER, Phys. Stat. Sol. 26, 241 (1968)

36. J.L. BIRMAN, M. LAX AND R. LOUDON, Phys. Rev. 145, 620 (1966)

37. G.W. LUDWIG AND M. AVEN, J. Appl. Phys. 38, 5326 (1967)

38. C. HILSUM AND H.D. REES, Electronics Lett. 6, 277 (1970)

39. J. APPERSON, Y. VOROBIOV, AND G.F.J. GARLICK, Brit. J. Appl. Phys. 18, 389 (1967)

40. N. HOLONYAK, S.J. BEVACQUA, C.V. BIELAU AND S.J. LUBOWSKI, Appl. Phys. Lett. 3, 47 (1963)

41. E. HAGA AND H. KIMURA, J. Phys. Soc. Japan 19, 1596 (1964)

42. H. EHRENREICH, J. Phys. Chem. Solids 2, 131 (1957)

43. W. FAWCETT, A.D. BOARDMAN AND S. SWAIN, J. Phys. Chem. Solids 31, 1963 (1970)

44. P.M. BOERS, Phys. Lett. 34A, 329 (1971)

45. D.H. PAXMAN AND R.J. TREE, Electronics Lett. 7, 1 (1971)

46. F. BONEK AND H. HILLBRAND, Electronics Lett. 7, 634 (1971)

47. J.G. RUCH, Appl. Phys. Lett. 20, 253 (1972)

48. E.G.S. PAIGE, in 'Prog. in Semiconductors' 8, pp. 1-244 (1964)

49. M. CARDONA, J. Phys. Chem. Solids 24, 1543 (1963)

50. M. CARDONA AND D.I. GREENAWAY, Phys. Rev. 125, 1291 (1962)

51. E. HAGA AND H. KIMURA, J. Phys. Soc. Japan, 18, 777 (1963)

52. J.L. BIRMAN, Phys. Rev. 127, 1093 (1962)

53. J.L. BIRMAN, Phys. Rev. 131, 1489 (1963)

54. W.G. SPITZER AND J.M. WHELAN, Phys. Rev. 114, 59 (1959)

55. H. EHRENREICH, Phys. Rev. 120, 951 (1960)

56. W.M. BECKER, A.K. RAMDAS AND H.Y. FAN, J. Appl. Phys. 32, 2094 (1961)

57. H. EHRENREICH, J. Appl. Phys. 32, 2155 (1961)

58. E.M. CONWELL in 'High Field Transport in Semiconductors' p. 154, Academic Press, New York, (1967)

59. A.W. LIVINGSTONE, Thesis, St. Andrews 1972.

60. J.W. ALLEN, A.W. LIVINGSTONE AND K. TURVEY to be published in Solid State Electronics.

61. M.D.S. RYALL Private communication.

62. L.Y. MARKOVSKII, I. MIRONOV AND Y.S. RYZHKIN, Optics and Spectroscopy 27, 84 (1969)

63. G.B. STRINGFELLOW AND R.H. BUBE, Phys. Rev. 171, 903 (1968)

64. L.Y. MARKOVSKII, I. MIRONOV AND Y.S. RYZHKIN, Bull. Acad. Sci. U.S.S.R. 33, 887 (1969)

65. S. IIDA, J. Phys. Soc. Japan 25, 177 (1968)

66. A.G. FISCHER in 'Radiative Recombination in Semiconductors', p. 259, Paris 1964, Dunod.

67. S. ASANO, N. YAMASHITA, M. OISHI AND K. OMORI, J. Phys. Soc. Japan 24, 1302 (1968)

68. M. AVEN AND H.H. WOODBURY, Appl. Phys. Lett. 1, 53 (1962)

69. D.W. LANGER AND H.J. RICHTER, Phys. Rev. 146, 554 (1966)

70. S. LARACH, J. Chem. Phys. 21, 756 (1953)

71. J. APPERSON, Y. VOROBIOV AND G.F.J. GARLICK, Brit. J. Appl. Phys. 18, 389 (1967)

72. H.W. LEVERENZ, in 'An Introduction to Luminescence' p. 204 Chapman and Hall, London (1950)

73. D.S. MC.CLURE, J. Chem. Phys. 39, 2850 (1963)

74. D. LANGER AND S. IBUKI Phys. Rev. 138A, 809, (1965)

75. S. BRAUN, H.G. GRIMMEISS AND J.W. ALLEN to be published.

76. E.M. WRAY, Private communication.

77. A.W. LIVINGSTONE, K. TURVEY AND J.W. ALLEN, to be published in Solid State Electronics.

78. C.E. BLIEL AND I. BROSER, J. Phys. Chem. Solids, 11 (1964)

79. A.G. FISCHER AND H.I. MOSS, J. Appl. Phys. 34, 2112 (1963)

80. D. WIGHT, Private communication.

81. A.W. LIVINGSTONE, Private communication.

82. H.W. LEVERENZ, in 'An Introduction to Luminescence', p.202 Chapman and Hall, London (1950).

83. W.G. GELLING AND J.H. HAANSTRA , Philips Research Reports 16, 371 (1961)

84. I.J. HEGYI, S. LARACH AND R.E. SCHRADER, J. Electrochem. Soc. 104, 717 (1957)

85. S. FUJIWARA AND M. FUKAI, J. Phys. Soc. Japan 23, 657 (1967)

86. S. FUJIWARA AND M. FAKAI, J. Phys. Soc. Japan 23, 669 (1967)

87. F.F. MOREHEAD, J. Phys. Chem. Solids 24, 37 (1963)

88. S. SHIONOYA, K. ERA AND Y. WASHIZAWA, J. Phys. Soc. Japan 21, 1624 (1966)

89. P. ZALM, G. DEIMER AND H.A. KLASENS, Philips Res. Repts. 9, 81 (1954)

90. R.C. PEEBLES, B.Sc. project, St. Andrews, 1972, and private communication.